

MATHEMATICAL MODELS FOR THE TIME DOMAIN
ANALYSIS OF HYDRAULIC SYSTEMS

Thesis for the Degree of Ph. D.
MICHIGAN STATE UNIVERSITY
Hinrich Robert Martens
1962

This is to certify that the
thesis entitled
MATHEMATICAL MODELS FOR THE TIME-DOMAIN
ANALYSIS OF HYDRAULIC SYSTEMS
presented by

Hinrich Robert Martens

has been accepted towards fulfillment
of the requirements for

Ph.D. degree in M.E.

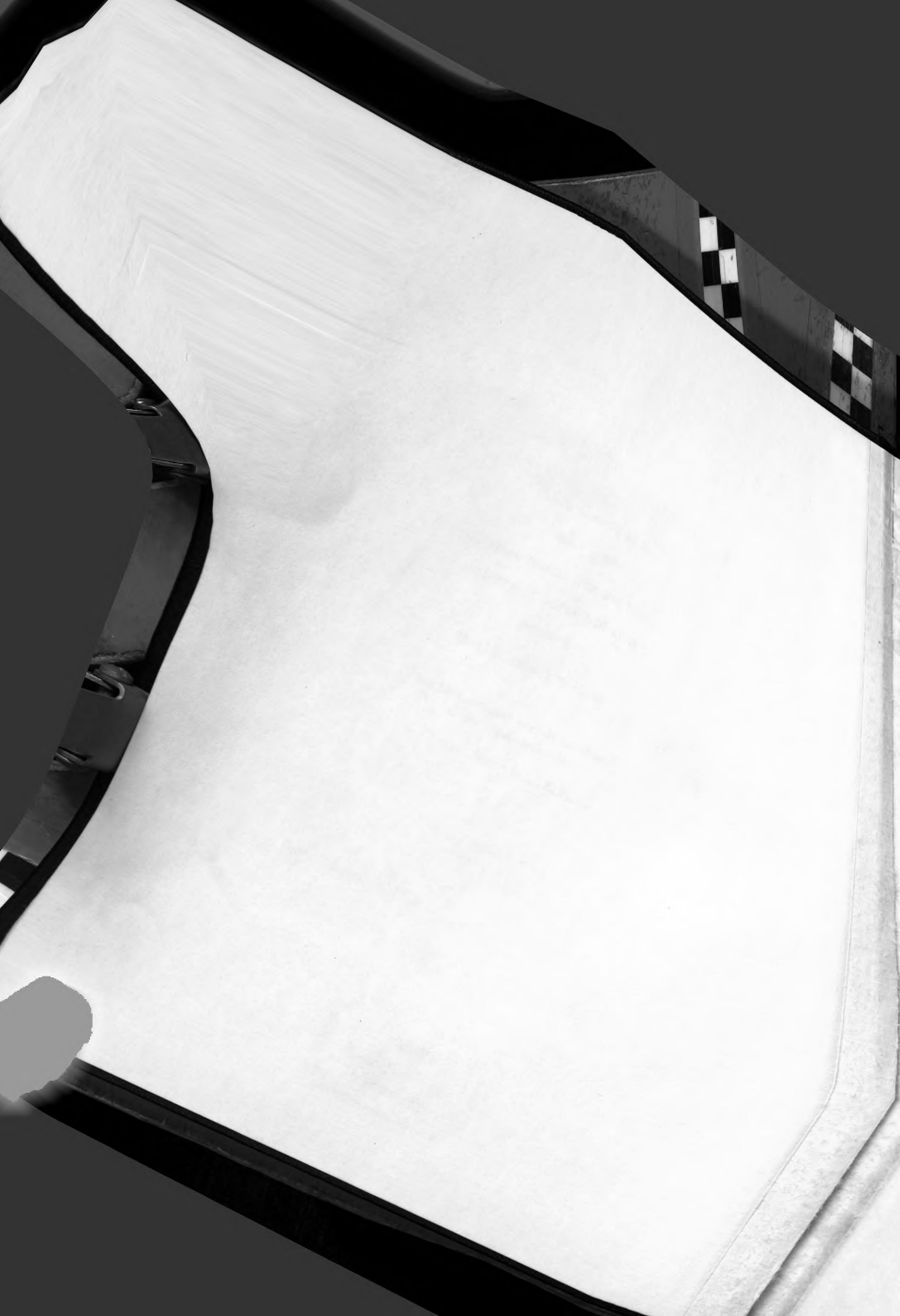
Francis S. Tse

Major professor

Date August 2, 1962

O-169





**MATHEMATICAL MODELS FOR THE TIME-DOMAIN
ANALYSIS OF HYDRAULIC SYSTEMS**

By

Hinrich Robert Martens

AN ABSTRACT OF A THESIS

**Submitted to the
School of Advanced Graduate Studies of
Michigan State University
in partial fulfillment of the requirements
for the degree of**

DOCTOR OF PHILOSOPHY

Department of Mechanical Engineering

1962

ABSTRACT

MATHEMATICAL MODELS FOR THE TIME-DOMAIN ANALYSIS OF HYDRAULIC SYSTEMS

by Hinrich Robert Martens

Systematic procedures have recently been developed to formulate the mathematical models of systems of discrete physical components regardless of whether or not the characteristics of the components are linear or nonlinear. These formulation procedures lead to a time-domain mathematical model suitable for computer processing. When applied to hydraulic systems, this time-domain model makes it possible to include a multitude of continuous and discontinuous nonlinearities as they are encountered in modeling the characteristics of hydraulic components. When this facility is combined with the ability of the digital computer to obtain solutions the accuracy obtainable in the study of nonlinear systems is limited only by the accuracy with which the individual components can be modeled.

This thesis presents a general methodology for implementing these procedures in the analysis and design of hydraulic systems. Nonlinear mathematical models are established for a number of typical hydraulic components. Conditions and procedures are developed for the generation of time-domain models suitable for computer processing of typical subassemblies and functional hydraulic systems.

Hinrich Robert Martens

It is shown that the desired form of the mathematical models may always be established when the effect of hydraulic capacitance is included in the component models. The inclusion of leakage effects in the models of hydraulic components is readily accomplished although results indicate that they may be neglected in most cases.

Comparisons made at various stages and levels of system complexity establish a high level of correlation between solutions based on these models and the performance of the actual system.

MATHEMATICAL MODELS FOR THE TIME-DOMAIN
ANALYSIS OF HYDRAULIC SYSTEMS

By

Hinrich Robert Martens

A THESIS

Submitted to the
School of Advanced Graduate Studies of
Michigan State University
in partial fulfillment of the requirements
for the degree of

DOCTOR OF PHILOSOPHY

Department of Mechanical Engineering

1962

ACKNOWLEDGMENT

The author is very grateful to Dr. H. E. Koenig for his guidance and encouragement during the preparation of this thesis and during the period of research. The author also wishes to gratefully acknowledge the support of the National Science Foundation.

TABLE OF CONTENTS

SECTION	Page
I. INTRODUCTION	1
II. MATHEMATICAL MODELS OF CONTROL VALVES	4
III. MATHEMATICAL MODELS OF HYDRAULIC MACHINES.	29
IV. MATHEMATICAL MODELS OF HYDRAULIC LINES	48
V. FORMULATION AND SOLUTION OF TYPICAL SUBASSEMBLIES.	56
VI. FORMULATION AND SOLUTION OF TYPICAL SYSTEMS	90
VII. CONCLUSION	112

LIST OF FIGURES

Figure	Page
2.1.1 Single Orifice	4
2.1.2 Pressure-Flow Curve for Single Orifice	5
2.1.3 Flow Reaction Force as a Function of Valve Opening and Pressure	6
2.1.4 Flow Reaction Force for a Compensated Valve.	6
2.2.1 Terminal Graph of Basic Valve Configuration.	7
2.2.2 System Graph of the General Case	8
2.2.3 Steady State Flow Reaction Force	9
2.2.4 Three-Way Valve	10
2.2.5 Four-Way Valve	11
2.2.6 System Graph of Flow Source-Valve Combination.	14
2.3.1 Typical Four-Way Valve Electromagnetic Transducer Assembly	15
2.3.2 Typical Electrohydraulic Servo Valve	16
2.3.3 Jet-Pipe Valve	17
2.3.4 Push-Pull Ram Actuator	19
2.3.5 Booster Stage	20
2.3.6 PEGASUS Electrohydraulic Servo Valve	21
2.3.7 Double Flapper-Nozzle Valve.	22
2.3.8 Booster Stage	23
2.4.1 RAD 410 Servo Valve. System Graph	24
2.5.1 Typical Family of Pressure-Flow Curves	27
3.1.1 Basic Hydraulic Machines	29

LIST OF FIGURES (con't)

Figure	Page
3.3.1 Assembly Drawing of Axial Piston Machine	34
3.3.2 Terminal Graph	34
3.3.3 Terminal Graph of Subassembly	35
3.3.4 Plate Valve Position	36
3.3.5 Plate Valve Position	37
3.3.6 System Graph of Axial Piston Pump	38
3.3.7 Terminal Graph	40
3.3.8 Pump Friction for Variable Displacement Pump . . .	42
3.3.9 Effect of Coulomb Friction	43
3.3.10 Pump Displacement	44
3.3.11 Tilt-plate Torque vs Velocity	44
3.4.1 Fixed Displacement Machine Friction Characteristics	47
4.1.1 Hydraulic Line and Terminal Graph	49
4.1.2 Lumped Model with n Sections; Closed Ends	50
4.2.1 System Graph for Terminal Representation	52
4.2.2 Pressure Response for 16 m flexible line	55
5.1.1 Graph of Subassembly 1	57
5.2.1 Graph of a Two-Element Line in CO Representation	60
5.2.2 Graph of Subassembly 2	60
5.2.3 Effect of variation of capacitance on Velocity Response of Subassembly 2	64
5.2.4 Velocity Response Curves of Subassembly 2	65

LIST OF FIGURES (con't)

Figure	Page
5.2.5 Velocity Response Curves of Subassembly 2	66
5.2.6 Velocity Response Curves of Subassembly 2	67
5.3.1 Graph of Subassembly 3	69
5.3.2 Velocity Response Curves of Subassembly 3	72
5.3.3 Velocity Response Curves of Subassembly 3	73
5.4.1 Graph of Subassembly 4	74
5.5.1 Graph of Subassembly 5	76
5.6.1 Graph of Subassembly 6	78
5.6.2 Velocity Response Curves of Subassembly 6	81
5.6.3 Velocity Response Curves of Subassembly 6	82
5.7.1 Graph of Subassembly 7	80
5.7.2 Velocity Response Curves of Subassembly 7	85
5.7.3 Velocity Response Curves of Subassembly 7	86
5.8.1 Graph of Subassembly 8	88
6.1.1 Valve Controlled Positioning System	90
6.1.2 Valve Controlled Speed Control System	91
6.2.1 Position Response Curves of Positioning System	94
6.2.2 Pressure Response Curves of Positioning System	95
6.2.3 Valve Stem Position as a Function of Position Load Factor	96
6.3.1 Response Curves of Speed Control System	105
6.4.1 Pump Controlled Speed Control System	106

LIST OF FIGURES (con't)

Figure	Page
6.4.2 Speed Response Curves of Speed Control System . . .	109
6.4.3 Pressure Response Curves of Speed Control System	110

LIST OF APPENDICES

APPENDIX	Page
A. Numerical Values of Coefficients	113

I. INTRODUCTION

A complete analysis of systems of discrete parameter components describable by linear algebraic and differential equations is generally obtainable. Transform techniques which have been highly developed are effectively utilized. However, when systems contain nonlinearities transform procedures no longer apply. Hydraulic systems are a noted example.

The first attempts in the analysis of hydraulic systems have been based on linear approximations. In fact, this is still widespread practice. Despite the awareness of the inherent nonlinearities, an investigation based upon linear approximations offered the only alternative for lack of other approaches. With the development of techniques in handling nonlinear systems, a great deal of effort, for example, was directed at the study of hydraulic systems by means of describing function techniques (2, 3, 9). However, all these techniques lean heavily toward linearization. Thus either misrepresentation or erroneous prediction of the physical system is the consequence. As a result of the history of nonlinear studies of hydraulic systems, it has become of prominent importance that a more effective procedure is needed for a complete and reliable investigation.

Through the advance of automatic computing equipment, it is now practical to simulate the mathematical models of systems of discrete parameter components regardless of degree of com-

plexity and regardless of the nature of the nonlinearities appearing in the model. Systematic procedures have recently been developed to formulate the mathematical models of systems of discrete parameter components regardless of whether or not the characteristics of the components are linear (4). These formulation procedures lead to a time-domain mathematical model referred to as "normal form", i.e., a model of the form

$$\frac{d\bar{x}(t)}{dt} = \bar{F}(\bar{x}(t), \bar{y}(t))$$

where $\bar{x}(t)$ and $\bar{y}(t)$ are vectors of system variables. When applied to hydraulic systems, this time-domain model makes it possible to include a multitude of continuous and discontinuous nonlinearities as they are encountered in the description of hydraulic components. When this facility is combined with the ability of the digital computer to obtain solutions, the accuracy obtainable in the study of nonlinear systems is limited only by the accuracy with which the individual components can be modeled.

One example based upon a time domain study was introduced by Wang (5). He presented the mathematical model of an electro-hydraulic servomechanism and included a discussion of how this model was derived. However, a general and systematic procedure for mathematically modeling hydraulic systems in the time-domain has not been reported.

This thesis presents a systematic method for the analysis of nonlinear hydraulic systems which involves 1) establishing nonlinear models of hydraulic components, 2) establishing a nonlinear time-domain model of the hydraulic system in a form (normal form) suitable for computer processing and 3) actual

solution of the system model.

The type of nonlinearities include both continuous and discontinuous functions. Comparisons are made at various stages and levels of system complexity between computer solutions and actual performance characteristics.

Normal form formulation procedures require the following information: 1) a mathematical model of the components of the system and 2) a mathematical statement of the interconnection of the system components. The first requirement involves the modeling of the components in a way such that when the components are assembled to form a system a normal form system model can be generated.

The results of extensive research on the characteristics of hydraulic components and typical subassemblies available in the literature along with experimental investigations form the general basis for the development of the component models presented in this thesis.

II. MATHEMATICAL MODELS OF CONTROL VALVES

2.1 The Orifice

The basic component of a control valve is the orifice. As shown in Fig. 2.1.1, the orifice may be represented as a four-terminal component; two terminals for the measurement of force and displacement of the valve stem, and two terminals for the measurement of flow and pressure of the fluid.

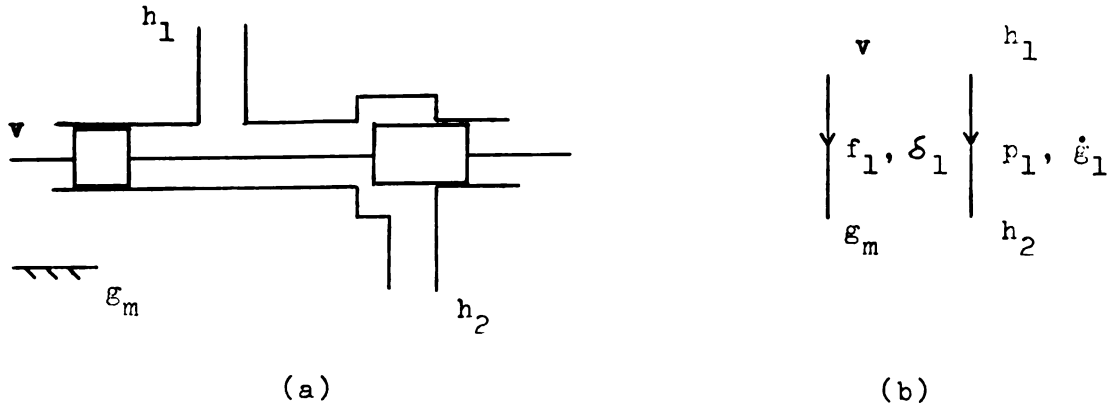


Fig. 2.1.1.--Single orifice. Schematic and terminal graph

The terminal equations associated with the terminal graph of Fig. 2.1.1(b) for a single orifice can be shown to have the form

$$\dot{g}_1 = K_v F_{13} (\Delta + \delta_1) \sqrt{p_1} \quad (2.1.1)$$

$$f_1 = B_1 (\dot{\delta}_1) + M_1 \ddot{\delta}_1 + K_{fb} (\delta_1) p_1 \quad (2.1.2)$$

where K_v = orifice flow coefficient

F_{13} = a switching function defined by

$$\begin{aligned} F_{13}(X) &= X & X &\geq 0 \\ &= 0 & X &< 0 \end{aligned} \quad (2.1.3)$$

$K_{fb}(\delta_1)$ = Flow reaction force coefficient

M_1 = Combined mass of stem and spool

$B_1(\dot{\delta}_1)$ = Compound friction function including the effects of viscous, dry, and static friction.

$\sqrt{}$ = a sign sensitive square root defined by

$$\sqrt{x} = \frac{x}{|x|} \sqrt{|x|} \quad (2.1.4)$$

Δ = Amount of Underlap or Overlap defined by

$$\Delta = \Delta_u > 0 \quad \text{for Underlap}$$

$$\Delta = \Delta_o < 0 \quad \text{for Overlap}$$

Equation (2.1.1) is sometimes called the orifice equation.

This equation is based on the usual assumptions that (1) all measurements are instantaneous, (2) the flow coefficient is a constant, and (3) the orifice area varies linearly with the stem displacement (8). A typical experimental pressure-flow curve is shown in Fig. 2.1.2.

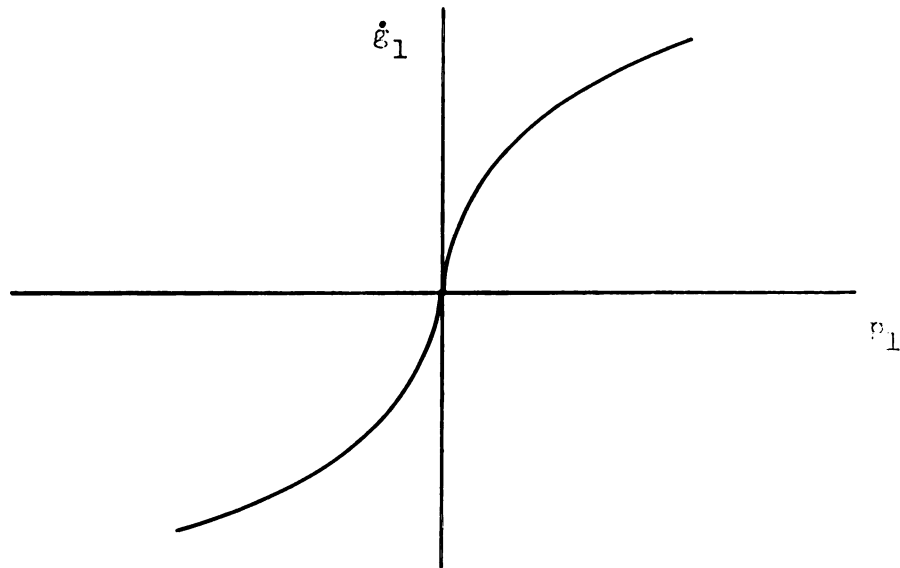


Fig. 2.1.2.--Pressure-flow curve for single orifice ($\delta_v = \text{constant}$)

Because of uneven pressure distribution in the valve spools during flow, a force term must be included in (2.1.2).

This flow reaction force is normally a function of both valve opening and pressure drop across the valve. A typical set of curves is shown in Fig. 2.1.3.

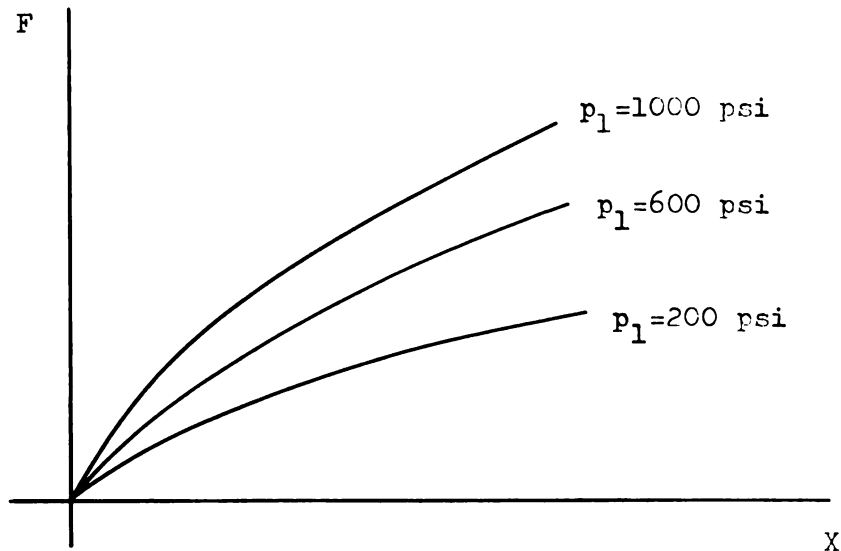


Fig. 2.1.3.--Flow reaction force as a function of valve opening (X) and pressure.

Since the force-displacement gradient is positive, the valve tends to close under flow condition. This, of course, is a desirable stability feature used to a great advantage in more complicated valve configurations. Through suitable geometric design, the flow reaction force may be controlled to a minimum, yet exhibit a desirable degree of stability (8). Figure 2.1.4 shows the flow reaction curves for an orifice which has been compensated. Note that the curve now is essentially independent of the pressure drop.

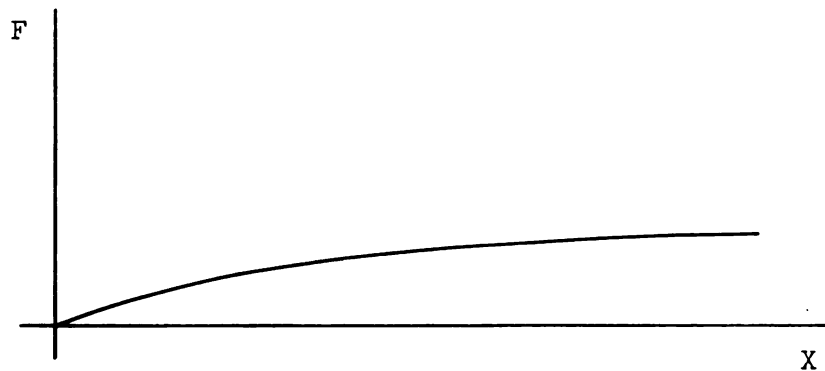


Fig. 2.1.4.--Flow reaction force for a compensated valve

2.2 Basic Valve Configurations.

Although a single orifice may be used as a control element

in a hydraulic system, a functional combination of several orifices is usually more effective. Several basic valve configurations are considered in this section and convenient terminal representations developed. All terminal representations are given in terms of the terminal graph of Fig. 2.2.1. Of interest is information regarding the force and displacement variables of the valve stem shaft, and pressure and flow variables of the various ports to which system connections are made. These are normally the two load ports, h_1 and h_2 , a supply port, h_3 , and a return port, g_h . Terminal g_h is conveniently

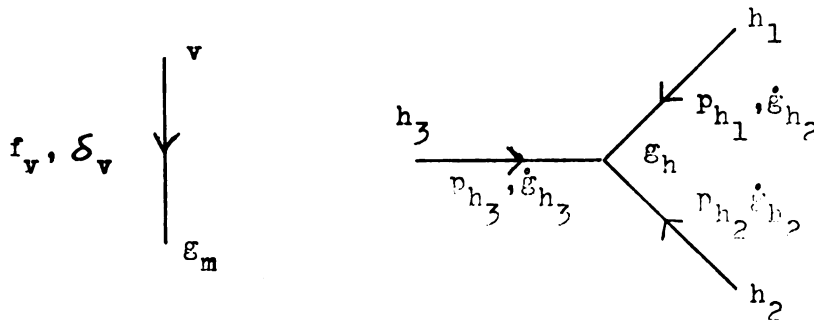


Fig. 2.2.1.--Terminal graph of basic valve configuration taken as the atmospheric reference. It will be seen later that only when the terminal g_h is included in a system graph can systems whose component characteristics depend on the atmospheric reference be properly formulated.

Consider first the mathematical model of a general valve configuration. From this the characteristics of other configurations are obtained as special cases or modifications. A valve configuration consisting of four orifices is considered as the general case. A larger number of orifices may be used to form a control valve. Such an example was presented by Dushkes (10).

Blackburn has shown that a four-orifice valve is most effectively analyzed when the valve is compared with a four-

arm bridge (7). Accordingly, in the system graph in Fig. 2.2.3, elements 1, 2, 3, 4 constitute the four orifices. In general, the orifices may be fixed or variable, and the supply may be either a constant pressure or constant flow source.

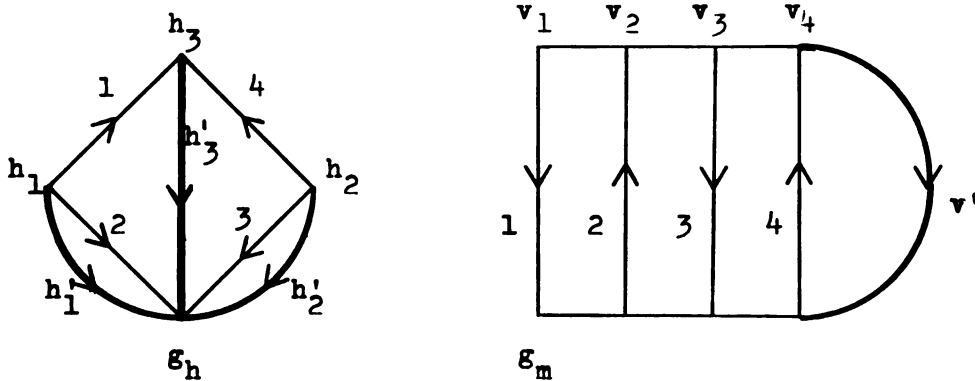


Fig. 2.2.3.--System graph of the general case

If the elements in the graph representing external measurements (measure graph) constitute a tree, all orifice elements can be made chord elements. For the given nonlinear forms this is a necessary condition to arrive at mathematical models explicit in the terminal variables. Since the respective orifice-across variables appear implicitly they must be related, through the circuit equations, to those tree-across variables that either are specified or otherwise known. Combination of the relatively simple graph equations with the orifice terminal equations yield the desired terminal representation.

$$\begin{aligned}
\dot{g}_{h_1} &= K_v (F_{13}(\Delta + \delta_v) \sqrt{p_{h_1} - p_{h_3}} + F_{13}(\Delta - \delta_v) \sqrt{p_{h_1}}) \\
\dot{g}_{h_2} &= K_v (F_{13}(\Delta - \delta_v) \sqrt{p_{h_2} - p_{h_3}} + F_{13}(\Delta + \delta_v) \sqrt{p_{h_2}}) \\
\dot{g}_{h_3} &= K_v (F_{13}(\Delta + \delta_v) \sqrt{p_{h_3} - p_{h_1}} + F_{13}(\Delta - \delta_v) \sqrt{p_{h_3} - p_{h_2}}) \\
f_v &= L_v(d/dt) \delta_v + K_{fv}(\delta_v)
\end{aligned}
\tag{2.2.1}$$

where $L_v(d/dt) \equiv M_v d/dt + B_v(\dot{\delta}_v)d/dt$

K_{fv} = positive gradient coefficient of the flow reaction force.

In the development of this result all orifices are considered identical although other conditions may also be considered.

As long as valve configurations exhibit symmetric design features, the steady-state flow reaction forces may be very effectively shaped by design to give a characteristic, as indicated for example, in Fig. 2.2.4.

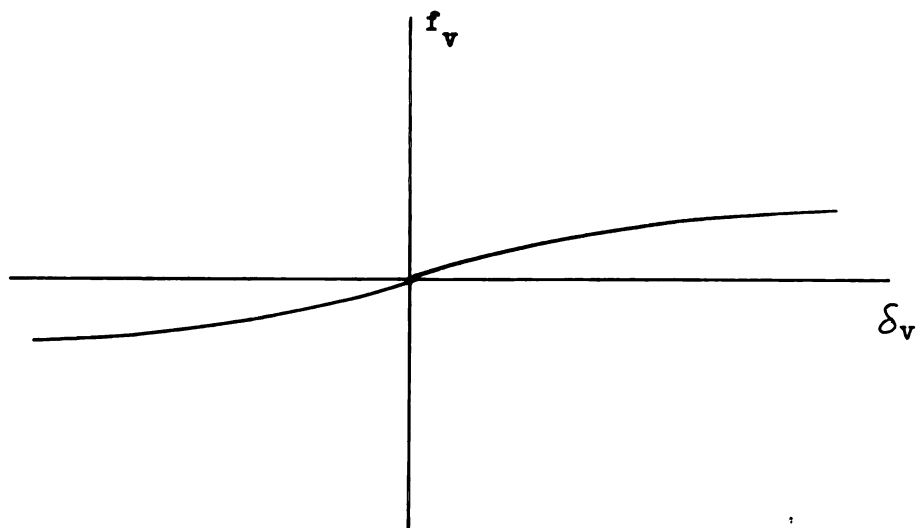


Fig. 2.2.4.--Steady-state flow reaction force

Several special cases are now considered. These special cases give the terminal equations of typical commercially produced control valves.

The Three-way Valve with Constant Pressure Supply

The schematic of a typical three-way valve is shown in Fig. 2.2.5. It consists of two variable orifices, both of which are underlapped. The terminal representation of the three-way valve may be obtained from (2.2.1) by making the following simplifications:

$$\text{Set } p_{h_3} = p_s$$

$$p_{h_2} = p_s/2$$

Orifices 1, 2 variable with $\Delta = \Delta_u \geq |\delta_v|$

Orifices 3, 4 nonexistent.

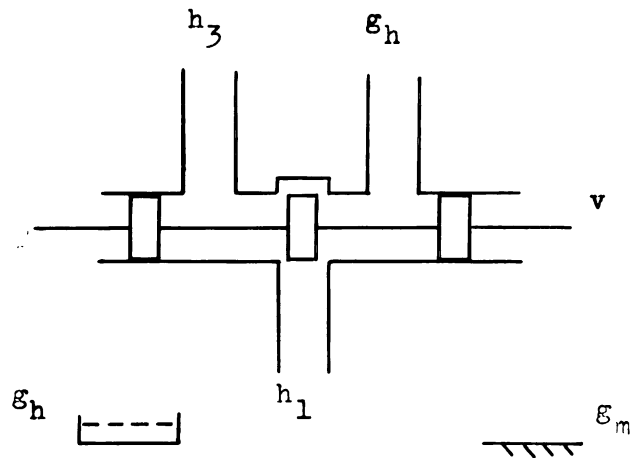


Fig. 2.2.5.--Three-way valve

This equation then reduces to

$$\dot{g}_{h_1} = K_v((\Delta_u + \delta_v) \sqrt{p_{h_1} - p_s} + (\Delta_u - \delta_v) \sqrt{p_{h_1}})$$

$$p_{h_2} = p_s/2$$

$$f_v = M_v d^2/dt^2 \delta_v + B_v(\dot{\delta}_v) + K_{fv}(\delta_v)$$

(2.2.2)

A typical system connection with a three-way valve shows the load inserted between h_1 and h_2 , so that p_{h_1} is controlled by the

valve and p_{h_2} is biased at half the system pressure.

The Four-way Valve with Constant Pressure Supply

The schematic of a typical four-way valve is shown in Fig. 2.2.6. It consists of 4 variable orifices all of which are of equal dimensions.

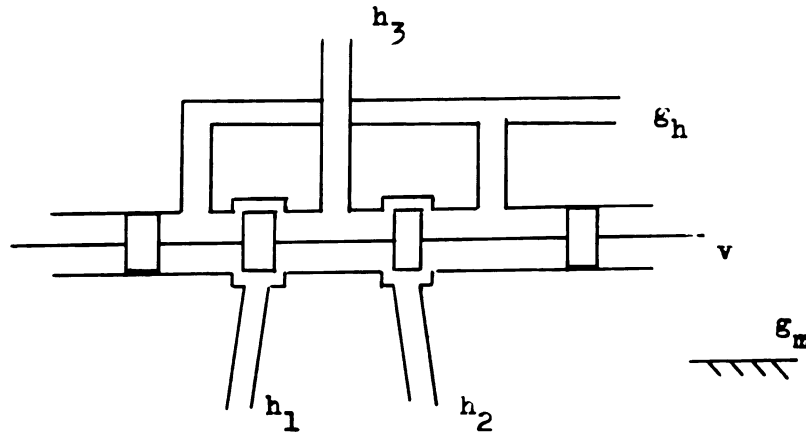


Fig. 2.2.6.--Four-way valve

The orifices may be either overlapped or underlapped. Consequently, Δ is included as arbitrary parameter. By simply setting $p_{h_3} = p_s$ in (2.2.1), there results

$$\begin{aligned} \dot{g}_{h_1} &= K_v [F_{13}(\Delta + \delta_v) \sqrt{p_{h_1} - p_s} + F_{13}(\Delta - \delta_v) \sqrt{p_{h_1}}] \\ \dot{g}_{h_2} &= K_v [F_{13}(\Delta - \delta_v) \sqrt{p_{h_2} - p_s} + F_{13}(\Delta + \delta_v) \sqrt{p_{h_2}}] \\ f_v &= L_v(d/dt)\delta_v + K_{fv}(\delta_v) \\ M_v d^2/dt^2 \delta_v + B_v(\dot{\delta}_v) d/dt \end{aligned} \quad (2.2.3)$$

This result is valid for all values of valve lapping Δ . When $\Delta = 0$, the valve is of zero-lap design, and (1.2.3) reduces to

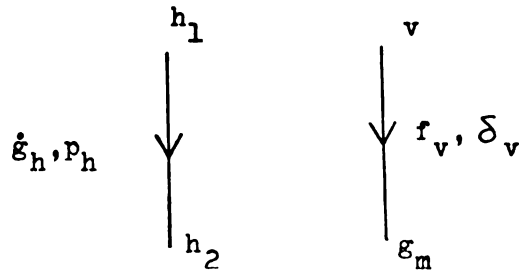
$$\begin{aligned} \dot{g}_{h_1} &= K_v |\delta_v| \sqrt{p_{h_1} - F_{12}(\delta_v)p_s} \\ \dot{g}_{h_2} &= K_v |\delta_v| \sqrt{p_{h_2} - F_{12}(-\delta_v)p_s} \end{aligned} \quad (2.2.4)$$

where F_{12} is a switching function defined by

$$\begin{aligned} F_{12}(X) &= +1 & X &\geq 0 \\ &= 0 & X &< 0 \end{aligned} \quad (2.2.5)$$

Equations (2.2.3) and (2.2.4) are associated with the terminal graph of Fig. 2.2.1. As mentioned before, the hydraulic reference is required in many system studies. In cases where the hydraulic reference may be omitted and $\Delta = 0$, (2.2.4) may be simplified to give the following terminal representation:

$$\begin{aligned} \dot{g}_h &= \frac{K_v}{\sqrt{2}} |\delta_v| \sqrt{p_h - F_{14}(\delta_v) p_s} \\ f_v &= L_v (d/dt) \delta_v + K_{fb}(\delta_v) \end{aligned} \quad (2.2.6)$$



where F_{14} is a switching function defined by

$$F_{14}(X) = \begin{bmatrix} +1 \\ 0 \\ -1 \end{bmatrix} \quad \text{for} \quad \begin{bmatrix} X > 0 \\ X = 0 \\ X < 0 \end{bmatrix} \quad (2.2.7)$$

The Four-way Valve with Constant Flow Supply

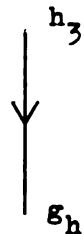
The design of a four-way valve operating from a constant flow supply is basically identical to the schematic of Fig.

2.2.5. However, one important restriction must be imposed. The orifices must be underlapped so as to provide a shunt at all times, i.e.,

$$\Delta_u > \Delta_1 \geq |\delta_v| \quad (2.2.8)$$

The formulation of an explicit mathematical model is complicated by the condition that \dot{g}_s is a specified flow driver whose graph element must be included in the chord set. The difficulty is evident when one lets $\dot{g}_{h_3} = \dot{g}_s$ and $p_{h_3} = p_s$ in (2.2.1); this results in a model non-explicit in p_s . On the other hand, the selection of a different tree in the graph of Fig. 2.2.3, such that element h'_3 is a chord element, as it should be for a constant flow driver, interferes with the requirement of putting all orifice elements in the chord set.

An explicit terminal representation may be obtained when the connection line from the flow source to terminal h_3 of the valve is assumed to possess capacity. The capacity of the flow source to line connection may be represented by a single element with the terminal characteristics



$$d/dt p_e = \frac{1}{C_e} \dot{g}_e \quad (2.2.9)$$

where C_e is the capacitance of line.

The system graph showing the interconnection of the four-way valve with the flow source is shown in Fig. 2.2.7.

An explicit terminal representation may now be obtained by combining the graph equations and terminals equations (2.2.1) and (2.2.9).

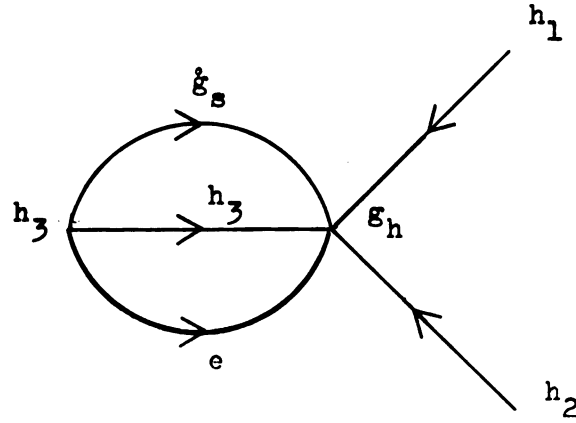


Fig. 2.2.7.--System graph of flow source-valve combination

$$\dot{g}_{h_1} = K_v ((\Delta_u + \delta_v) \sqrt{p_{h_1} - p_s} + (\Delta_u - \delta_v) \sqrt{p_{h_1}})$$

$$\dot{g}_{h_2} = K_v ((\Delta_u - \delta_v) \sqrt{p_{h_2} - p_s} + (\Delta_u + \delta_v) \sqrt{p_{h_2}})$$

$$d/dt p_s = \frac{1}{C_e} (K_v ((\Delta_u + \delta_v) \sqrt{p_{h_3} - p_s} + (\Delta_u - \delta_v) \sqrt{p_{h_2} - p_s}) + \dot{g}_s)$$

$$f_v = M_v d^2/dt^2 \delta_v + B_v (\dot{\delta}_v) + K_{fv} (\delta_v)$$

(2.2.10)

Terminal representations of any other valve configuration may be obtained on the basis of the techniques applied in the derivation of the above three cases. However, if an explicit mathematical model is to be realized it is necessary that all orifice elements be made part of the chord-set in the system graph. In pressure operated valves this requirement is easily satisfied; in flow operated valves special considerations must be taken by including the effect of capacitance of lines and oil volumes. Section 5.2 deals in more detail with this problem.

2.3. Valve Actuators

To effectively incorporate a control valve in a hydraulic system, provision must be made for controlling the stem position. An electromagnetic transducer may be used to directly manipulate the stem, as shown in Fig. 2.3.1.

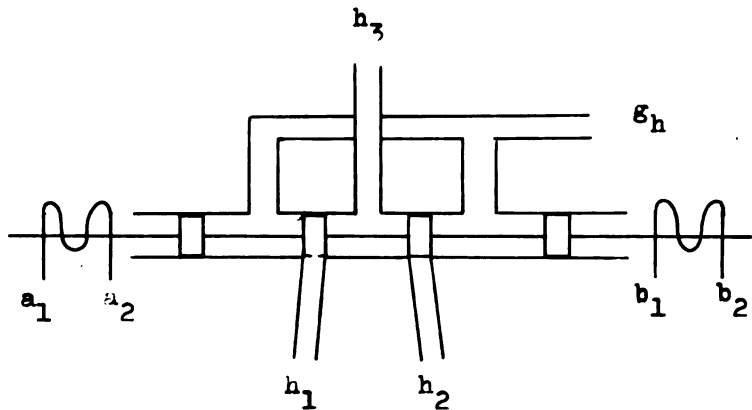


Fig. 2.3.1.--Typical four-way valve electromagnetic transducer assembly.

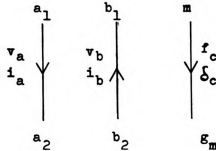
Quite frequently, however, the output impedance of such a transducer is not sufficiently low, unless the device is very large, to adequately handle the load requirements imposed by the valve-stem forces. A booster amplifier deriving its power from the hydraulic power supply is frequently used to amplify the action of the electromagnetic transducer. A typical design of this type is shown in Fig. 2.3.2. Such an assembly is referred to as an electrohydraulic servo valve.

In this section, the terminal characteristics of several typical actuating mechanisms are developed.

Electromagnetic Actuator

The terminal characteristics of an electromagnetic transducer are modeled by equations of the form

$$\begin{bmatrix} v_a \\ v_b \\ f_c \end{bmatrix} = \begin{bmatrix} R_{aa} + L_{aa} \frac{d}{dt} & 0 & K_{ac} \frac{d}{dt} \\ 0 & R_{aa} + L_{aa} \frac{d}{dt} & -K_{ac} \frac{d}{dt} \\ -K_{ac} & +K_{ac} & K_{cc} + B_{cc} \frac{d}{dt} + M_{cc} \frac{d^2}{dt^2} \end{bmatrix} \begin{bmatrix} i_a \\ i_b \\ \delta_c \end{bmatrix} \quad (2.3.1)$$



where R_{aa} = coil resistance

L_{aa} = coil inductance

K_{ac} , K_{ca} = electromechanical coupling constants

K_{cc} , B_{cc} , M_{cc} = mechanical constants.

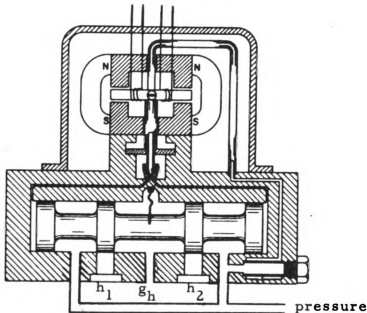


Fig. 2.3.2.--Typical four-way valve with electromagnetic transducer and booster stage.*

*Raymond Atchley Inc., Los Angeles, California, Model 410.

This linearized model of the electromagnetic transducer is usually quite justifiable for small signal operation of the component (8). The mechanical variables represent either rotation or translation whichever is more convenient.

Booster Amplifiers

Several effective designs for a booster amplifier are employed in the many commercially available servo valves. In order to define the terminal characteristics of a servo valve assembly it is convenient to consider the booster amplifier as a subassembly of the servo valve and derive its terminal characteristics separately. Two typical booster amplifiers are discussed here.

Booster Amplifier of RAD Model 410

The booster stage may be considered as a subassembly of three components, namely a jet-pipe valve, a push-pull hydraulic piston, and a position feedback spring. The terminal characteristics of the three components are considered first.

A. Jet-pipe valve

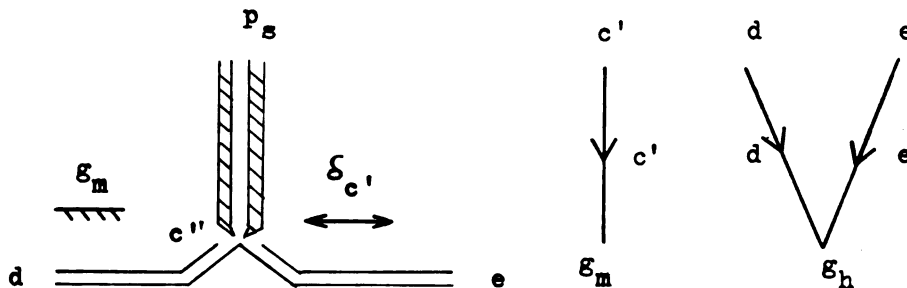


Fig. 2.3.3.--Jet pipe valve (a) schematic (b) terminal graph

For the terminal graph of Fig. 2.3.3(b), one has

$$\begin{bmatrix} f_c' \\ p_d \\ p_e \end{bmatrix} = \begin{bmatrix} 0 & 0 & 0 \\ k_d & R_d & 0 \\ -k_d & 0 & R_d \end{bmatrix} \begin{bmatrix} \delta_c' \\ \dot{g}_d \\ \dot{g}_e \end{bmatrix} + \begin{bmatrix} 0 \\ p_{s/2} \\ p_{s/2} \end{bmatrix} \quad (2.3.2)$$

Equations (2.3.2) may be derived from (2.2.3) of section 2.2. If in Fig. 2.2.6, orifices 1 and 2 are considered variable and orifices 3 and 4 are identical and fixed, and appropriate modifications are made in (2.2.10), the characteristics of the jet-pipe valve are obtained.

$$\dot{g}_{h_1} = K_v(\Delta + \delta_v) \sqrt{p_{h_1} - p_s} + K_1 \sqrt{p_{h_1}}$$

$$\dot{g}_{h_2} = K_v(\Delta - \delta_v) \sqrt{p_{h_2} - p_s} + K_1 \sqrt{p_{h_2}}$$

$$f_v = L_v(d/dt) \delta_v$$

$$K_{fv} \equiv 0, \quad \Delta > \delta_v$$

For small signal operation about the operating point

$$\begin{bmatrix} p_{h_1} \\ p_{h_2} \\ \delta_v \end{bmatrix} = \begin{bmatrix} p_{s/2} \\ p_{s/2} \\ 0 \end{bmatrix}$$

the equations are linearized to a form identical to 2.3.2., i.e.,

$$\begin{bmatrix} p_{h_1} \\ p_{h_2} \\ f_v \end{bmatrix} = \begin{bmatrix} \frac{p_{s/2}}{K_v(\Delta - K_1)} & 0 & \frac{p_{s/2}}{\Delta - K_1} \\ 0 & \frac{p_{s/2}}{K_v(\Delta - K_1)} & \frac{p_{s/2}}{\Delta - K_1} \\ 0 & 0 & L_m(d/dt) \end{bmatrix} \begin{bmatrix} \dot{g}_{h_1} \\ \dot{g}_{h_2} \\ \delta_v \end{bmatrix} + \begin{bmatrix} p_{s/2} \\ p_{s/2} \\ 0 \end{bmatrix}$$

It is assumed that the static pressure at the two receiving pipe openings varies linearly with the position of the jet about a point equal to one half the supply pressure p_s . Since the mechanical characteristics of the jet-pipe have been already

included in the description of the electromagnetic transducer, and since for small displacements about the outer position no net jet reaction force exists, the top row of (2.3.2) contains only zero entries.

B. Push-Pull Ram Actuator

For the terminal graph

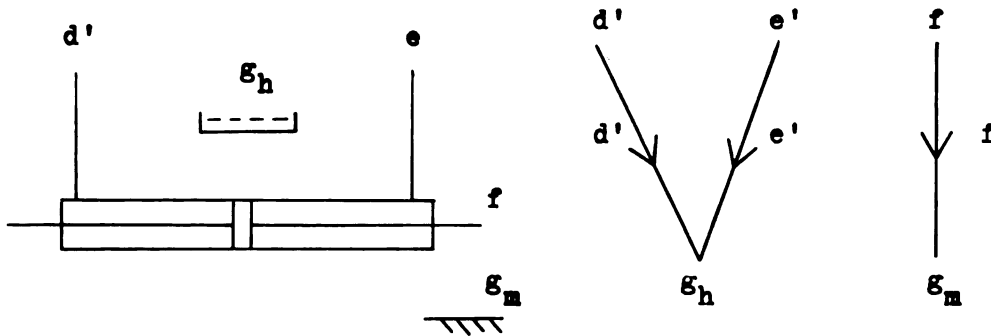


Fig. 2.3.4.--Push-pull ram actuator

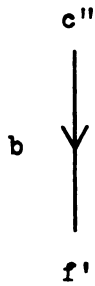
of Fig. 2.2.3, the terminal equations are

$$\begin{bmatrix} \dot{\delta}_{d'} \\ \dot{\delta}_{e'} \\ f_f \end{bmatrix} = \begin{bmatrix} 0 & 0 & d/dt A \\ 0 & 0 & -d/dt A \\ -A & A & L_f(d_m/dt) \end{bmatrix} \begin{bmatrix} p_{d'} \\ p_{e'} \\ \delta_f \end{bmatrix} \quad (2.3.3)$$

where A is the area of the spool ram, and $L_f(d/dt)$ is a second order differential operator. (See also section 3)

Any compressibility effects are negligible in (2.3.3) since the actual volume in question is very small.

C. Feedback Spring



$$f_b = K_b \delta_b \quad (2.3.4)$$

Components A, B, and C are now assembled for the booster stage subassembly according to the system graph of Fig. 2.3.4(a) and a terminal representation derived, retaining the three terminals as shown in Fig. 2.3.4(b).

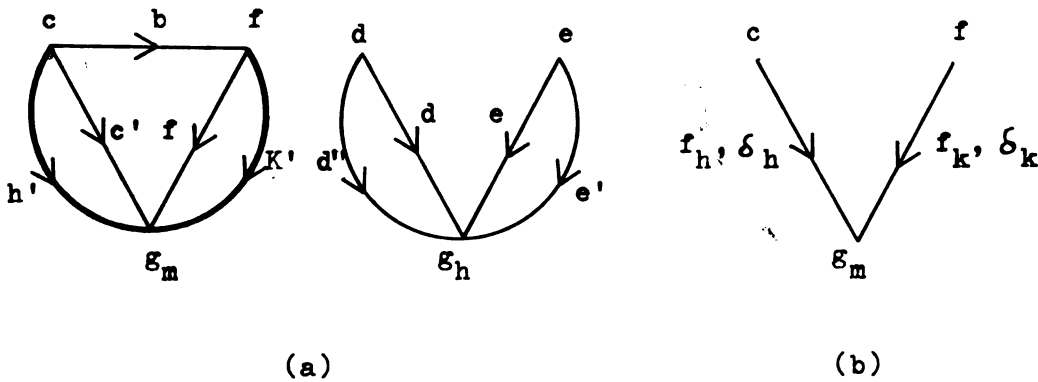


Fig. 2.3.5.--Booster stage: (a) system graph; (b) terminal graph

This results in

$$\begin{bmatrix} f_h \\ f_k \end{bmatrix} = \begin{bmatrix} K_b & -K_b \\ -K_b - 2AK_2 & M_d d^2/dt^2 + (Bd + 2A^2R)d/dt + K_b \end{bmatrix} \begin{bmatrix} \delta_h \\ \delta_k \end{bmatrix} \quad (2.3.5)$$

or when written in normal form

$$\begin{aligned} f_h &= K_b \delta_h - K_b \delta_k \\ d/dt \dot{\delta}_k &= -\frac{1}{M_d} ((Bd + 2A^2R) \dot{\delta}_k + K_b \delta_k - f_k + (K_b + 2A_{kd}) \delta_h) \\ d/dt \delta_k &= \dot{\delta}_k \end{aligned} \quad (2.3.6)$$

Booster Amplifier of Pegasus Model 120-F*

Terminal characteristics of essentially the same form as (2.3.5) may be derived for the booster amplifier of the Pegasus Model 120-F servo valve. As shown in Fig. 2.3.6 a dual flapper nozzle valve in combination with a push-pull ram actuator is utilized. As for the RAD design, the booster amplifier may be

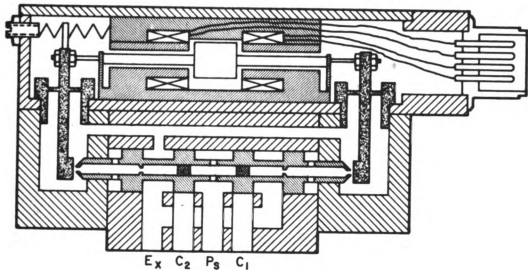


Fig. 2.3.6.--PEGASUS electrohydraulic servo valve conveniently modeled as a three-terminal subassembly made up of two components. The representations of the two components are given first.

Dual Flapper - Nozzle Valve Configuration

In Fig. 2.3.7 are shown a schematic of the flapper-nozzle configuration and a desired terminal graph.

The terminal equations for a linear model of the valve are

*Pegasus, Inc., Berkeley, Michigan.

$$\begin{bmatrix} f_c' \\ f_f' \\ p_d \\ p_e \end{bmatrix} = \begin{bmatrix} L_c(d/dt) & -K & 0 & 0 \\ -K_{jf} & L_f(d/dt) & 0 & 0 \\ K_{jp} & -K_{jp} & R & 0 \\ -K_{jp} & K_{jp} & 0 & R \end{bmatrix} \begin{bmatrix} \delta_c' \\ \delta_f' \\ \dot{\epsilon}_d \\ \dot{\epsilon}_e \end{bmatrix} + \begin{bmatrix} 0 \\ 0 \\ p_s/2 \\ p_s/2 \end{bmatrix} \quad (2.3.7)$$

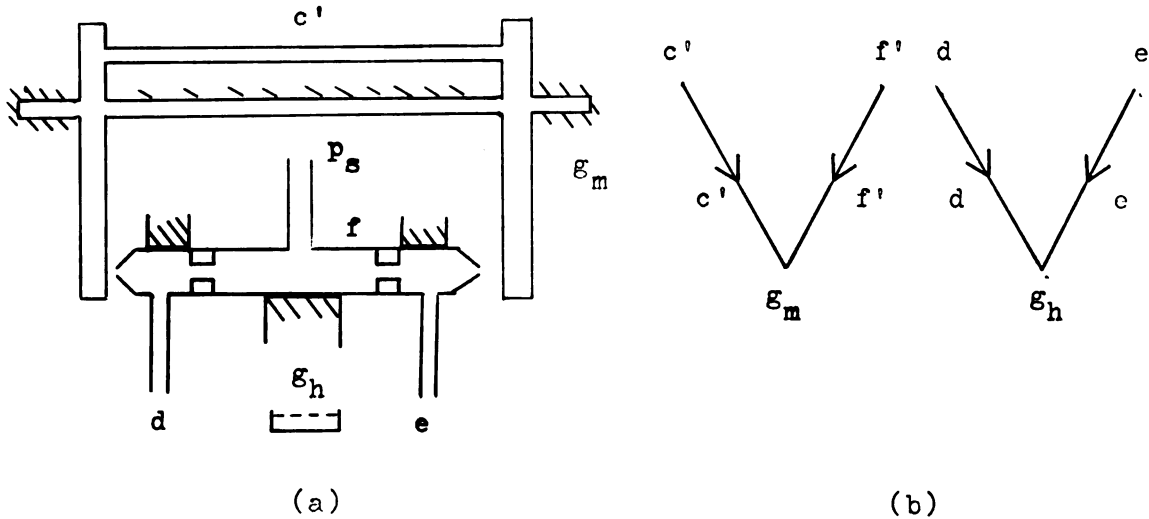


Fig. 2.3.7.--Double Flapper-Nozzle Valve

(a) Schematic (b) Terminal Graph

where $L_d(d/dt)$ = flapper characteristics

$L_f(d/dt)$ = nozzle characteristics

K_{jf} = jet force reaction coefficient

K_{jp} = jet pressure reaction coefficient

R = hydraulic resistance of restriction

The linear model is justified on the basis of small signal operation of the variables and the cancelling effect of the push-pull action. It may also be derived as a special case of (2.2.3).

The push-pull hydraulic position is represented by (2.2.3) and the graph of Fig. 2.3.4(b). The overall terminal representation of the booster subassembly is obtained upon combining (2.3.7) with (2.3.3), according to the system graph of Fig.

2.3.8 (a).

$$\begin{bmatrix} f_h \\ f_k \end{bmatrix} = \begin{bmatrix} L_h(d/dt) & -K_{fj} \\ -K_{fj} - 2A K_{pj} & L_k(d/dt) + 2A^2 R d/dt + 2AK_{pj} \end{bmatrix} \begin{bmatrix} \delta_h \\ \delta_k \end{bmatrix} \quad (2.3.8)$$

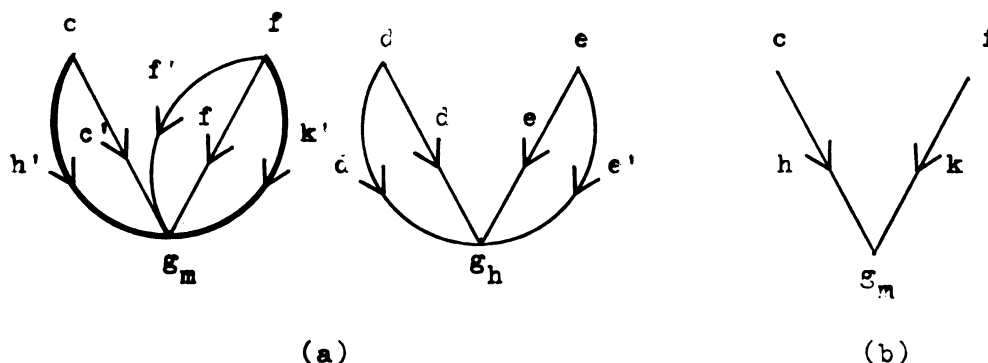


Fig. 2.3.8.--Booster stage (a) system graph (b) terminal graph

A comparison of (2.3.8) with (2.3.5) reveals complete agreement in terms of the form of the equations except for one term in the lower right hand corner of the coefficient matrix. In fact, it is this term which enters into the expression for the steady state output impedance of the booster stage. As the output impedance is, to a significant extent, a measure of the effectiveness of the booster amplifier, a comparison reveals that the dual flapper-nozzle assembly appears to be a more effective design.

RAD 410

Pegasus 120-F

$$\left. \frac{\delta_k}{f_k} \right]_{\delta_h=0} = \frac{1}{k_b}$$

$$\frac{1}{2AK_{pj}}$$

Steady State Output Impedances of Two Typical Booster Amplifiers

2.4 Terminal Representation of a typical electrohydraulic servo-valve

When equations (2.2.10), (2.3.1) and (2.3.5) are combined

according to the system graph of Fig. 2.4.1, the overall terminal representation of the electrohydraulic servovalve of Fig. 2.3.2 is obtained as

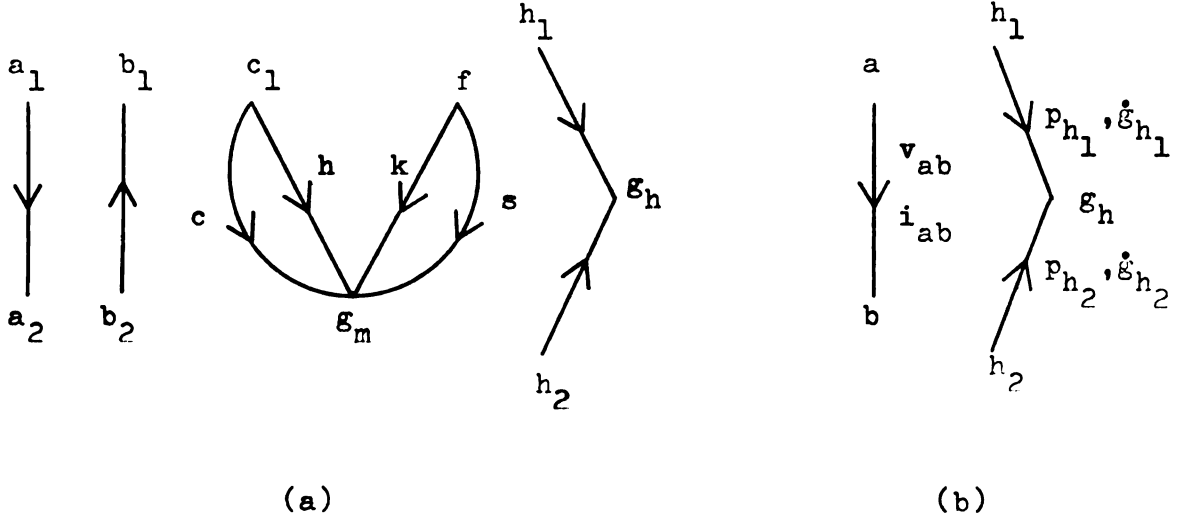


Fig. 2.4.1.--Model RAD 410 Servo Valve (a) System Graph
(b) Terminal Graph

$$\frac{d}{dt} \begin{bmatrix} i_{ab} \\ \dot{\delta}_c \\ \delta_c \\ \dot{\delta}_s \\ \delta_s \end{bmatrix} = \begin{bmatrix} -1/L_{aa}(R_{aa}i_{ab} - v_{ab} + K_{ac}\dot{\delta}_c \\ -1/M_{cc}(B_{cc}\dot{\delta}_c + (K_{cc} + K_b)\delta_c - K_{ca}(i_{ab})) \\ \dot{\delta}_c \\ -1/M_s(A^2R + B_s(\dot{\delta}_s))\dot{\delta}_s + K_b\delta_s + (K_b + AK_d)\delta_c K_{fbs}(\delta_s) \\ \dot{\delta}_s \end{bmatrix} \quad (2.4.1)$$

$$\begin{aligned} \dot{g}_{h1} &= K_v(F_{13}(\Delta - \delta_v) \sqrt{p_{h1} - p_s} + F_{13}(\Delta - \delta_v) \sqrt{p_{h1}}) \\ \dot{g}_{h2} &= K_v(F_{13}(\Delta - \delta_v) \sqrt{p_{h2} - p_s} + F_{13}(\Delta + \delta_v) \sqrt{p_{h2}}) \end{aligned}$$

2.5 Experimental Evaluation of Terminal Equations

Although the coefficients in (2.4.1) are shown as explicit functions of the component parameters, these relations cannot be used directly to determine the magnitudes of the coefficients. Further, since not all variables appearing in the model are accessible for external measurement, many of the coefficients cannot be determined directly from measurement.

A fairly good approximation to the terminal representation of the servo valve may be obtained by considering the valve to be a second order system. In this approximation, the coefficients L_{aa} , M_{cc} , and B_{cc} are neglected. If in addition, the flow reaction force, $K_{fbs}(\delta_s)$, on the valve stem is neglected the form of the model reduces to two first order differential and three algebraic equations.

$$\frac{d}{dt} \begin{bmatrix} \dot{\delta}_v \\ \delta_v \end{bmatrix} = \begin{bmatrix} -2\zeta\omega_n & -\omega_n^2 \\ 1 & 0 \end{bmatrix} \begin{bmatrix} \dot{\delta}_v \\ \delta_v \end{bmatrix} + \begin{bmatrix} \omega_n^2 k_{avab} \\ 0 \end{bmatrix} \quad (2.5.1)$$

$$i_{ab} = R_{aa} v_{ab}$$

$$\begin{aligned} \dot{g}_{h_1} &= K_v (F_{13}(\Delta + \delta_v) \sqrt{p_{h_1} - p_s} + F_{13}(\Delta - \delta_v) \sqrt{p_{h_2}}) \\ \dot{g}_{h_2} &= K_v (F_{13}(\Delta - \delta_v) \sqrt{p_{h_2} - p_s} + F_{13}(\Delta + \delta_v) \sqrt{p_{h_1}}) \end{aligned} \quad (2.5.2)$$

To complete the mathematical model of the servo valve it is necessary to determine the numerical values of ζ , ω_n , Δ , k_a , K_v and R_{aa} . All of these coefficients are usually obtainable from the manufacturer's specifications. In general, these coefficients may also be determined experimentally by selection of suitable test conditions. These test conditions are simple for a servo valve with a zero-lap design ($\Delta = 0$). The test procedures outlined below refer specifically to a zero-lap servo valve.

a) No-load Gain Characteristics

To determine the gain characteristics of a zero-lapped servo valve it is convenient to eliminate the hydraulic reference from the terminal graph. Then the two algebraic flow equations

are reduced to a single equation.

$$\dot{g}_h = \frac{K_v}{\sqrt{2}} |\delta_v| \sqrt{p_h - F_{14}(\delta_v) p_s} \quad (2.5.3)$$

By short-circuiting h_1 and h_2 , the valve load terminals, p_h is set to zero. For the steady state, δ_v may be expressed in terms of v_{ab} . Thus, a convenient relation involving only terminal variables results which may be employed to experimentally determine the steady-state flow vs. input gain characteristics.

$$\dot{g}_h = - \frac{K_v}{\sqrt{2}} k_a \sqrt{p_s} v_{ab} \quad (2.5.4)$$

Although (2.5.4) was developed for a steady-state measurement, it will also serve as a basis for a frequency response test. For

$$v_{ab}(t) = V_{ab} \sin \omega t$$

(2.5.4) in combination with the second-order valve model of (2.5.2) yields

$$\dot{g}_h(t) = G \sin (\omega t + \phi)$$

It is therefore possible from the resulting frequency response to determine the constants ξ and ω_n in (2.5.1). Due to the fact that δ_v , the valve stem position, is not a terminal variable, one cannot find the individual factors of the product $K_v k_a$; only their combined value is experimentally available.

b) The Pressure-Flow Characteristics

On the basis of one of the flow equations of (2.5.2), one may specify convenient test conditions to obtain a pressure-flow characteristic for a zero-lapped valve. For the second equation, let

$$\delta_v > 0$$

so that

$$\dot{q}_{h_2} = K_v \delta_v \sqrt{p_{h_2}}$$

Again for the steady state, δ_v is expressed in terms of v_{ab} so that

$$\dot{q}_{h_2} = K_v k_a v_{ab} \sqrt{p_{h_2}} \quad (2.5.5)$$

Equation (1.5.5) is the expression for a family of square-root curves with v_{ab} as a parameter, as shown in Fig. 2.5.1.

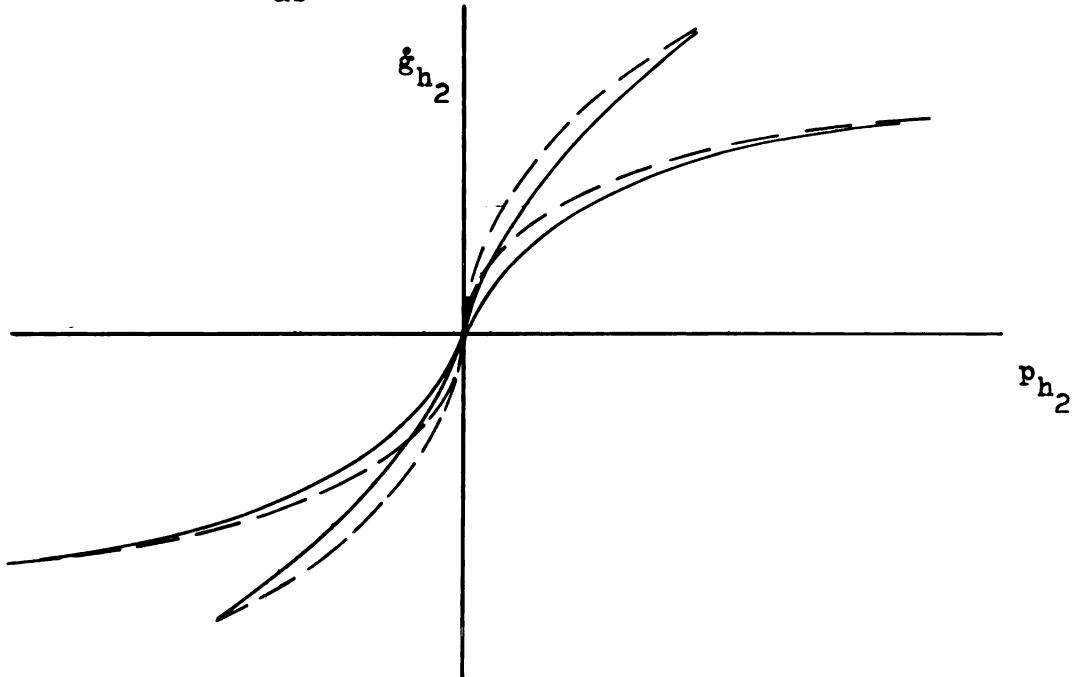


Fig. 2.5.1.--Typical family of pressure flow curves:
(a) experimental (solid) (b) Calculated (dotted).

Equation (2.5.5) and the curves of Fig. 1.5.1 not only provide a second method for determining the gain characteristic of a servo valve, but they also offer a very effective check on the assumption of the form of the orifice flow equations.

Usually the electro-hydraulic servo valve is operated in connection with a servo amplifier. The mathematical model for such a combination is obtained very readily by realizing that the

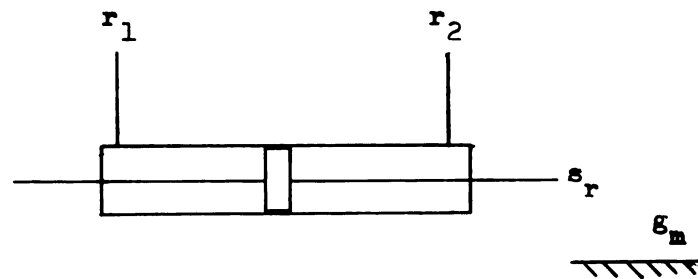
amplifier has essentially a zero-output impedance and negligible time-dependent characteristics. For such a combination (2.5.1) and (2.5.2) may be used as the mathematical model, with the equation containing i_{ab} omitted.

III. MATHEMATICAL MODELS OF HYDRAULIC MACHINES

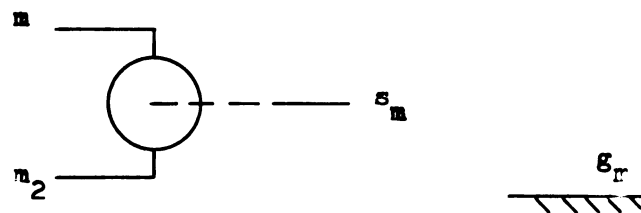
3.1 Gytrators as Mathematical Models for Machines

Three basic types of positive displacement machines are of interest in the study of hydraulic systems. They are shown in Fig. 3.1.1.

1. Hydraulic Cylinder



2. Hydraulic Motor



3. Variable Displacement Hydraulic Pump

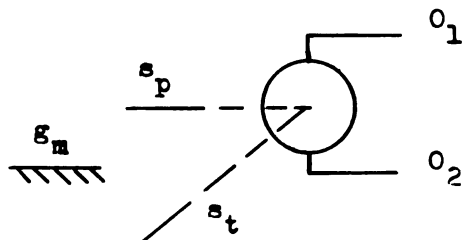


Fig. 3.1.1.--Basic hydraulic machines

All three types are classified as multi-terminal components, whose terminal representations involve measurement of hydraulic and mechanical variables. When treated as "ideal" components, i.e., no internal "losses", the mathematical models for all three of these components are of a form referred to as "gyrators". Such models include only two hydraulic terminals as shown below.

For instance, the terminal representation of an ideal cylinder is

$$\begin{bmatrix} \dot{g}_1 \\ f_2 \end{bmatrix} = \begin{bmatrix} 0 & A_p \\ -A_p & 0 \end{bmatrix} \begin{bmatrix} p_1 \\ \dot{\delta}_2 \end{bmatrix} \quad \begin{array}{c} r_1 \\ \downarrow \dot{g}_1, p_1 \\ r_2 \end{array} \quad \begin{array}{c} s_r \\ \downarrow f_2, \dot{\delta}_2 \\ s_m \end{array} \quad (3.1.2)$$

where A_p = crosssectional area.

For an ideal fixed motor one has

$$\begin{bmatrix} \dot{g}_1 \\ \tau_2 \end{bmatrix} = \begin{bmatrix} 0 & V \\ -V & 0 \end{bmatrix} \begin{bmatrix} p_1 \\ \dot{\phi}_2 \end{bmatrix} \quad \begin{array}{c} m_1 \\ \downarrow \dot{g}_1, p_1 \\ m_2 \end{array} \quad \begin{array}{c} s_m \\ \downarrow \tau_2, \dot{\phi}_2 \\ s_m \end{array} \quad (3.1.3)$$

where V = volumetric displacement/rad.

An ideal pump is given by

$$\begin{bmatrix} \tau_1 \\ \dot{g}_2 \end{bmatrix} = \begin{bmatrix} 0 & -V_t \phi_t \\ +V_t \phi_t & 0 \end{bmatrix} \begin{bmatrix} \dot{\phi}_1 \\ p_2 \end{bmatrix} \quad \begin{array}{c} o_1 \\ \downarrow \tau_1 \dot{\phi}_1 \\ o_2 \end{array} \quad \begin{array}{c} s_d \\ \downarrow \dot{g}_2, p_2 \\ s_m \end{array} \quad (3.1.4)$$

where $V_t \phi_t$ = volumetric displacement/rad.

and ϕ_t = volumetric control variable.

It is well recognized, however, that the internal losses in hydraulic machines are not in the least negligible. The losses which have to be considered are due to the inertial and

frictional properties of the moving parts of the machines. This includes all mechanical and hydraulic effects. Since the frictional properties in part depend on the pressures developed inside the machines during operation, the terminal graphs must be constructed to include the hydraulic reference as one terminal. Thus in the terminal representation for an ideal machine both the form of the equations and terminal graph must be changed to appropriately include loss characteristics.

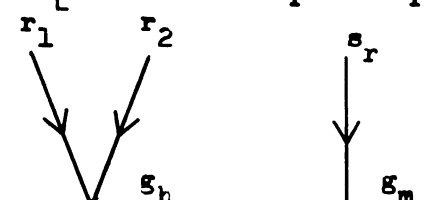
Some basic assumptions are made to hold in general in the developments for terminal characteristics of the machines.

1. All mechanical and hydraulic friction effects appear lumped.
2. All mechanical and hydraulic inertia effects appear lumped.
3. Leakage flows are assumed zero, unless otherwise stated.
4. Oil compressibility is neglected, unless stated otherwise.

3.2 Hydraulic Cylinder

The representation is given in two forms. The first form neglects compressibility; the second form includes it.

Without compressibility, the terminal characteristics are

$$\begin{bmatrix} \dot{g}_{r1} \\ \dot{g}_{r2} \\ f_r \end{bmatrix} = \begin{bmatrix} 0 & 0 & A \\ 0 & 0 & -A \\ -A & A & M_r d/dt + F_r(\dot{\delta}_r) \end{bmatrix} \begin{bmatrix} p_{r1} \\ p_{r2} \\ \delta_r \end{bmatrix}$$


(3.2.1)

where $M_r = M_p + A^2 I_p$

M_p = total mechanical mass

I_p = total hydraulic inertance

$$F_r(\dot{\delta}_r) = F_r + F_{14}(\dot{\delta}_r)(f_{cr} + F_{cr}(p_{r1} + p_{r2}))$$

with $\dot{\delta}_r = 0$

for $f_r < f'_{cr} + F'_{cr}(p_{r1} + p_{r2})$ and whenever $\dot{\delta}_r$ changes sign

f_{cr} = constant Coulomb friction.

The primed quantities are the respective stiction terms.

The Coulomb friction characteristics and the stiction are attributable to the seal pressure which is a function of the operating pressures.

When oil compressibility effects are included the terminal representation is modified:

$$\begin{bmatrix} \dot{g}_{r1} \\ \dot{g}_{r2} \\ f_r \end{bmatrix} = \begin{bmatrix} \beta/V(\delta_r)d/dt & 0 & A_r \\ 0 & \beta/V(-\delta_r)d/dt & -A_r \\ -A_r & A_r & M_r d/dt + F_r(\dot{\delta}_r) \end{bmatrix} \begin{bmatrix} p_{r1} \\ p_{r2} \\ \dot{\delta}_r \end{bmatrix} \quad (3.2.2)$$

where $V(\delta_r)$ = total volume enclosed in one side of cylinder.

Equations (3.2.2) may be written in normal form:

$$d/dt \begin{bmatrix} p_{r1} \\ p_{r2} \end{bmatrix} = \frac{1}{\beta} \begin{bmatrix} V(\delta_r) & 0 & -AV(\delta_r) \\ 0 & V(-\delta_r) & AV(-\delta_r) \end{bmatrix} \begin{bmatrix} \dot{g}_{r1} \\ \dot{g}_{r2} \\ \dot{\delta}_r \end{bmatrix} \quad (3.2.3)$$

$$d/dt \dot{\delta}_r = -\frac{1}{M_r} (F_r \dot{\delta}_r + F_{14}(\dot{\delta}_r)(f_{cr} + F_{cr}(p_{r1} + p_{r2})))$$

$\dot{\delta}_r = 0$ whenever $\dot{\delta}_r$ changes sign and as long as

$$f_r < f'_{cr} + F'_{cr}(p_{r1} + p_{r2})$$

3.3 Variable Displacement Hydraulic Pump*

The type of variable displacement pump most commonly encountered is the axial piston machine. This unit consists of a set of small pistons and cylinders uniformly arranged in a cylinder block as shown in Fig. 3.3.1.

The piston rods engage through a ball and socket joint in the drive shaft flange which in turn is rigidly connected to the drive shaft. The cylinder block's motion is slaved to the drive shaft by a universal joint. A plate valve containing two oval shaped slots directs the flow of oil. In operation, each piston draws oil into the cylinder block bores via the inlet port during one half of each revolution and forces it out through the outlet port during the other half. Twice each revolution the plate valve seals off any oil flow between the two adjacent cylinder bores and the ports. The tilt-angle of the yoke supporting the cylinder block determines the length of the stroke of the pistons, and thus the oil flow in pump operation.

The terminal variables used in modeling the component are identified by the terminal graph of Fig. 3.3.2.

*This development is based upon an earlier development by Koenig & Blackwell, Electromechanical System Theory, McGraw Hill, 1961, page 233.

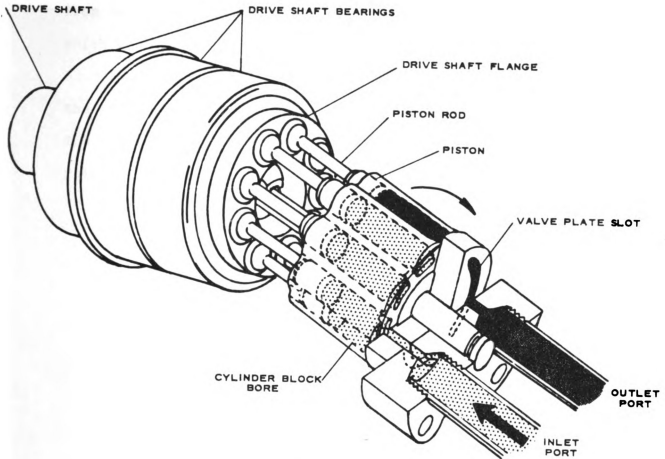


Fig. 3.3.1.--Assembly drawing of axial piston machine*

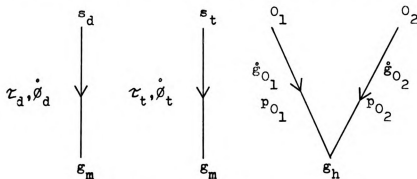


Fig. 3.3.2.--Terminal graph

The form of the equations relating these variables can be derived from the characteristics of the various elementary components which go to make up the unit.

As a first step one may consider the characteristics of the tilt plate with the piston rods removed from their sockets. The machine is assumed to have 7 pistons. The equations relating the variables

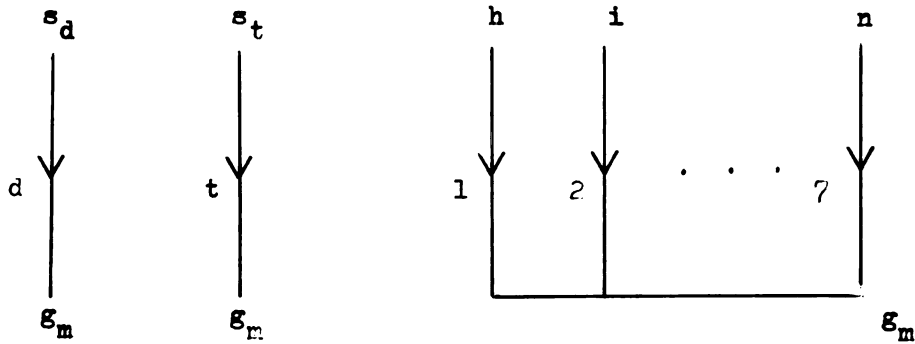


Fig. 3.3.3.--Terminal graph of subassembly
of the terminal graph of Fig. 3.3.3 are

$$\begin{bmatrix} \tau_d \\ \tau_t \end{bmatrix} = \begin{bmatrix} B_d + J_d d/dt & 0 \\ 0 & J_t d/dt \end{bmatrix} \begin{bmatrix} \dot{\phi}_d \\ \dot{\phi}_t \end{bmatrix}$$

$$- k_t \sin \phi_t \begin{bmatrix} \sin \phi_d & \sin (\phi_d - \alpha) & \dots & \sin (\phi_d - 6\alpha) \\ -\cos \phi_d & -\cos (\phi_d - \alpha) & \dots & -\cos (\phi_d - 6\alpha) \end{bmatrix} \begin{bmatrix} f_1 \\ f_2 \\ \vdots \\ f_7 \end{bmatrix} \quad (3.3.1)$$

$$\begin{bmatrix} \delta_1 \\ \delta_2 \\ \vdots \\ \delta_7 \end{bmatrix} = k_t \sin \phi_t \begin{bmatrix} \cos \phi_d \\ \cos (\phi_d - \alpha) \\ \vdots \\ \cos (\phi_d - 6\alpha) \end{bmatrix} \quad (3.3.2)$$

where the subscript d refers to all axially rotating parts.

Consider now a relative motion between the rotating cylinder block and the plate valve through an angle of $\frac{2\pi}{7}$. In particular let the motion be according to Fig. 3.3.4 and 3.3.5, first from $-\frac{\pi}{7} < \phi_d < 0$ then from $0 < \phi_d < +\frac{\pi}{7}$. It is assumed that when $\phi_d = 0$ the port of cylinder 1 is completely closed by the plate valve. However, for any small angle $\phi_d = \pm \varepsilon$, the piston port is connected to either the O_1 or O_2 region.

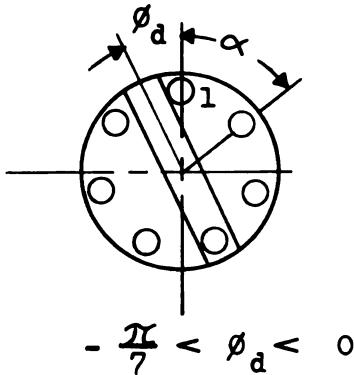


Fig. 3.3.4

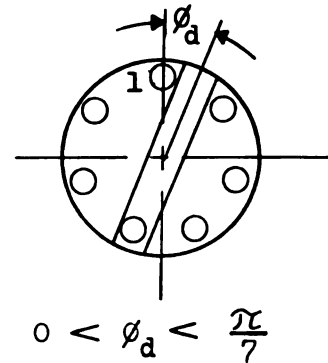


Fig. 3.3.5

As one of the cylinders (1) passes from one pressure region to the other, the equations relating terminal variables of the cylinder block are shown below.

$$\begin{bmatrix} f'_1 \\ f'_2 \\ f'_3 \\ f'_4 \\ \cdot \\ \cdot \\ \cdot \\ f'_7 \\ \dot{g}_{01} \\ \dot{g}_{02} \end{bmatrix} = \begin{bmatrix} L(\frac{d}{dt}) & 0 & 0 & 0 & 0 & 0 & 0 & 0 & 0 & -A_p \\ 0 & L(\frac{d}{dt}) & 0 & 0 & 0 & 0 & 0 & 0 & 0 & -A_p \\ 0 & 0 & \cdot & & & & \cdot & 0 & -A_p & \\ \cdot & & & \cdot & & & & 0 & -A_p & \\ \cdot & & & & \cdot & & & -A_p & 0 & \\ \cdot & & & & & 0 & 0 & -A_p & 0 & \\ f'_7 & 0 & & & & 0 & L(\frac{d}{dt}) & -A_p & 0 & \\ \dot{g}_{01} & 0 & 0 & 0 & 0 & A_p & A_p & A_p & G_{011} & G_{012} \\ \dot{g}_{02} & +A_p & A_p & A_p & A_p & 0 & 0 & 0 & G_{021} & G_{022} \end{bmatrix} \begin{bmatrix} \delta'_1 \\ \delta'_2 \\ \cdot \\ \cdot \\ \cdot \\ \cdot \\ \delta'_7 \\ p_{01} \\ p_{02} \end{bmatrix}$$

(3.3.3)

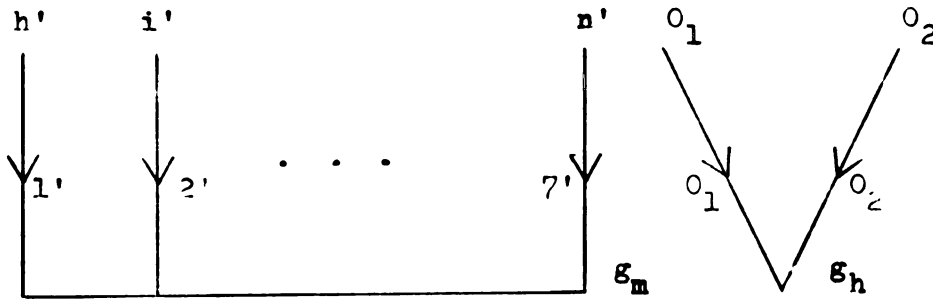
where $L(d/dt) = B_p + M_p d/dt$

B_p = total frictional characteristics of a piston

M_p = total inertial characteristics of a piston

A_p = crosssectional area of piston

G_{0ij} = leakage coefficient between regions i and j



For the range $0 < \phi_0 < \frac{\pi}{7}$ the system of equations is identical to (3.3.3) except that the 8th and 9th term in the first row are interchanged.

When the pistons are assembled with the cylinder block the terminal graphs of the two subassemblies are assembled as shown by the system graph of Fig. 3.3.6.

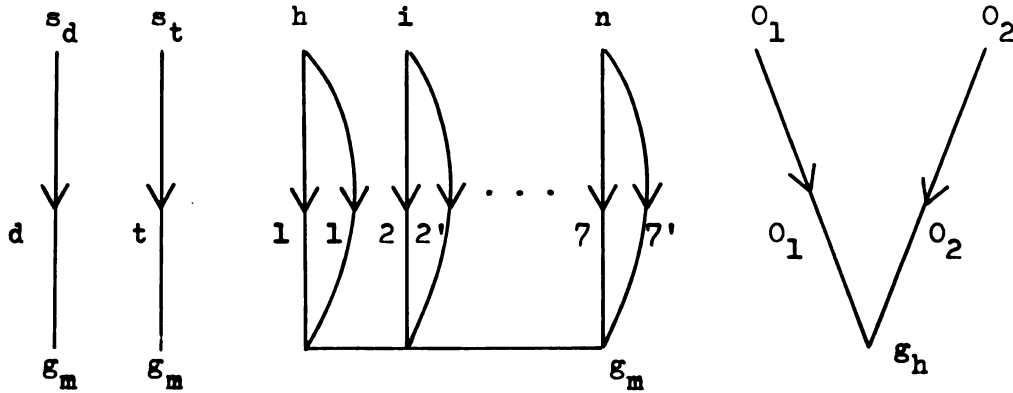


Fig. 3.3.6.--System graph of axial piston pump

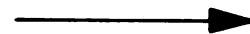
Now through use of the simple cutset and circuit equations of the system graph, (3.3.3) are first substituted into (3.3.7) and the result is then combined with (3.3.2) to yield

$$\begin{bmatrix} \tau_d \\ \tau_t \end{bmatrix} = \begin{bmatrix} B_d + J_d \frac{d}{dt} & 0 \\ 0 & B_t + J_t \frac{d}{dt} \end{bmatrix} \begin{bmatrix} \dot{\phi}_d \\ \dot{\phi}_t \end{bmatrix} + \frac{7}{2} k_t^2 B_p \begin{bmatrix} \sin^2 \phi_t \\ -\sin \phi_t \end{bmatrix} \begin{bmatrix} \dot{\phi}_d \\ \dot{\phi}_t \end{bmatrix} + \frac{7}{2} k_t^2 M_p \begin{bmatrix} \sin^2 \phi_t & \dot{\phi}_d \\ -\sin \phi_t & \end{bmatrix} \quad (3.3.5)$$

$$-k_t A_p \phi_t \begin{bmatrix} \sin(\phi_d - 4\alpha) + \dots + \sin(\phi_d - 6\alpha) \sin \phi_d + \dots + \sin(\phi_d - 3\alpha) \\ -\cos(\phi_d - 4\alpha) - \dots - \cos(\phi_d - 6\alpha) - \cos \phi_d - \dots - \cos(\phi_d - 3\alpha) \end{bmatrix} \begin{bmatrix} p_{01} \\ p_{02} \end{bmatrix}$$

and

$$\begin{bmatrix} \dot{g}_{01} \\ \dot{g}_{02} \end{bmatrix} = K_t A_p \begin{bmatrix} \dot{\phi}_d \phi_t \sin(\phi_d - 4\alpha) + \dots + \sin(\phi_d - 6\alpha) \\ \dot{\phi}_d \phi_d \sin \phi_d + \dots + \sin(\phi_d - 3\alpha) \end{bmatrix} \quad (3.3.6)$$



$$\begin{bmatrix} -\dot{\phi}_t \cos(\phi_d - 4\alpha) + \dots + \cos(\phi_d - 6\alpha) \\ -\dot{\phi}_t \cos \phi_d + \dots + \cos(\phi_d - 3\alpha) \end{bmatrix} + \begin{bmatrix} G_{011} & G_{012} \\ G_{021} & G_{022} \end{bmatrix} \begin{bmatrix} p_{01} \\ p_{02} \end{bmatrix}$$

Similarly, a set of equations corresponding to (3.3.5) and (3.3.6) may be obtained for the range $0 < \phi_d < \frac{\pi}{7}$. It is evident that the case $\phi_d = 0$ is the common borderline between the ranges $-\frac{\pi}{7} < \phi_d < 0$ and $0 < \phi_d < \frac{\pi}{7}$ and requires no special consideration.

Note that the expressions relating the torques to the pressures and the flows to the displacements are functions of the shaft position ϕ_d . Due to the periodic pattern of the switching action of the plate valve the above equations, as set up for the range $-\frac{\pi}{7} < \phi_d < \frac{\pi}{7}$, hold for other ranges as well. Since the shaft torque τ_d and tilt-plate torque τ_t contain a ripple at a frequency seven times the frequency of rotation.

These pulses are noticable only at very low speeds. Similar pulses of course, appear in the flow variables.

When the torques and flows are averaged (3.3.5) and (3.3.6) over the range $-\frac{\pi}{7} < \phi_d < 0$ and $0 < \phi_s < \frac{\pi}{7}$ the terminal equations reduce to

$$\begin{bmatrix} \tau_d \\ \tau_t \\ \dot{g}_{01} \\ \dot{g}_{02} \end{bmatrix} = \begin{bmatrix} B_d(\phi_t) + J_d(\phi_t) \frac{d}{dt} & B_{dt}(\phi_t) & -V_t \phi_t & V_t \phi_t \\ -K_{td} \phi_t^2 \dot{\phi}_d & B'_t \phi_t + J'_t \frac{d}{dt} + J''_t \phi_t & 0 & 0 \\ V_t \phi_t & 0 & G_{011} & G_{012} \\ -V_t \phi_t & 0 & G_{012} & G_{022} \end{bmatrix} \begin{bmatrix} \dot{\phi}_d \\ \dot{\phi}_t \\ p_{01} \\ p_{02} \end{bmatrix}$$

(3.3.7)

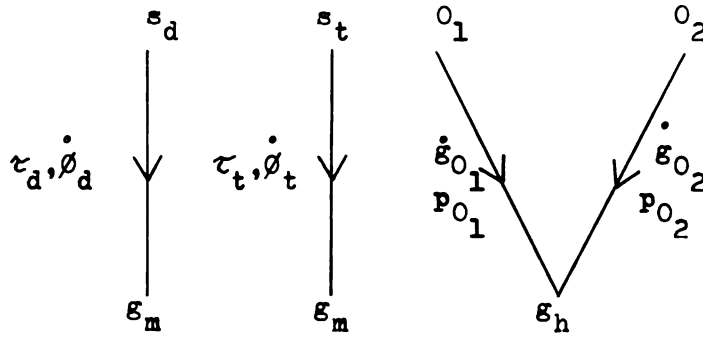


Fig. 3.3.7.--Terminal graph

where the coefficients are related specifically to the detailed characteristics of each component in the assembly by:

$$B_d(\phi_t) = B_d + \frac{7}{2} K_t^2 B_p \phi_t^2$$

$$B_{dt}(\phi_t) = 7 K_t^2 M_p \phi_t$$

$$J_d(\phi_t) = J_d + \frac{7}{2} K_t^2 M_p \phi_t^2$$

$$B'_t = B_t - \frac{7}{2} K_t^2 B_p$$

$$J'_t = J_t - \frac{7}{2} K_t^2 M_p \phi_t^2$$

$$J''_t = \frac{7}{2} K_t^2 M_p \phi_t^2$$

$$K_{td}(\phi_t) = \frac{7}{2} K_t^2 M_p \phi_t^2$$

$$V_t = \frac{7}{2\pi} K_t^2 A_p$$

The term $K_{dc} \phi_t$ can be identified as the volumetric displacement per radian. This can be seen by calculating V_p , the volume displaced per piston per revolution. It is equal to the length of stroke times the area of the piston.

$$V_p = 2 \sin \phi_t K_t A_p \doteq 2 \phi_t K_t A_p$$

Hence, the total volume of the pump per radian is

$$V_m = \frac{7}{2\pi} V_p$$

or

$$V_m = \frac{7}{\pi} \phi_t K_t A_p$$

Equations (3.3.7) and (3.3.8) associated with the terminal graph of Fig. 3.3.7 represent the terminal characteristics of the

variable displacement axial piston pump. An inspection of equations (3.3.8) shows that a determination of the coefficients of equation (3.3.7) is highly impractical. Despite the fact that the coefficients are expressed explicitly in terms of the characteristics of the individual parts of the pump, many of the characteristics take on meaning only with the parts installed in the pump. Thus, experimental means must be employed to find the coefficients. Through suitable test conditions, one can single out the coefficients of equation (3.3.7). Furthermore, using the form of equations (3.3.7) as a guide, meaningful relations can be established.

Pump friction test.

The following test conditions are specified: $p_{01} = p_{02} = 0$, $\dot{\phi}_t = 0$, and ϕ_t taken as a parameter. For steady state conditions, then, the curves of Fig. 3.3.8 can be obtained.

If the test conditions are altered, such as to introduce the effect of pressure on the Coulomb friction, one obtains the curves of Fig. 3.3.9, for which $p_c = p_d = P$, $\dot{\phi}_t = 0$ and $\phi_t = 0$.

On the basis of these curves and equations (3.3.7), one can establish the following steady state torque equation for the pump

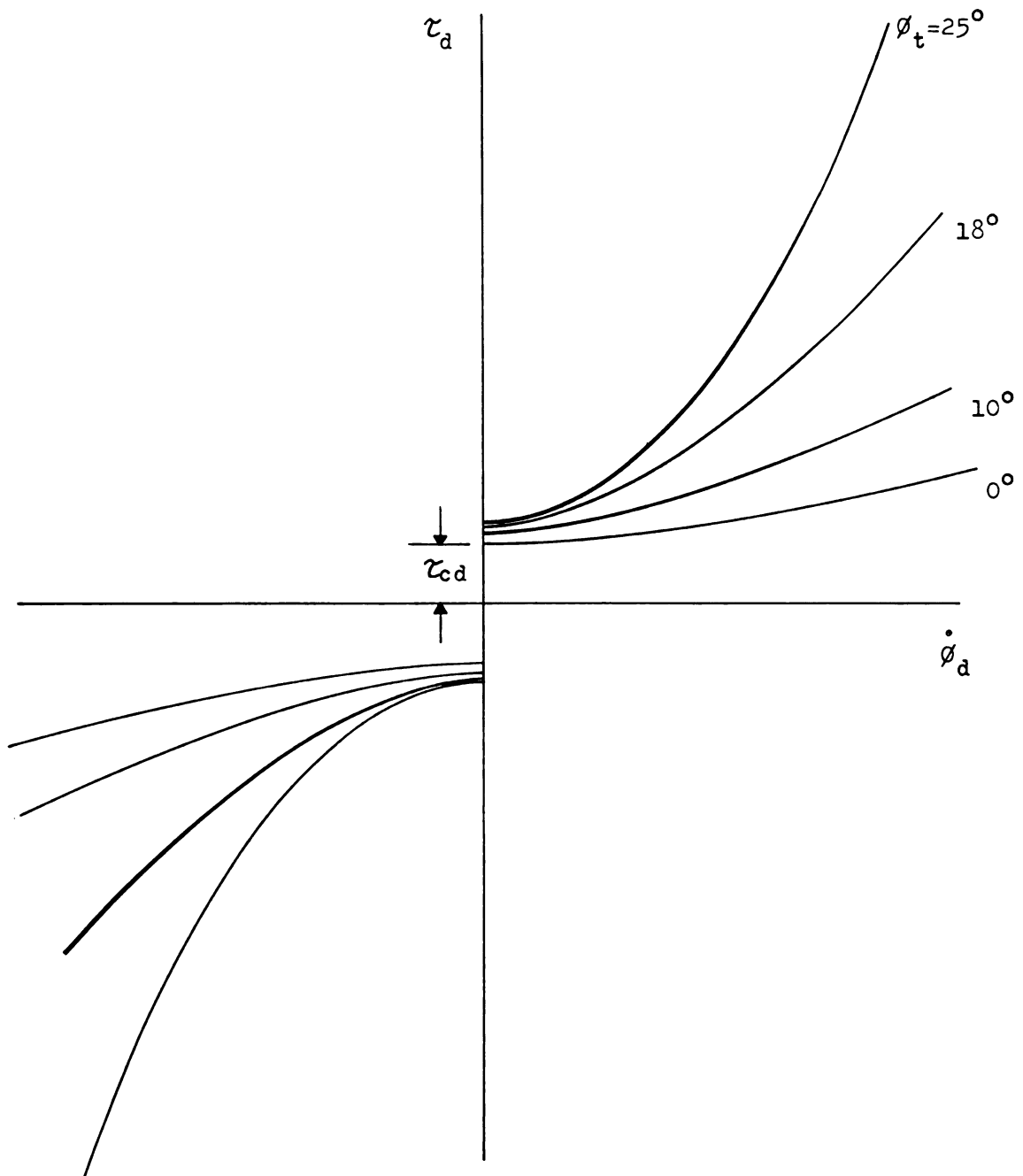


Fig. 3.3.8.--Pump friction for variable displacement pump

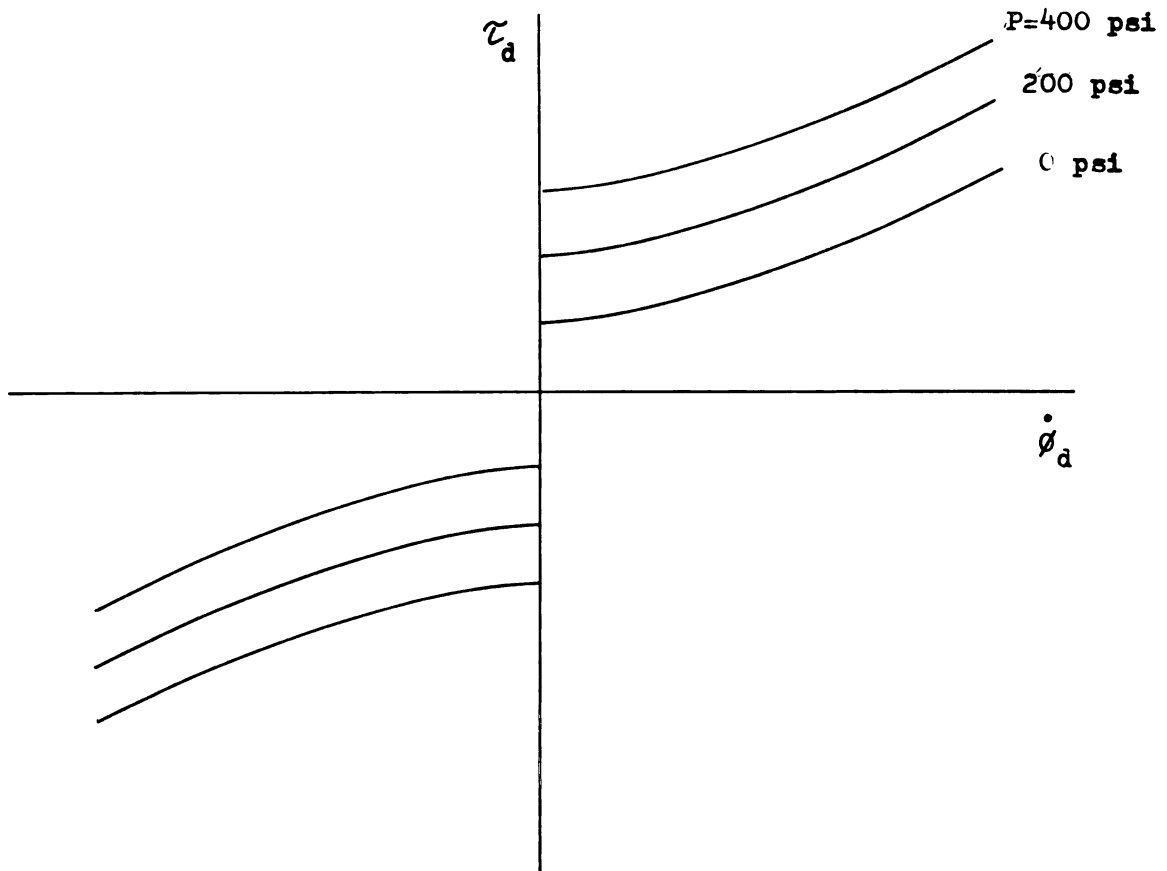


Fig. 3.3.9.--Effect of Coulomb friction

drive shaft:

$$\tau_d = (B_d + B_t \dot{\phi}_t^2) \dot{\phi}_d + \dot{\phi}_d / |\dot{\phi}_d| (\tau_{cd} + B_{cd}(p_{O_1} + p_{O_2}))$$

with stiction component (3.3.9)

$$\tau_{sd} = \tau'_c + B'_c(p_{O_1} + p_{O_2})$$

The coefficient V_t is easily calculated. Nevertheless, a laboratory measurement will also quickly lead to a result.

$$p_{O_1} = p_{O_2} = 0, \dot{\phi}_d = \text{constant}, \dot{\phi}_t = 0$$

A $\dot{\phi}_{O_1}$ vs $\dot{\phi}_t$ curve is obtained as shown in Fig. 3.3.10.

A great amount of simplification in (3.3.8) is precipitated by the experimental result that all terms containing M_p are significant.

The only term yet to be determined is the diagonal entry

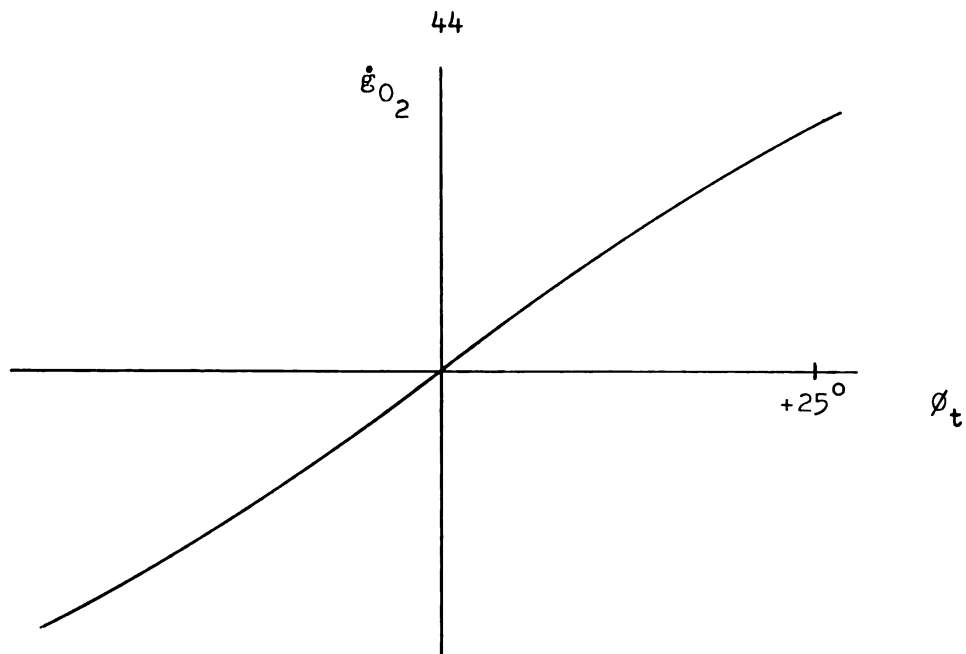


Fig. 3.3.10.--Pump displacement relating τ_t with $\dot{\phi}_t$. Experimental results indicate friction characteristics of the nature

$$\tau_t = \dot{\phi}_t / |\dot{\phi}_t| (\tau_{ct} + B_{ct}(p_{01} + p_{02}))$$

with a stiction torque

$$\tau_t = \tau_{ct} + B'_{ct}(p_{01} + p_{02})$$

as indicated by the curves of Fig. 3.3.11.

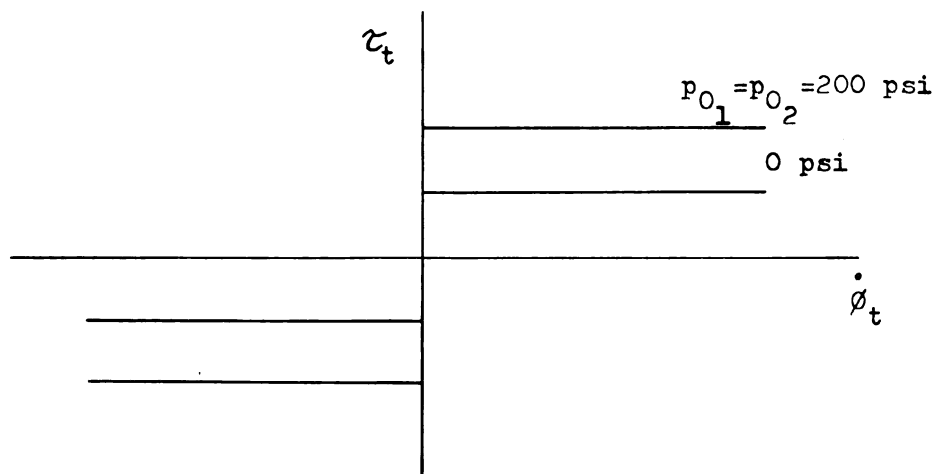


Fig. 3.3.11.--Tilt-plate torque vs velocity

No significant viscous friction term is present.

In correspondence with the measured characteristics, a meaningful terminal representation is now given in normal form

$$\begin{aligned}
 d/dt \dot{\phi}_d &= -1/J_d((B_d + B_{dt}\dot{\phi}_t^2) \dot{\phi}_s - V_t \phi_t(p_{01} - p_{02}) - \tau_d \\
 &\quad + F_{14}(\dot{\phi}_d)(\tau_{cd} + B_{cd}(p_{01} + p_{02}))) \\
 d/dt \dot{\phi}_t &= -1/J_t(B_t \dot{\phi}_t - \tau_t \\
 &\quad + F_{14}(\dot{\phi}_t)(\tau_{ct} + B_{ct}(p_{01} + p_{02}))) \\
 \dot{\phi}_t &= 0 \text{ for } \tau_t < \tau'_{ct} + B'_{ct}(p_{01} + p_{02})
 \end{aligned} \tag{3.3.14}$$

$$\begin{bmatrix} \dot{g}_c \\ \dot{g}_d \end{bmatrix} = V_t \dot{\phi}_d \begin{bmatrix} 1 \\ -1 \end{bmatrix} \phi_t + \begin{bmatrix} G_{011} & G_{012} \\ G_{012} & G_{022} \end{bmatrix} \begin{bmatrix} p_c \\ p_d \end{bmatrix}$$

Since normally $\dot{\phi}_d \neq 0$, no stiction characteristics need be considered for the drive shaft.

3.4. Fixed Displacement Motor.

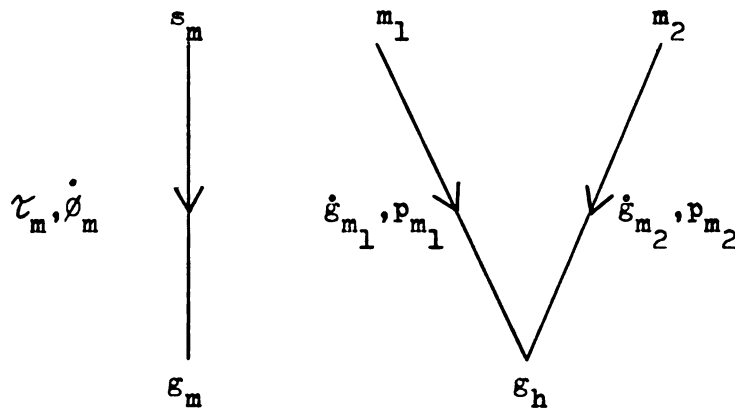
The terminal representation of the fixed displacement motor evolves quite automatically as a special case of the previous development. By setting

$$\begin{aligned}
 \dot{\phi}_t &= 0 \\
 \phi_t &= \text{constant}
 \end{aligned}$$

one has immediately:

$$\begin{aligned}
 d/dt \dot{\phi}_m &= -1/J_m(B_m \dot{\phi}_m - V_m(p_{m1} - p_{m2} - p_{m2}) - \tau_m \\
 &\quad + F_{14}(\dot{\phi}_m)(\tau_{cm} + B_{cm}(p_{m1} + p_{m2}))) \\
 \text{with } \dot{\phi}_m &= 0 \\
 \text{for } \tau_m &< \tau'_{cm} + B'_{cm}(p_{m1} + p_{m2})
 \end{aligned} \tag{3.4.1}$$

$$\begin{bmatrix} \dot{g}_{m1} \\ \dot{g}_{m2} \end{bmatrix} = V_m \begin{bmatrix} 1 \\ -1 \end{bmatrix} \dot{\phi}_m + \begin{bmatrix} G_{m11} & G_{m12} \\ G_{m12} & G_{m11} \end{bmatrix} \begin{bmatrix} p_{m1} \\ p_{m2} \end{bmatrix}$$



The frictional characteristics must again be determined through a laboratory measurement. Since a motor may be operated as a pump also, the frictional characteristics may be determined through two independent procedures. First, in motor operation, and under no-load steady state conditions ($\tau_m = 0$, $\dot{\phi}_m = \text{constant}$) the frictional characteristics may be determined through a measurement of differential port pressure and flow. Secondly, in pump operation, and also under no-load steady state conditions ($p_{m_1} = p_{m_2} = 0$, $\dot{g}_{m_1} = -\dot{g}_{m_2} = \text{constant}$) a measurement of torque and velocity will reveal the frictional characteristics. The two results may be checked against one another very effectively by plotting on the same figure the hydraulic measurements from the motor operation on a $(p_{m_1} - p_{m_2}) \cdot V_m$ vs \dot{g}_{m_1} scale and the mechanical measurements from the pump operation on a τ_m vs $V_m \cdot \dot{\phi}_m$ scale. The results from a typical machine are shown in Fig. 3.4.1.

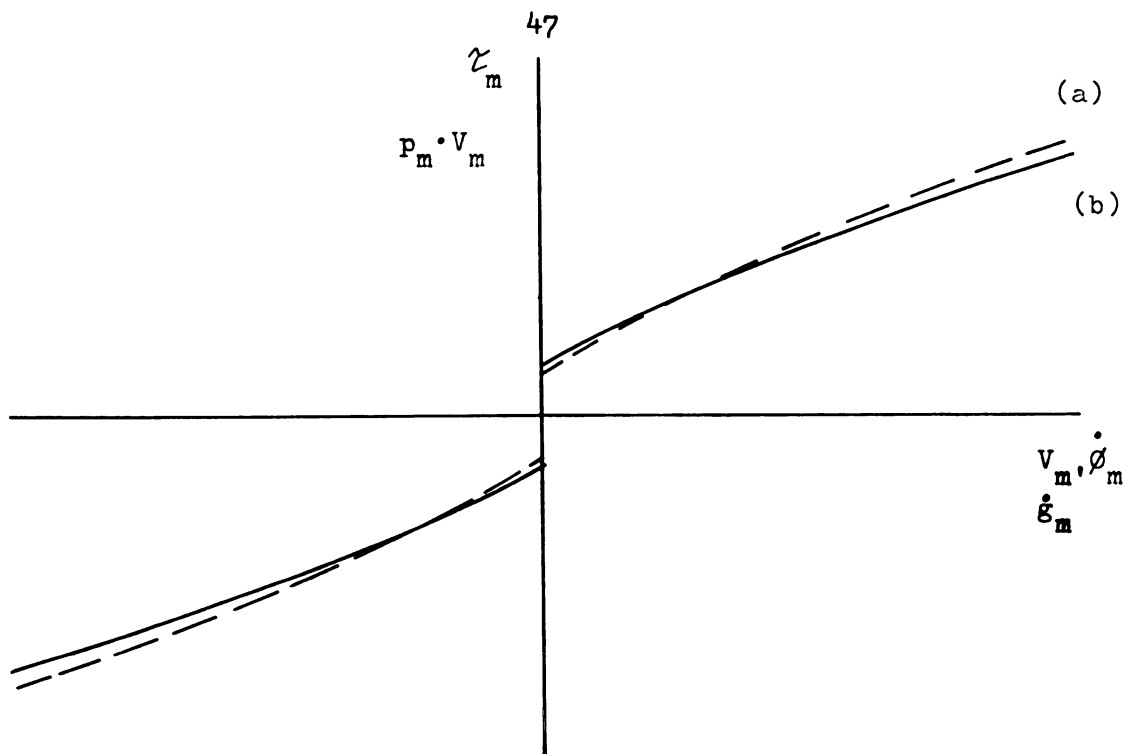


Fig. 3.4.1.--Fixed displacement machine friction characteristics (a) pump friction (b) motor friction.

IV. MATHEMATICAL MODELS OF HYDRAULIC LINES

In this section several models of hydraulic lines are developed. They are based upon lumped parameter approximations, so that they may be effectively used to establish a system model in normal form.

In the modeling process emphasis is placed more on the presentation of models for convenient system formulation than a study of time dependent fluid-flow. From this point of view the derived models will be representative of terminal measurements rather than an analytical account of fluid particle behavior. Included in the modeling process are the effects of resistance, inertance, fluid compressibility and line elasticity.

A hydraulic line, or a section of a hydraulic line, is viewed as a three-terminal component - the two ends of the line and a hydraulic reference which may be viewed as the atmospheric region surrounding the line. That this latter point is required in models that include fluid compressibility and line elasticity is evident from the manner in which the hydraulic capacity is measured. This effect is measured by closing one end of the line to the atmosphere and supplying the other end from a hydraulic power supply. The pressure and flow measurements under these conditions are identified by element 1 in the terminal graph of Fig. 4.1.1.

The hydraulic capacitance is to include the effect of both

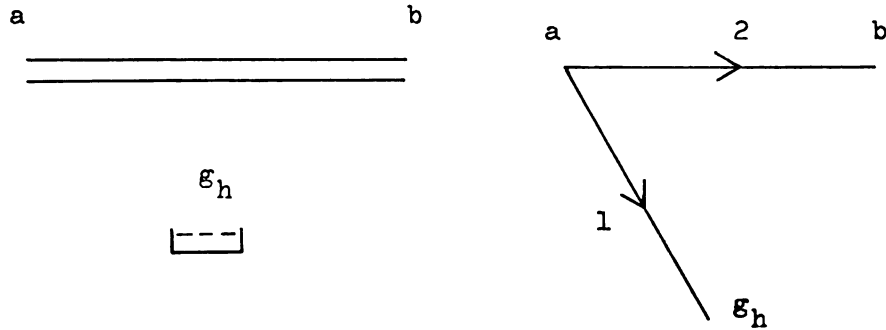


Fig. 4.1.1.--Hydraulic line and terminal graph
line elasticity and fluid compressibility. It is defined by

$$\epsilon_1 = C(p_1)p_1 \quad (4.1.1)$$

where $C = (K_e + \frac{V}{\beta})$

and K_e = coefficient of elastic expansion of line

V = total volume included

β = Bulk Modulus.

The elastic expansion coefficient should be treated as a function of the pressure as the elastic characteristics of lines are generally nonlinear; this is true in particular for flexible hoses.

The resistance and inertance effects are conveniently modeled in terms of pressure and flow measurements between the two ends of the line. These measurements are indicated by element 2 in the terminal graph of Fig. 4.1.1.

The inertance coefficient I is easily calculated from the specific density, ρ , of the fluid, the hose length, L , and area A , by

$$I = \int \frac{L}{A} \quad (4.1.2)$$

On the basis of typical measurements the terminal equation for element 2 is established as

$$p_2 = R * (\dot{g}_2)^K + I \frac{d}{dt} \dot{g}_2 \quad (4.1.3)$$

where R is the resistance

K a number normally of the range $1 \leq K \leq 2$

$$*(X)^\alpha = \frac{X}{|X|} (|X|)^\alpha$$

By forming an assembly of line sections such as modeled by the terminal graph of Fig. 4.1.1 lumped parameter models of hydraulic transmission lines are obtained. The number of R-I elements and C elements depends on the length of line and the accuracy desired. An example is shown in Fig. 4.1.2, by the graph of a lumped model with n sections.

For the convenience of later applications of lumped models the following terminology is introduced. The graph of Fig. 4.1.2 is called a closed-closed (CC) graph, as both the first and last elements of the graph are C-elements. In contrast,

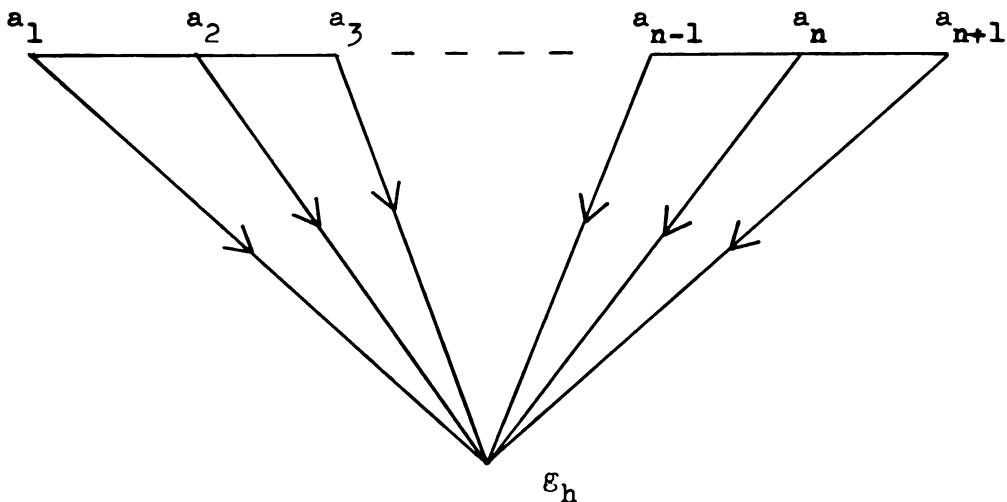


Fig. 4.1.2.--Lumped model with n-sections, closed ends

an open-open graph (OO) begins and ends with an R-I element. Thus, an n-section (CC) lumped parameter model has (n+1) C-elements and n R-I elements, while an (OO) model with n sections contains n-1 C elements and n R-I elements.

The values of the individual elements of the graph are computed on the basis of their relation to the measurements indicated by the graph of Fig. 4.1.1.

Under steady-state flow conditions only resistive effects enter into a pressure-flow measurement. One has then the relationship

$$R = \sum_{i=1}^n R_i \quad (4.1.4)$$

When one end is blocked off, the line becomes simply a fluid storage unit. Thus, under steady-state conditions, only capacitive effects are measured so that

$$C = \sum_{i=1}^{n+1} C_i \quad (4.1.5)$$

The line inertance is simply related to the section inertances by

$$I = \sum_{i=1}^n I_i \quad (4.1.6)$$

2.2 Models of Lines

The terminal representation for the lumped parameter models of hydraulic lines may be given in (CC), (OO), (OC), or (CO) form. For a particular application, the choice will depend upon how the representation "fits" together with the rest of the system in order to achieve normal form representation.

The terminal representation for a line with three sections is now being developed in (CC) forms

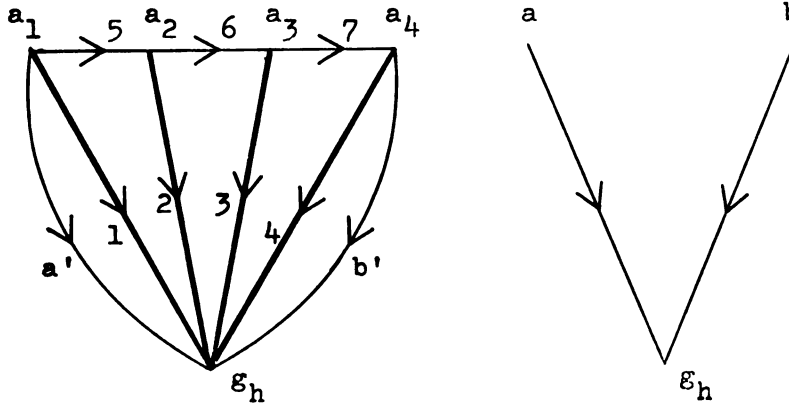


Fig. 4.2.2.--System graph for terminal representation

The terminal equations for the elements in the system of Fig. 4.2.2 are

$$\frac{d}{dt} \begin{bmatrix} p_1 \\ p_2 \\ p_3 \\ p_4 \end{bmatrix} = \begin{bmatrix} \frac{1}{C} & 0 & 0 & 0 \\ 0 & \frac{1}{C} & 0 & 0 \\ 0 & 0 & \frac{1}{C} & 0 \\ 0 & 0 & 0 & \frac{1}{C} \end{bmatrix} \begin{bmatrix} \dot{g}_1 \\ \dot{g}_2 \\ \dot{g}_3 \\ \dot{g}_4 \end{bmatrix}$$

(4.2.1)

$$\frac{d}{dt} \begin{bmatrix} \dot{g}_5 \\ \dot{g}_6 \\ \dot{g}_7 \end{bmatrix} = \begin{bmatrix} +\frac{1}{I} & 0 & 0 & -\frac{R}{I} & 0 & 0 \\ 0 & +\frac{1}{I} & 0 & 0 & -\frac{R}{I} & 0 \\ 0 & 0 & +\frac{1}{I} & 0 & 0 & -\frac{R}{I} \end{bmatrix} \begin{bmatrix} p_5 \\ p_6 \\ p_7 \\ \dot{g}_5 \\ \dot{g}_6 \\ \dot{g}_7 \end{bmatrix}$$

The terminal equations of the capacitive elements appear explicit in the derivative of the across variable; hence elements 1, 2, 3, and 4 are contained in the tree. Since these elements complete the tree, the measure graph elements a and b must go into the chordset. Upon expressing the right hand column

vector of equation (4.2.1) in terms of the branch across and chord through variables we have

$$d/dt \begin{bmatrix} p_1 \\ p_2 \\ p_3 \\ p_4 \\ \dot{g}_5 \\ \dot{g}_6 \\ \dot{g}_7 \end{bmatrix} = \begin{bmatrix} 0 & \dots & 0 & -\frac{1}{C} & 0 & 0 \\ 0 & & & \frac{1}{C} & -\frac{1}{C} & 0 \\ \vdots & & & 0 & 0 & \frac{1}{C} \\ 0 & \dots & 0 & 0 & 0 & -\frac{1}{C} \\ \frac{1}{I} & -\frac{1}{I} & 0 & 0 & -\frac{R}{I} & 0 \\ 0 & \frac{1}{I} & -\frac{1}{I} & 0 & 0 & -\frac{R}{I} \\ 0 & 0 & \frac{1}{I} & -\frac{1}{I} & 0 & -\frac{R}{I} \end{bmatrix} \begin{bmatrix} p_1 \\ p_2 \\ p_3 \\ p_4 \\ \dot{g}_5 \\ \dot{g}_6 \\ \dot{g}_7 \end{bmatrix} + \begin{bmatrix} -\frac{1}{C} & 0 \\ 0 & 0 \\ 0 & 0 \\ 0 & -\frac{1}{C} \\ 0 & 0 \\ 0 & 0 \\ 0 & 0 \end{bmatrix} \begin{bmatrix} \dot{g}_a \\ \dot{g}_b \end{bmatrix} \quad (4.2.2)$$

The terminal representation is completed by introducing the remaining terminal variables

$$\begin{bmatrix} p_1 \\ p_4 \end{bmatrix} = \begin{bmatrix} p_a \\ p_b \end{bmatrix}$$

and by changing from the measure graph to the terminal graph:

$$d/dt \begin{bmatrix} p_a \\ p_b \\ p_2 \\ p_3 \\ \dot{g}_5 \\ \dot{g}_6 \\ \dot{g}_7 \end{bmatrix} = \begin{bmatrix} 0 & \dots & 0 & -\frac{1}{C} & 0 & 0 \\ \cdot & & & 0 & 0 & -\frac{1}{C} \\ \cdot & & & \frac{1}{C} & -\frac{1}{C} & 0 \\ 0 & \dots & 0 & 0 & \frac{1}{C} & -\frac{1}{C} \\ \frac{1}{I} & 0 & -\frac{1}{I} & 0 & -\frac{R}{I} & 0 \\ 0 & 0 & \frac{1}{I} & -\frac{1}{I} & 0 & -\frac{R}{I} \\ 0 & -\frac{1}{I} & 0 & \frac{1}{I} & 0 & -\frac{R}{I} \end{bmatrix} \begin{bmatrix} p_a \\ p_b \\ p_2 \\ p_3 \\ \dot{g}_5 \\ \dot{g}_6 \\ \dot{g}_7 \end{bmatrix} + \begin{bmatrix} \frac{1}{C} & 0 \\ 0 & \frac{1}{C} \\ 0 & 0 \\ \cdot & \cdot \\ \cdot & \cdot \\ 0 & 0 \end{bmatrix} \begin{bmatrix} \dot{g}_a \\ \dot{g}_b \end{bmatrix} \quad (4.2.3)$$

Equations (4.2.3) show that there are exactly two terminal equations and five auxiliary equations to describe, in CC form, a three-section hydraulic line. The total number of equations for a line thus corresponds to the total number of elements chosen to describe the line.

The development of the terminal representation for an OO model is handled similarly. Again, a three section model is considered and the result is

$$d/dt \begin{bmatrix} \dot{g}_a \\ \dot{g}_b \\ p_1 \\ p_2 \\ \dot{g}_4 \end{bmatrix} = \begin{bmatrix} -\frac{R}{I} & 0 & -\frac{1}{I} & 0 & 0 \\ 0 & -\frac{R}{I} & 0 & -\frac{1}{I} & 0 \\ \frac{1}{C} & 0 & 0 & 0 & -\frac{1}{C} \\ 0 & \frac{1}{C} & 0 & 0 & \frac{1}{C} \\ 0 & 0 & \frac{1}{I} & -\frac{1}{I} & -\frac{R}{I} \end{bmatrix} \begin{bmatrix} \dot{g}_a \\ \dot{g}_b \\ p_1 \\ p_2 \\ \dot{g}_4 \end{bmatrix} + \begin{bmatrix} \frac{1}{I} & 0 \\ 0 & \frac{1}{I} \\ 0 & 0 \\ 0 & 0 \\ 0 & 0 \end{bmatrix} \begin{bmatrix} p_a \\ p_b \end{bmatrix} \quad (4.2.5)$$

It is to be noted that a CC representation has both terminal variables explicit in the derivatives of the across variables. Exactly the opposite is true for a OO representation. In a CO or OC representation, the terminal equations are explicit in the derivatives of exactly one across and one through terminal variable.

It is significant to note that a normal form representation, as obtained for these two examples directly, is an immediate consequence of the topological development of the graphs of lumped parameter models of lines.

Fig. 4.2.3 shows a comparison between the measured and computed pressure response of a closed line. The computed result is based upon a 4-section CC model.

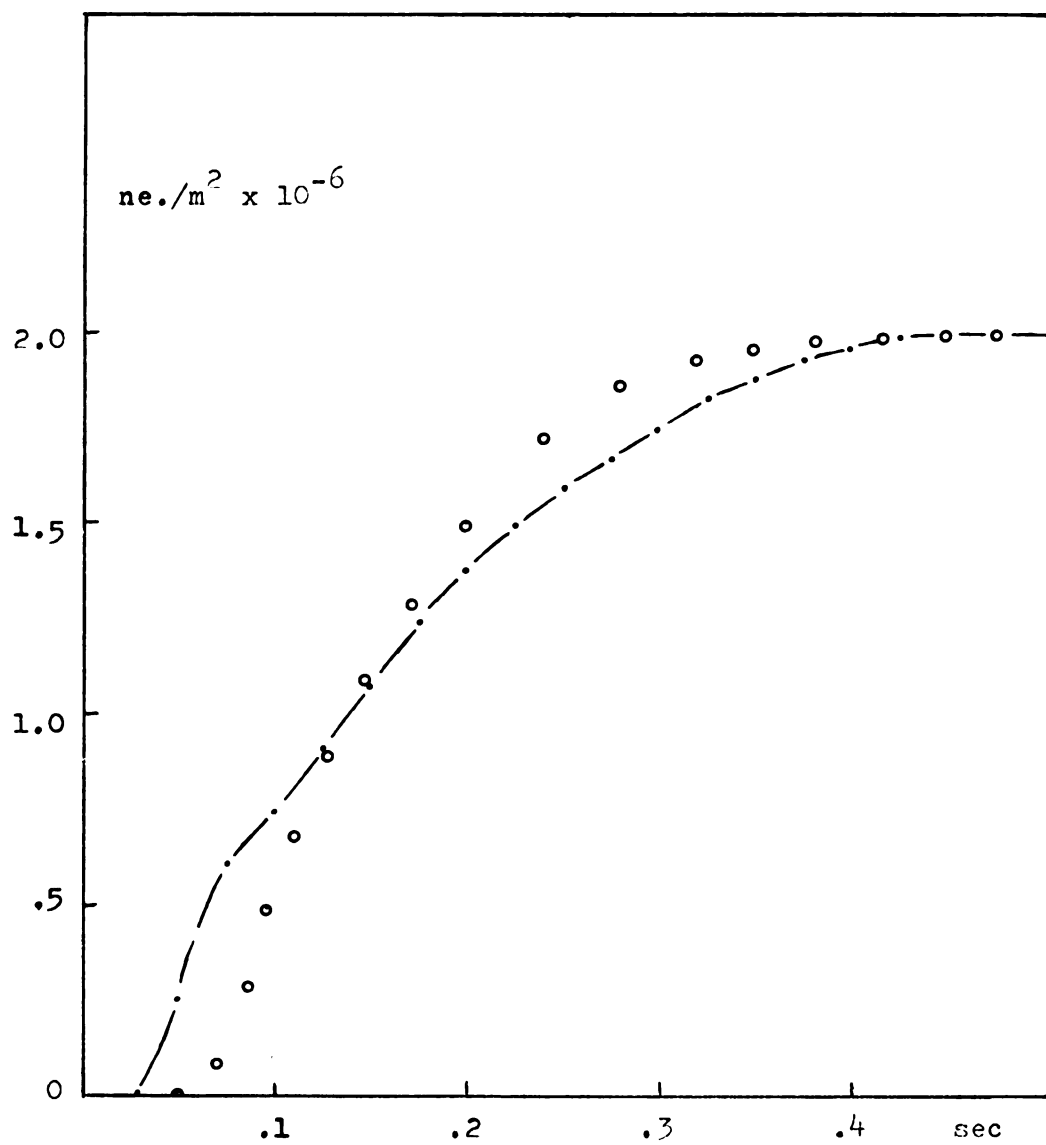


Fig. 4.2.3.--Pressure response for 16 m flexible line.

V. FORMULATION AND SOLUTION OF TYPICAL SUBASSEMBLIES

In the foregoing section, detailed mathematical models of typical hydraulic system components were developed. Some of the typical nonlinear phenomena inherent in the characteristics of hydraulic components were included in the models. Two classes of nonlinearities may be identified in the models. One class consists of nonlinear functional forms which are generally continuous functions of one or several variables. Examples include the square root relation of the orifice equation, or the quadratic form of the pump flow equation. The other class consists of nonlinear functional forms which are discontinuous or have discontinuous derivatives. The switching functions F_{12} , F_{13} and F_{14} , or the Coulomb friction are examples of this class. Also included are the limits on the range of values the variables may assume, which are imposed during the solution process. These limits depend on the geometric design of the components and other physical restrictions.

In the formulation of a mathematical model of a system consisting of typical hydraulic components, two factors act as a guide. First, the desired mathematical model is to be in a form amenable to existing solution techniques, either analytical or computational. It will be seen that a normal form model offers the only acceptable mathematical form in the presence of the nonlinearities. Secondly, for simplicity, only

as many of the detailed characteristics of the system components as are necessary for a meaningful analysis are to be included in the mathematical model. The second factor clearly requires a knowledge of the solution prior to passing judgement whether or not a particular characteristic has any significant effect on the solution, i.e., the only way to determine whether certain simplifying approximations are acceptable is to compare computed results with actual performance. In keeping with this objective several typical subassemblies are analyzed and their predicted performance is compared with measured performance.

5.1 Valve-Motor. (Subassembly 1)

This subassembly consists of a fixed displacement motor cascaded with a four-way valve operating from a constant pressure supply. The terminal equations of the two components are given by equations (2.2.3) and (3.4.1), respectively. It is assumed that no appreciable capacitive effect is present in the connection lines between the components. The graph of this subassembly is shown in Fig. 5.1.1.

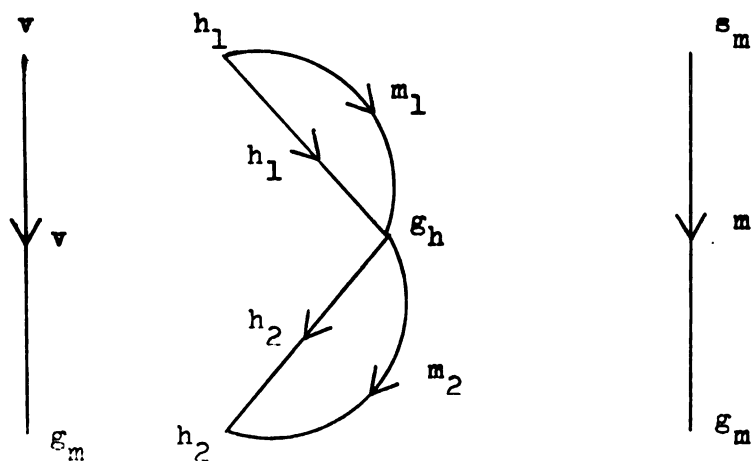


Fig. 5.1.1.--Graph of subassembly 1

By using the simple graph equations of Fig. 5.1.1, a

mathematical model in the form of three simultaneous differential and algebraic equations is obtained.

$$0 = V_m \dot{\phi}_m + K_v (F_{13} (\Delta + \delta_v) \sqrt{p_{h1} - p_s} + F_{13} (\Delta - \delta_v) \sqrt{p_{h1}}) \\ + G_{m11} p_{h1} - G_{m12} p_{h2} \quad (5.1.1)$$

$$0 = -V_m \dot{\phi}_m + K_v (F_{13} (\Delta - \delta_v) \sqrt{p_{h2} - p_s} + F_{13} (\Delta + \delta_v) \sqrt{p_{h2}}) \\ - G_{m12} p_{h1} + G_{m11} p_{h2}$$

$$d/dt \dot{\phi}_m = -\frac{1}{J_m} (B_m \dot{\phi}_m - V_m (p_{h1} - p_{h2}) - \tau_m \\ + F_{14} (\dot{\phi}_m) (\tau_{mc} + B_{mc} (p_{h1} + p_{h2})))$$

To investigate the performance of this subassembly it is necessary to determine a solution vector $(p_{h1}(t), p_{h2}(t), \dot{\phi}_m(t))$ when the initial conditions $(p_{h1}(0), p_{h2}(0), \dot{\phi}_m(0))$ and the input function $\delta_v(t)$ are specified. An analytical solution process is unobtainable. On the other hand, the direct generation of a solution by a computer is not feasible either, due to the implicit form of the algebraic equations. Automatic computation procedures based upon successive approximations such as the Newton-Raphson method, or the Seidel iteration may be solved for p_{h1} and p_{h2} for any $\dot{\phi}_m$ calculated on a point for point basis from a numerical integration of the differential equation. Actual solution attempts on this basis, however, have not been successful for the following three factors.

- (1) Presence of the switching function.

- (2) Rapidly changing pressures.
- (3) Smallness of the leakage coefficients.

For the slightly less general case of a zero-lapped valve ($\Delta = 0$) and no motor leakage, equations (5.1.1) may be reduced to a single equation.

The result is

$$\begin{aligned} d/dt \dot{\phi}_m = - \frac{1}{J_m} (B_m \dot{\phi}_m - V_m F_{14}(\delta_v)(p_s - 2(\frac{V_m \dot{\phi}_m}{K_v \delta_v})^2) \\ - \tau_m + F_{14}(\dot{\phi}_m)(\tau_{mc} + B_{mc} p_s)) \end{aligned} \quad (5.1.2)$$

Equation (4.1.2) is a mathematical model of subassembly 1 in the form of a single differential equation. In order to generate a solution, the following condition must be satisfied.

$$p_s - 2(\frac{V_m \dot{\phi}_m}{K_v \delta_v})^2 \geq 0 \quad (5.1.3)$$

This condition implies that the pressures are limited to the following range.

$$p_v \leq (p_{h_1}, p_{h_2}) \leq p_s, \text{ where } p_v > 0 \quad (5.1.5)$$

The lower limit is set by the vapor pressure of the fluid. The upper limit, however, is a restriction which is not necessarily valid under certain transient conditions. It is quite likely that for sudden changes in $\delta_v(t)$ the system pressures can increase beyond the supply pressure. This is particularly true when $\delta_v(t)$ is set to zero from a non zero value so that the motor is forced to come to an instantaneous halt.

5.2 Valve-Short-Line-Motor. (Subassembly 2)

The following system configuration is essentially identical to the previous one. However, while in the previous case compressibility is neglected, the effect of line capacity of the short

lines in this subassembly is taken into consideration.

For a short line, an adequate representation may be obtained through a two-element lumped-parameter model as indicated by the graph of Fig. 5.2.1 and (5.2.1).

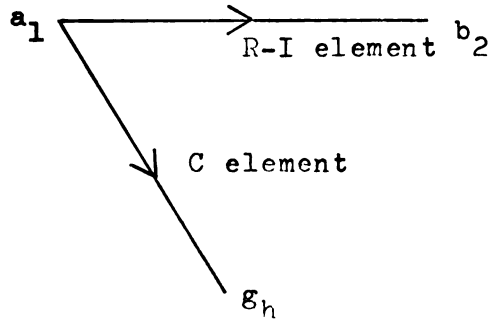


Fig. 5.2.1.--Graph of a two-element line in (CO) representation

$$\frac{d}{dt} \begin{bmatrix} p_{a_1} \\ \dot{g}_{b_1} \end{bmatrix} = \begin{bmatrix} \frac{1}{C} & 0 & 0 \\ 0 & \frac{1}{I} & -\frac{R}{I} \end{bmatrix} \begin{bmatrix} \dot{g}_{a_1} \\ p_{b_1} \\ \dot{g}_{b_1} \end{bmatrix} \quad (5.2.1)$$

Identical equations are used for the second line.

The mathematical model of this subassembly is formulated according to the graph of Fig. 5.2.2.

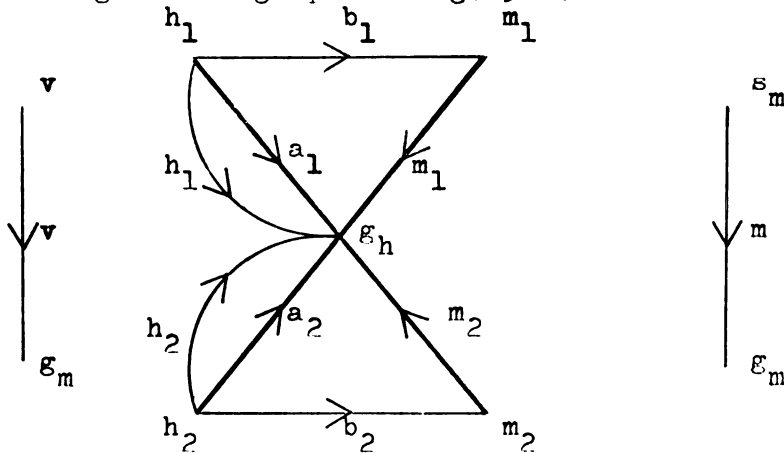


Fig. 5.2.2.--Graph of subassembly 2

The formulation tree is selected by observing the rules of normal form formulation (4): the terminal equation of the capacitive elements of the lines, a_1 and a_2 , have the across

variable explicit in the first derivative and the terminal equations of elements b_1 and b_2 have the through variable explicit in the first derivative. Thus, a unique tree is determined.

First, combining the terminal equations of the capacitive elements of the line with the motor flow equations as dictated by the cutset equations of the system graph, gives

$$\frac{d}{dt} p_{a_1} = - \frac{1}{C_1} (\dot{g}_{h_1} + V_m \dot{\phi}_{m_1} + G_{m_1} p_{m_1} - G_{m_2} p_{m_2}) \quad (5.2.2)$$

$$\frac{d}{dt} p_{a_2} = - \frac{1}{C_1} (\dot{g}_{h_2} - V_m \dot{\phi}_{m_1} - G_{m_{12}} p_{m_1} + G_{m_1} p_{m_2})$$

Secondly, combining the remaining line equations with the circuit equations and the motor flow equations gives

$$\begin{aligned} p_{m_1} &= p_{a_1} - V_m (R_1 \dot{\phi}_m + I_1 \frac{d}{dt} \dot{\phi}_m) \\ p_{m_2} &= p_{a_2} + V_m (R_1 \dot{\phi}_m + I_1 \frac{d}{dt} \dot{\phi}_m) \end{aligned} \quad (5.2.3)$$

Equations (5.2.3) are subtracted and added and the respective results are substituted into the remaining motor equations (3.4.4). In addition, the valve equations (2.2.3) are substituted into (5.2.2). With the assumption that for a short line R_1 and I_1 are small, i.e.,

$$\begin{bmatrix} p_{a_1} \\ p_{a_2} \end{bmatrix} = \begin{bmatrix} p_{m_1} \\ p_{m_2} \end{bmatrix}$$

the final result is obtained as

$$\begin{aligned}
d/dt \, p_{h_1} &= -\frac{1}{C_1} (V_m \dot{\phi}_m + K_v (F_{13} (\Delta + \delta_v) \sqrt{p_{h_1} - p_s} + F_{13} (\Delta - \delta_v) \sqrt{p_{h_1}}) \\
&\quad + G_{m_{11}} p_{h_1} - G_{m_{12}} p_{h_2}) \\
d/dt \, p_{h_2} &= -\frac{1}{C_1} (V_m \dot{\phi}_m + K_v (F_{13} (\Delta - \delta_v) \sqrt{p_{h_2} - p_s} + F_{13} (\Delta + \delta_v) \sqrt{p_{h_2}}) \\
&\quad - G_{m_{12}} p_{h_1} + G_{m_{22}} p_{h_2}) \tag{5.2.4}
\end{aligned}$$

$$\begin{aligned}
d/dt \, \dot{\phi}_m &= -\frac{1}{J'_m} (B'_m \dot{\phi}_m - V_m (p_{h_1} - p_{h_2}) - \tau_m \\
&\quad + F_{14} (\dot{\phi}_m) (\tau_{mc} + B_{mc} (p_{h_1} + p_{h_2})))
\end{aligned}$$

$$\text{where } J'_m = J_m + 2V^2 I$$

$$B'_m = B_m + 2V^2 R$$

Equations (5.2.4) represent three simultaneous first order nonlinear differential equations. They are in normal form and hence a computer solution is directly applicable.

Of interest is a comparison of (5.2.4) and (5.1.3). One may consider the limit as the parameters of the lines, C_1 , R_1 , and I_1 , vanish in (5.2.4). As I and R vanish, the third equation becomes identical to the corresponding equation of (5.1.3). As C_1 vanishes, the two top equations of (5.2.4) become algebraic and identical to the algebraic equations of (5.1.3). On the basis of this relationship, (5.2.4) may be effectively employed to find an approximate solution to (5.1.3).

Although the derivatives of the pressure may become rather large for small values of C_1 and thus cause numerical problems in the solution, accuracy may be maintained through time scaling of analog computer solutions or by reducing the

increment of integration in a digital computer solution. The curves of Fig. 5.2.3 show a sequence of solutions for various values of C_1 to demonstrate the implications of the capacity assumption. The effects of stiction and leakage are neglected. To avoid any possible difficulties introduced by the discontinuities when $\delta_v(t)$ is taken as a step function, $\delta_v(t)$ is taken as the solution of a first order differential equation. Curves A, B, C are the solution of the differential equations for three different values of capacitance, which correspond to the following physical lines.

A - 30 cm of $\frac{1}{4}$ " I.D. flexible hose

B - 100 cm of $\frac{1}{4}$ " I.D. copper tubing

C - 10 cm of $\frac{1}{4}$ " I.D. copper tubing

Curve D is the solution to the single differential equation (5.1.6). It is quite clearly demonstrated that cases C and D are not distinguishable. Already solution B is a very good approximation to the equations describing the incompressible case. Curve E represents the measured characteristic for conditions corresponding to the solution indicated by curve A.

To enhance the significance of this comparison, it is important to keep J_m as small as possible, so that the time constant of the motor differential equation is in magnitude close to the time constants of the pressure equations. For instance, for a large inertial load, the effect of a change in C_1 is almost negligible.

The curves of Fig. 5.2.4 and 5.2.5 show velocity responses of the subassembly to various magnitudes of inputs. Computed and experimental results are shown for two types of lines,

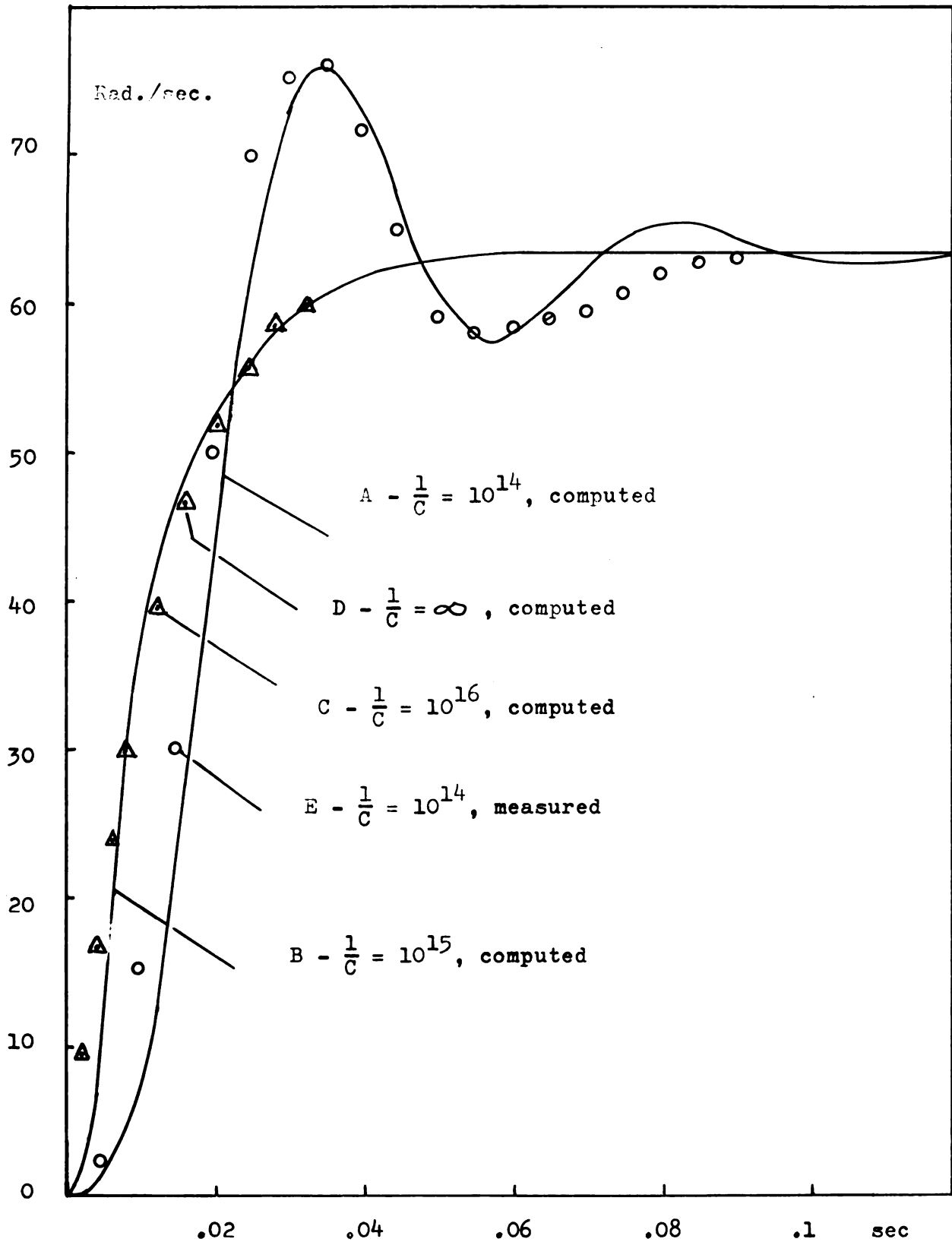


Fig. 5.2.3.--Effect of variation of capacitance on velocity response (Subassembly 2).

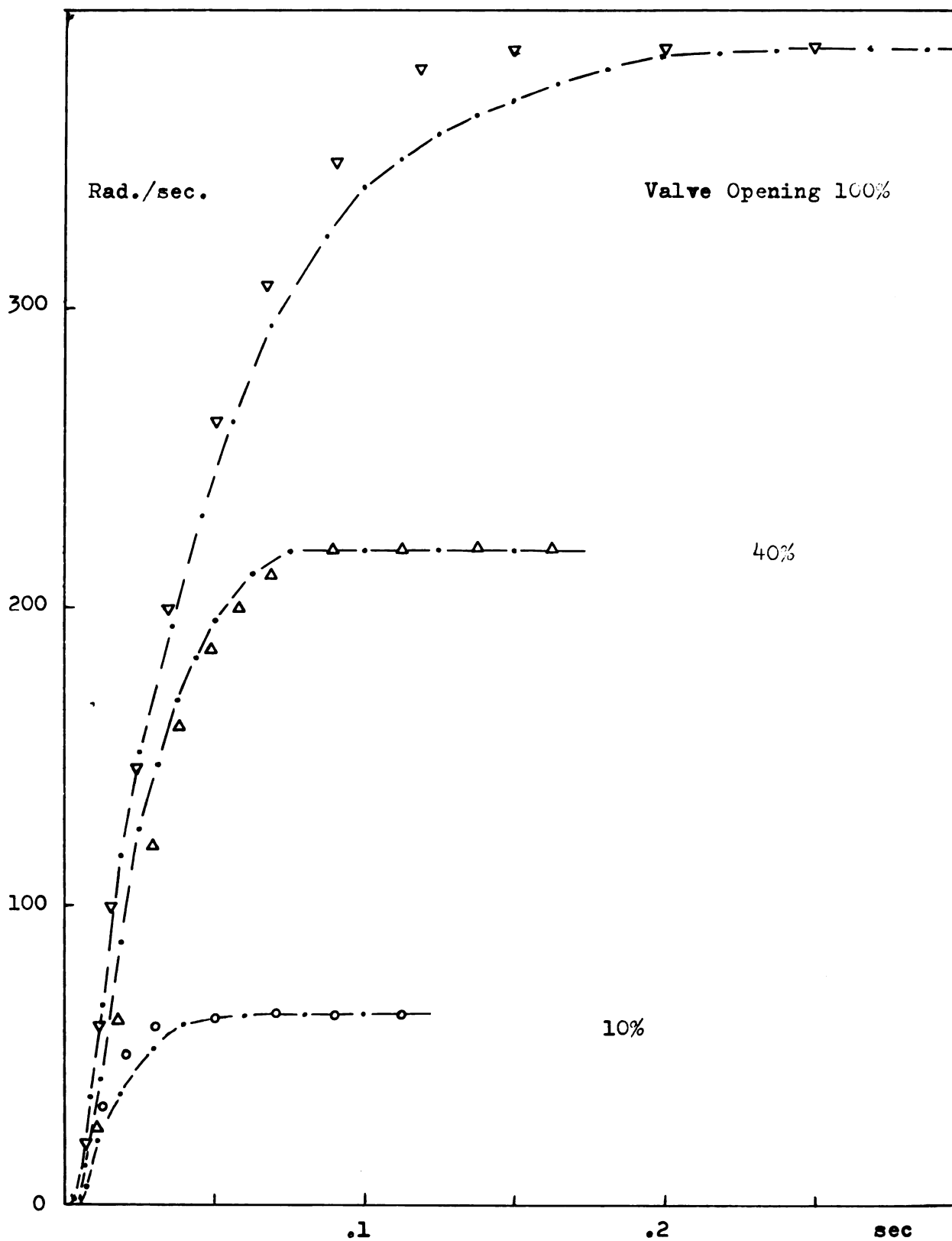


Fig. 5.2.4.--Response curves for subassembly 2; lines: 50 cm copper

300

200

100

0

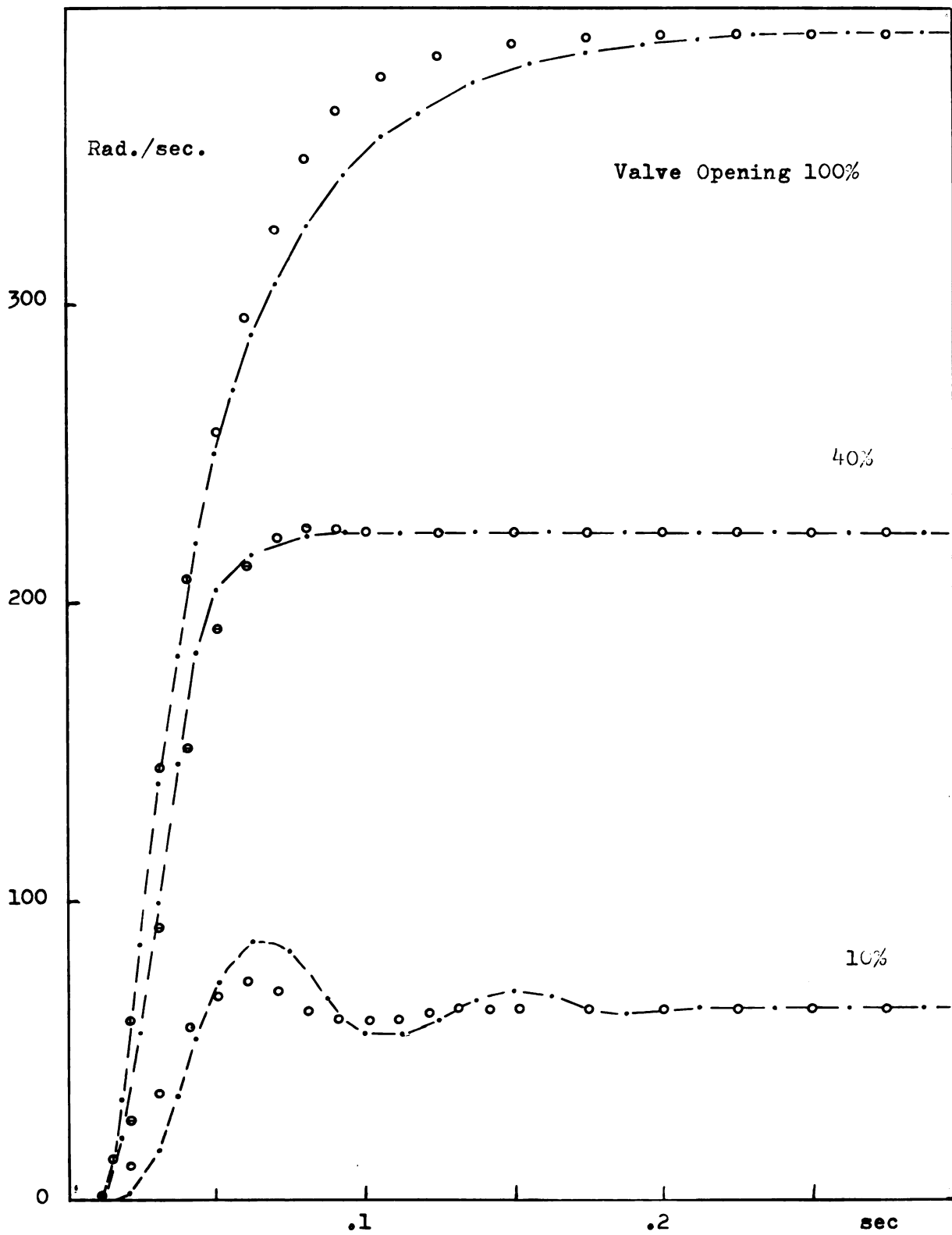


Fig. 5.2.5.--Response curves for subassembly 2; lines: 1 m flexible

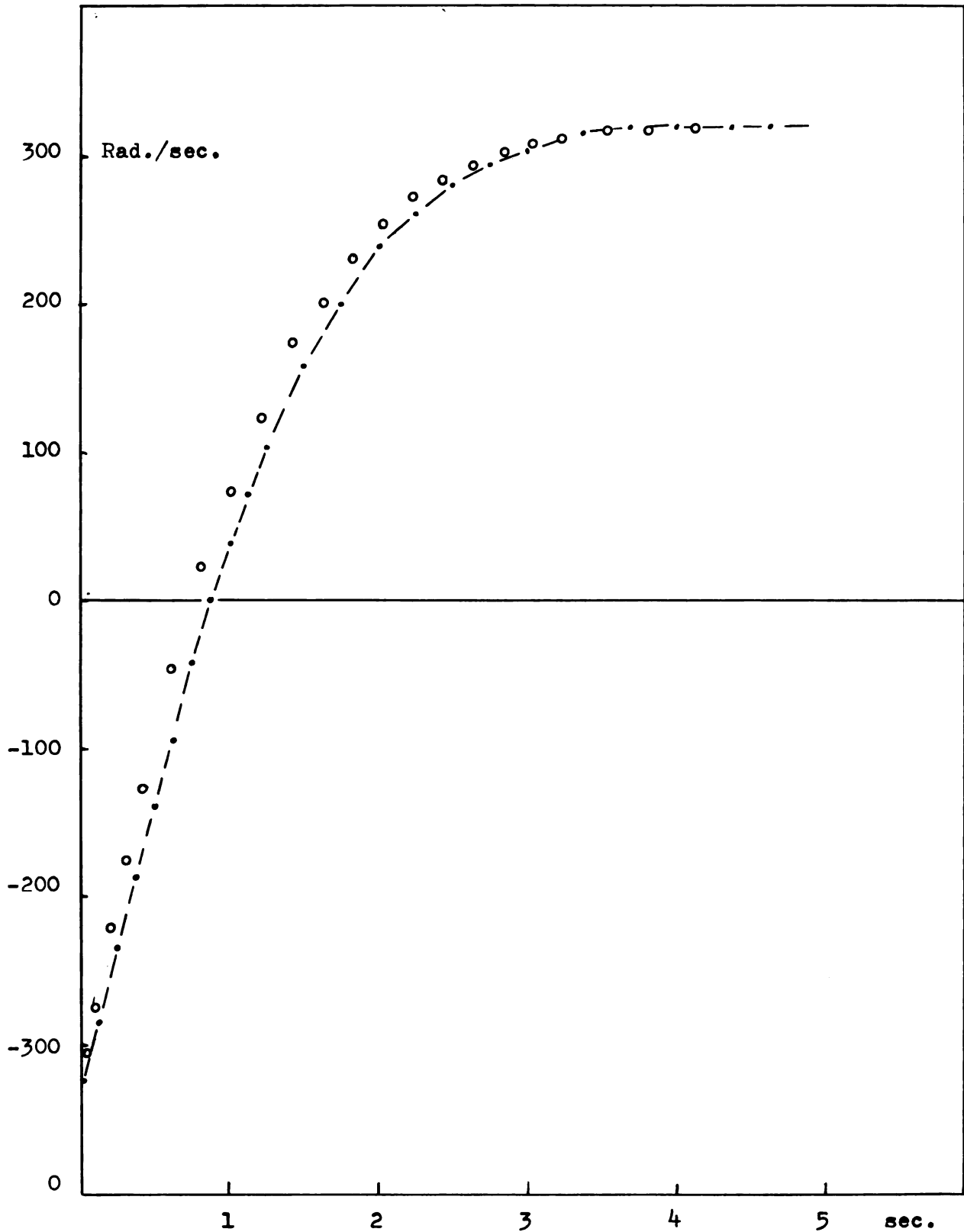


Fig. 5.2.6.--Square-wave response curves for subassembly 2 with load; lines: 1 m flexible.

representing a capacity ratio of approximately 10. A comparison of the curves reveals significant differences between the two sets of curves only for small valve openings. Two important conclusions may be drawn from this observation: (1) The damping effect of the control valve on the dynamic response of the subassembly increases with an increase in valve opening. (2) The effect of a change in capacitance of the amount indicated in the lines is relatively insignificant for valve openings above 10% of full opening.

As will be seen later in section 5, the variation of the damping effect of the control valve as a function of the valve opening has an extreme influence on the stability behavior of a closed loop system containing this subassembly. The other conclusion establishes the validity of the technique of including a capacity in the system in order to facilitate the computer solution.

An interesting observation is obtained when the effect of the presence of leakage in the mathematical model is investigated. It is immaterial whether or not the leakage terms are included in the model, since for the numerical magnitudes involved no detectable influence was discerned in the solutions presented by the previous figures.

Fig. 5.2.6 shows the computed and experimental results of a square wave response of this subassembly with a large inertia load connected.

5.3 Valve Long-Line Motor. (Subassembly 3)

In order to obtain a mathematical model in normal form for this subassembly it is necessary that the lines be modeled in

CC form. This condition is evident from an inspection of the system graph and the terminal equations of the components.

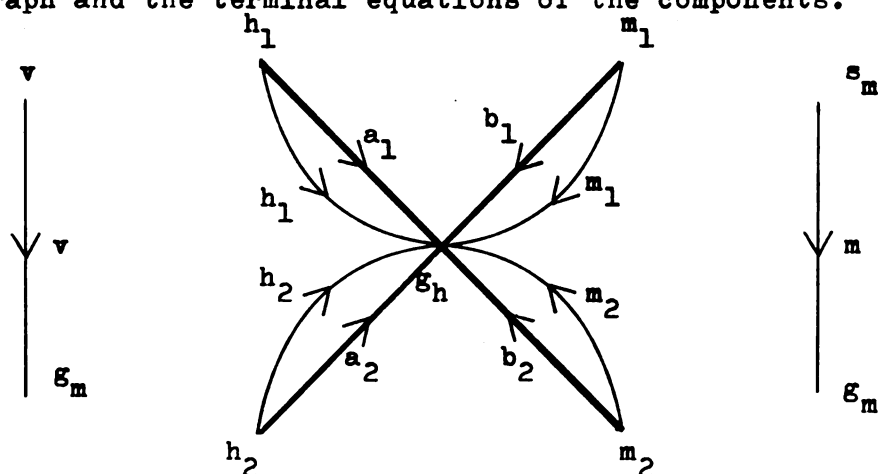


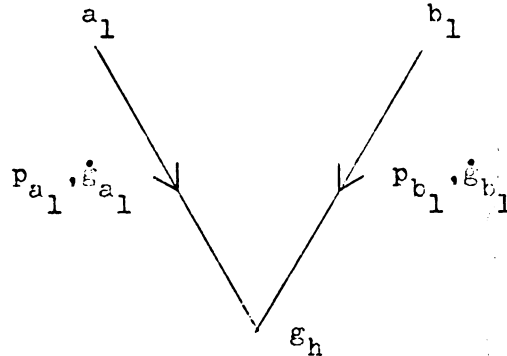
Fig. 5.3.1.--Graph of subassembly 3

To avoid nonlinear algebraic equations in the final mathematical model elements a_1 and a_2 must be branch elements and as such their across variables must be explicit in the first derivatives. This condition is achieved by a closed representation for the lines at those ends to which the valve is connected.

The motor equations require that p_{m_1} and p_{m_2} be solved explicitly. These pressures may be solved by the differential equations of the line when a closed representation is chosen for the other end also.

Let it be assumed that the characteristics of the lines are adequately given by a 5-element representation. A three-terminal representation for a 5-element line is

$$\frac{d}{dt} \begin{bmatrix} p_{a1} \\ p_{b1} \\ p_{c1} \\ \dot{g}_{ac1} \\ \dot{g}_{cb1} \end{bmatrix} = \begin{bmatrix} 0 & 0 & 0 & -\frac{1}{C} & 0 \\ 0 & 0 & 0 & 0 & -\frac{1}{C} \\ 0 & 0 & 0 & \frac{1}{C} & \frac{1}{C} \\ \frac{1}{I} & 0 & -\frac{1}{I} & -\frac{R}{I} & 0 \\ 0 & \frac{1}{I} & -\frac{1}{I} & 0 & -\frac{R}{I} \end{bmatrix} \begin{bmatrix} p_{a1} \\ p_{b1} \\ p_{c1} \\ \dot{g}_{ac1} \\ \dot{g}_{cb1} \end{bmatrix} + \begin{bmatrix} \frac{1}{C} & 0 \\ 0 & \frac{1}{C} \\ 0 & 0 \\ 0 & 0 \\ 0 & 0 \end{bmatrix} \begin{bmatrix} \dot{g}_{a1} \\ \dot{g}_{b1} \end{bmatrix} \quad (5.3.1)$$



The development leading to (5.3.1) runs parallel to the development of equations (4.2.3). Again, it is quite permissible to let the C and R coefficients of (5.3.1) be functions of the pressures and flows, respectively.

The model of the subassembly is obtained by combining (5.3.1) with the other component equations as dictated by the graph equations of Fig. 5.3.1.

Fig. 5.3.2 shows a set of velocity response curves for this subassembly. The computed results are based on the model given by (5.3.3). The measured characteristics clearly show the transportation lag characteristic of long lines. The computed results also give correct indication of this lag, but include a certain amount of oscillation not present in the measured result. This is, of course, attributable to the particular mathematical model chosen to describe the lines. If the lines are represented by a lumped parameter model containing more elements, thus forming a better approximation, the

$$\begin{aligned}
 \frac{d}{dt} \begin{bmatrix} p_{h1} \\ p_{h2} \\ p_{c1} \\ p_{c2} \\ \dot{g}_{ac1} \\ \dot{g}_{ac2} \\ \dot{g}_{cb1} \\ \dot{g}_{cb2} \\ p_{m1} \\ p_{m2} \\ \dot{\phi}_m \end{bmatrix} &= \begin{bmatrix} -\frac{1}{C}(\dot{g}_{ac1} + K_v F_{13}(\Delta + \delta_v) \sqrt{p_{h1} - p_s} + F_{13}(\Delta - \delta_v) \sqrt{p_1}) \\ -\frac{1}{C}(\dot{g}_{ac2} + K_v F_{13}(\Delta - \delta_v) \sqrt{p_{h2} - p_s} + F_{13}(\Delta + \delta_v) \sqrt{p_2}) \\ \frac{1}{C}(\dot{g}_{ac1} + \dot{g}_{cb1}) \\ \frac{1}{C}(\dot{g}_{ac2} + \dot{g}_{cb2}) \\ -\frac{1}{I}(\dot{R}\dot{g}_{ac1} + p_{c1} - p_{h2}) \\ -\frac{1}{I}(\dot{R}\dot{g}_{ac2} + p_{c2} - p_{h2}) \\ -\frac{1}{I}(\dot{R}\dot{g}_{cb1} + p_{c1} - p_{m1}) \\ -\frac{1}{I}(\dot{R}\dot{g}_{cb2} + p_{c2} - p_{m2}) \\ -\frac{1}{C}(\dot{g}_{cb1} + V_m \dot{\phi}_m) \\ -\frac{1}{C}(\dot{g}_{cb2} - V_m \dot{\phi}_m) \\ -\frac{1}{J_m}(B_m \dot{\phi}_m - V_m(p_{m1} - p_{m2}) - \tau_m \\ + F_{14}(\dot{\phi}_m)(\tau_{mc} + B_{mc}(p_{m1} + p_{m2}))) \end{bmatrix} \quad (5.3.3)
 \end{aligned}$$

predicted response is found to agree more closely with the measured response.

Fig. 5.3.3 shows another velocity response of this subassembly with an inertia load connected. The measured result coincides very closely with the mathematical solution in this case. Since the inertia load is the primary time lag effect, effects due to any differences between the physical and mathematical model of the lines are concealed.

5.4 Valve Short-Line cylinder. (Subassembly 4)

A combination of components occurring frequently as subassembly in a hydraulic control system is a valve-line-cylinder combination. The formulation for this subassembly is identical in structure to the subassemblies 1, 2, and 3. One can obtain the corresponding mathematical models for the valve-line-cylinder subassembly directly from equations (5.1.1), (5.2.4), and (5.3.3) by simply replacing motor parameters by corresponding

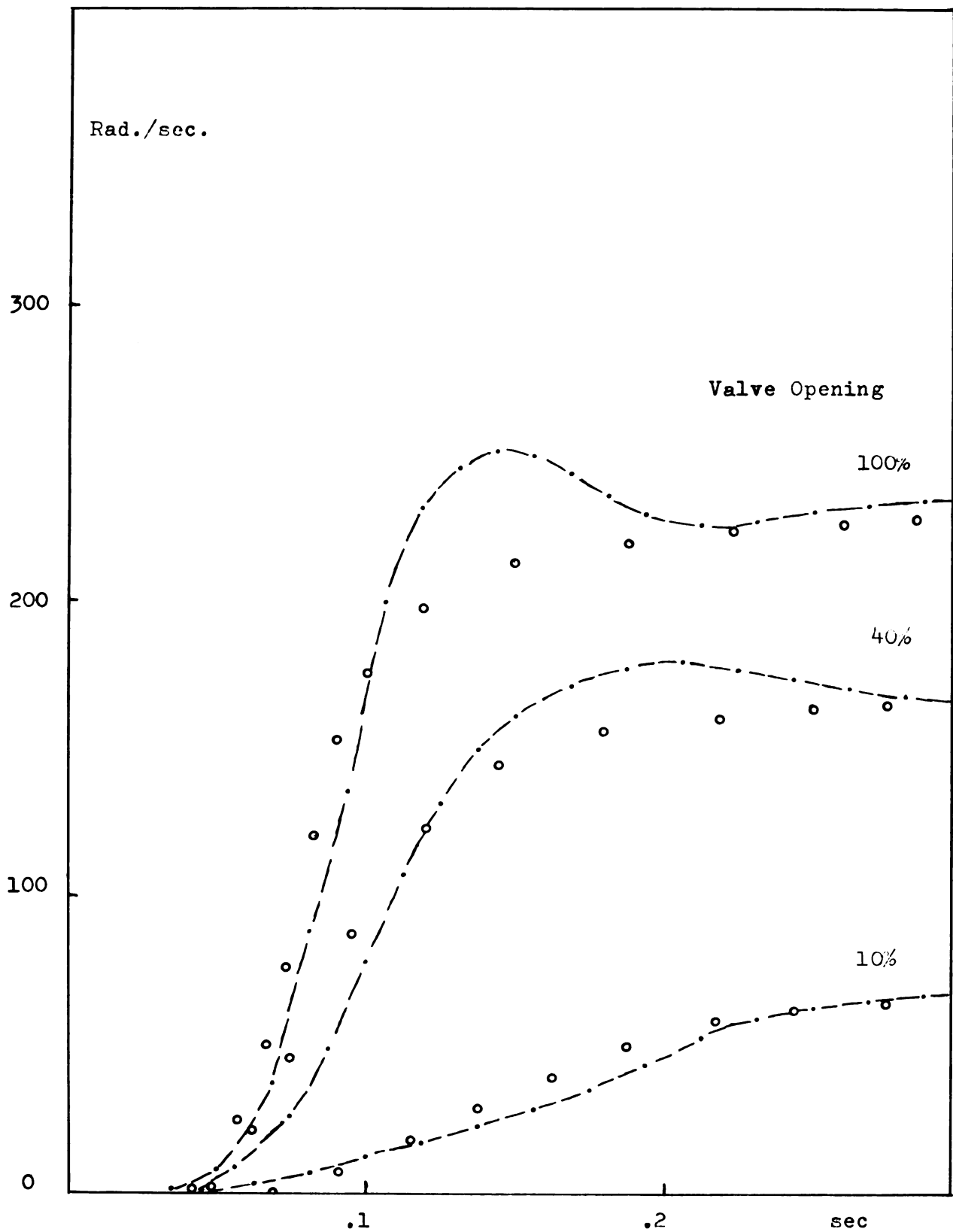


Fig. 5.3.2.--Response curves for subassembly 3. Lines: 16 m flexible

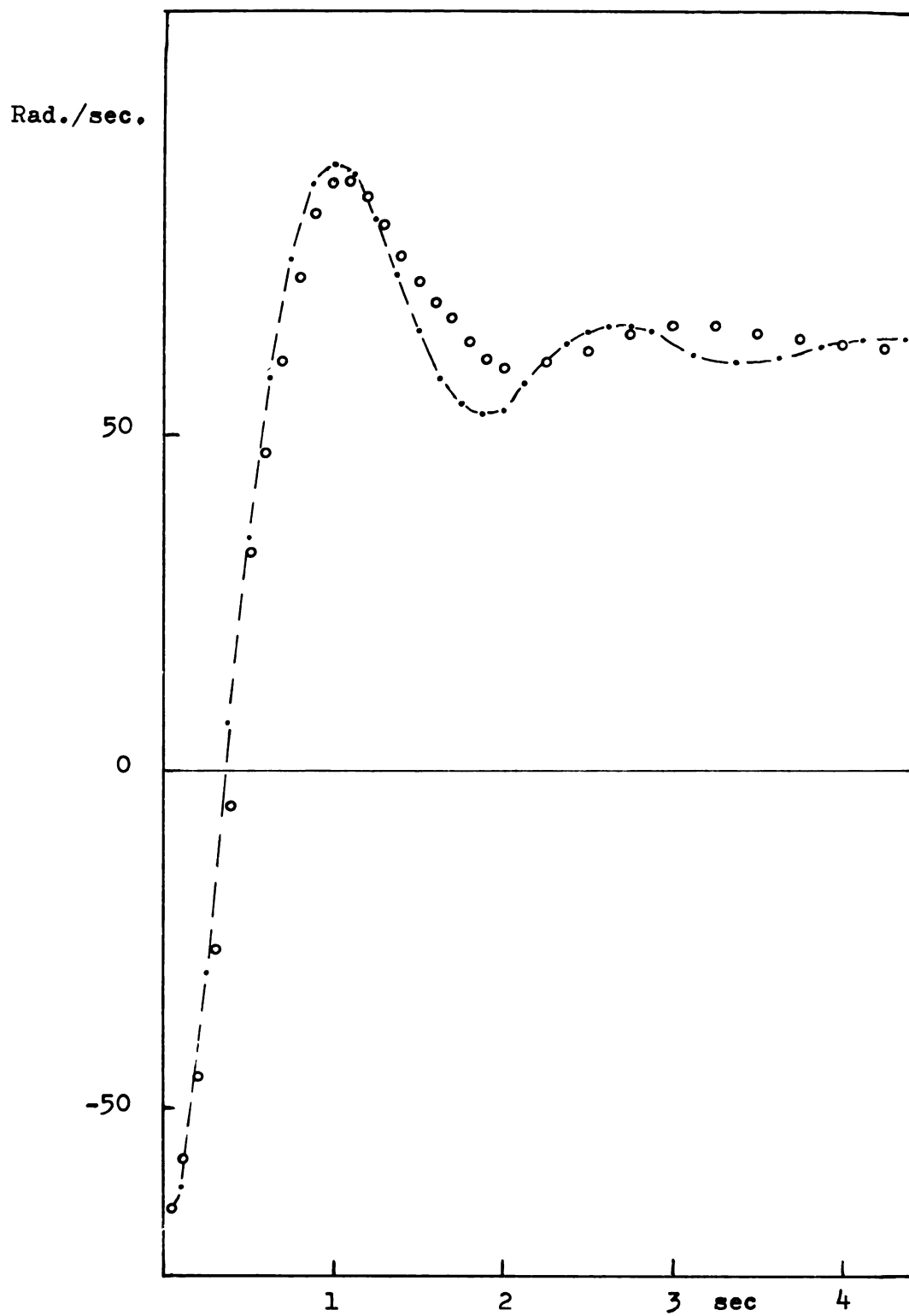


Fig. 5.3.3.--Response curves for subassembly 3 with load.
Lines: 16 m flexible.

piston parameters. In all three cases it is, however, assumed that the capacity of the cylinder chambers is negligible. Special consideration must be given to applications where the chamber capacity is not negligible. This particular case is discussed here.

For this subassembly the following components are used: (1) a four-way valve, (2) a short line modeled in terms of two elements and (3) a cylinder with appreciable chamber capacity. The system graph of the subassembly is shown in Fig. 5.4.1.

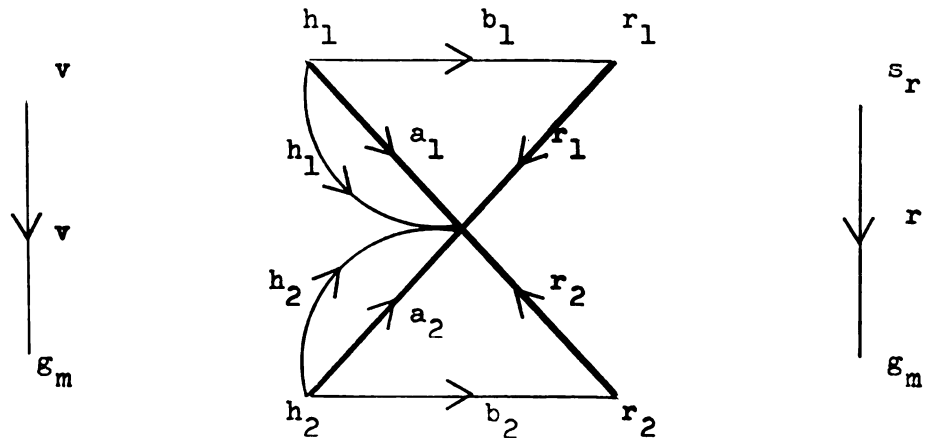


Fig. 5.4.1.--Graph of subassembly 4

The equations for the subassembly are found to be

$$\frac{d}{dt} \begin{bmatrix} p_{h1} \\ p_{h2} \\ \dot{g}_{b1} \\ \dot{g}_{b2} \\ p_{r1} \\ p_{r2} \\ \dot{\delta}_r \\ \delta_r \end{bmatrix} = \begin{bmatrix} -\frac{1}{C_1} (K_v(F_{13}(\Delta + \delta_v) \sqrt{p_{h1} - p_s} + F_{13}(\Delta - \delta_v) \sqrt{p_{h1}}) + \dot{g}_{b1}) \\ -\frac{1}{C_1} (K_v(F_{13}(\Delta - \delta_v) \sqrt{p_{h2} - p_s} + F_{13}(\Delta + \delta_v) \sqrt{p_{h2}}) + \dot{g}_{b2}) \\ -\frac{1}{I} (R \dot{g}_{b1} - p_{h1} + p_{r1}) \\ -\frac{1}{I} (R \dot{g}_{b2} - p_{h2} + p_{r2}) \\ -\frac{1}{C(\delta_r)} (\dot{g}_{b1} + A_p \dot{\delta}_r + G_{r11} p_{r1} - G_{r12} p_{r2}) \\ -\frac{1}{C(-\delta_r)} (\dot{g}_{b2} - A_p \dot{\delta}_r - G_{r12} p_{r1} + G_{r11} p_{r2}) \\ -\frac{1}{M_r} (B_r \dot{\delta}_r - A_p (p_{r1} - p_{r2}) - f_r + F_{14}(\delta_r)(f_{rc} + B_{rc}(p_{r1} + p_{r2}))) \\ \dot{\delta}_r \end{bmatrix} \quad (5.4.1)$$

From (5.4.1), it is seen that 8 differential equations are required when the capacitive effects of the line and the cylinder are taken into account separately. When the two capacitive effects are lumped together, as may well be done for a short line, equations (5.4.1) reduce to a set of equations similar to (5.2.4).

$$\frac{d}{dt} \begin{bmatrix} p_{r1} \\ p_{r2} \\ \dot{\delta}_r \\ \delta_r \end{bmatrix} = \begin{bmatrix} -\frac{1}{C(\delta_r)} (K_v(F_{13}(\Delta + \delta_v) \sqrt{p_{r1} - p_s} + F_{13}(\Delta - \delta_v) \sqrt{p_{r1}}) + A_p \dot{\delta}_r) \\ -\frac{1}{C(-\delta_r)} (K_v(F_{13}(\Delta - \delta_v) \sqrt{p_{r2} - p_s} + F_{13}(\Delta + \delta_v) \sqrt{p_{r2}}) - A_p \dot{\delta}_r) \\ -\frac{1}{M_r} (F_r \dot{\delta}_r - A_p (p_{r1} - p_{r2}) - f_r + F_{14}(\delta_r)(f_{rc} + B_{rc}(p_{r1} + p_{r2}))) \\ \dot{\delta}_r \end{bmatrix} \quad (5.4.2)$$

where $C(\delta_r)$ = combined capacitance of one line and one side of cylinder.

Solutions as predicted by the mathematical model (5.4.2) agree closely with experimental results. This was shown earlier by Wang (5). Due to lack of suitable experimental facilities, the effect of a change in capacitance as a function of piston rod position could not effectively be demonstrated.

5.5 Pump Motor. (Subassembly 5)

The combination of a variable displacement pump and a fixed displacement motor is also a basic subassembly in hydraulic systems. It is frequently employed to serve as an infinitely variable speed transmission. The terminal representations of the two components are given by equations (3.3.14) and (3.4.1). If the subassembly is connected according to the graph of Fig. 5.5.1, the mathematical model (5.5.1) and (5.5.2) is obtained.

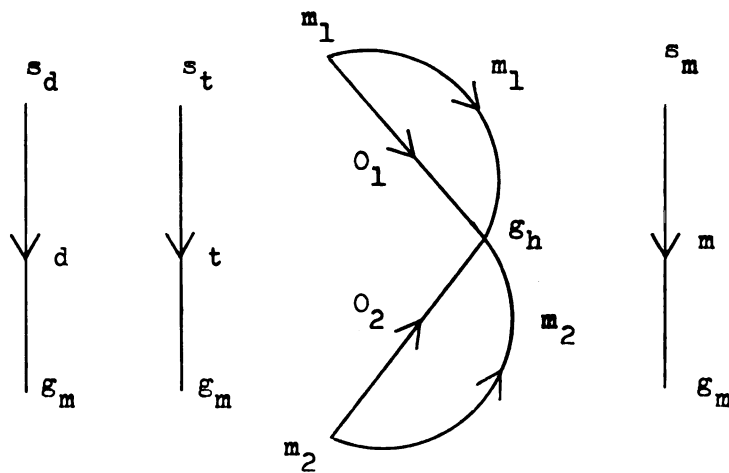


Fig. 5.5.1.--Graph of subassembly 5

The resulting mathematical model clearly is not in normal form since a combination of nonlinear algebraic and differential equations is involved. The difficulty involved in realizing an exact solution is increased by the fact that a lower limit on the pressures must be observed. This lower limit is set by the pressure at which the make-up fluid is supplied to the system. Normally, proper limiting of variables is handled utilizing information on their derivatives. Since in (5.5.1) and (5.5.2), the pressure derivatives do not appear, it is extremely difficult to properly determine when the pressure limits are in effect. As an auxiliary measure, one might use information on

$$\frac{d}{dt} \begin{bmatrix} \dot{\phi}_t \\ \phi_t \\ \dot{\phi}_d \\ \dot{\phi}_m \end{bmatrix} = \begin{bmatrix} -\frac{1}{J_t}(B_t \dot{\phi}_t - \tau_t + F_{14}(\dot{\phi}_t)(\tau_{tc} + B_{tc}(p_{01} + p_{02}))) \\ \dot{\phi}_t \\ -\frac{1}{J_d}(B_d \dot{\phi}_d - \tau_d - V_t(p_{01} - p_{02})\phi_t + F_{14}(\dot{\phi}_d)(\tau_{dc} + B_{dc}(p_{01} + p_{02}))) \\ -\frac{1}{J_m}(B_m \dot{\phi}_m - \tau_m - V_m(p_{01} - p_{02}) + F_{14}(\dot{\phi}_m)(\tau_{dm} + B_{dm}(p_{01} + p_{02}))) \end{bmatrix} \quad (5.5.1)$$

$$0 = \begin{bmatrix} V_m \\ -V_m \end{bmatrix} \dot{\phi}_m + \dot{\phi}_d \begin{bmatrix} V_t \\ -V_t \end{bmatrix} \phi_t + \begin{bmatrix} (G_{01} + G_{m1}) & -(G_{012} + G_{m12}) \\ -(G_{012} + G_{m12}) & (G_{01} + G_{m1}) \end{bmatrix} \begin{bmatrix} p_{01} \\ p_{02} \end{bmatrix} \quad (5.5.2)$$

the velocities $\dot{\phi}_d$ and $\dot{\phi}_m$ and position ϕ_t . By monitoring the change in these three variables, sufficient information can be made available to decide at what points the pressures should be limited. This technique is discussed in detail in the next section.

For the less general case in which the drive shaft speed $\dot{\phi}_d$ is held constant, the system equations reduce to

$$\frac{d}{dt} \begin{bmatrix} \dot{\phi}_t \\ \phi_t \end{bmatrix} = \begin{bmatrix} -\frac{1}{J_t}(B_t \dot{\phi}_t - \tau_t + F_{14}(\dot{\phi}_t)(\tau_{tc} + B_{tc}(p_{01} + p_{02}))) \\ \dot{\phi}_t \end{bmatrix}$$

$$\dot{\phi}_m = -\frac{V_t}{V_m} \dot{\phi}_d \phi_t - \left[(G_{01} + G_{m1}) - (G_{012} + G_{m12}) \right] \begin{bmatrix} p_{01} \\ p_{02} \end{bmatrix} \quad (5.5.2)$$

$$0 = B_m \dot{\phi}_m - \tau_m - V_m(p_{01} - p_{02}) + F_{14}(\dot{\phi}_m)(\tau_{mc} + B_{mc}(p_{01} + p_{02}))$$

Equations (5.5.2) indicated that $\dot{\phi}_m$ is algebraically related to ϕ_t , i.e., the output speed changes instantaneously with the

tiltplate angle, regardless of load effects.

The development of the mathematical models of the valve-motor and pump-motor subassemblies, namely, equations 5.1.1 and 5.5.1, were based on the assumption that the effect of oil compressibility can be negligible. In both cases, the mathematical models appeared as combinations of nonlinear algebraic and differential equations, i.e., not in normal form. When, however, oil compressibility is included, a normal form model will result. This was already demonstrated in subassembly 2. Subassembly 6 demonstrates this for the pump motor combination.

5.6 Pump Short-Line Motor (Subassembly 6)

When the effects of a short line are added to the configuration of subassembly 5, a normal form model is made possible. The effects of a short line are accounted for in precisely the same manner as for subassembly 2. The system graph for subassembly 6 is shown in Fig. 5.6.1.

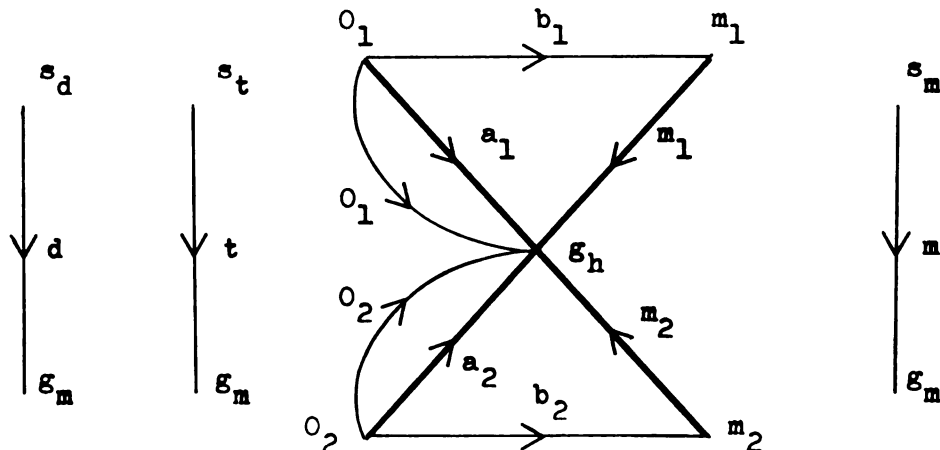


Fig. 5.6.1.--Graph of subassembly 6

Following the formulation procedure of subassembly 2, the normal form representation for subassembly 6 is obtained.

$$\frac{d}{dt} \begin{bmatrix} \dot{\phi}_t \\ \phi_t \\ \dot{\phi}_d \\ p_{O_1} \\ p_{O_2} \\ \dot{\phi}_m \end{bmatrix} = \begin{bmatrix} -\frac{1}{J_t}(B_t \dot{\phi}_t - \tau_t + F_{14}(\dot{\phi}_t)(\tau_{tc} + B_{tc}(p_{O_1} + p_{O_2}))) \\ \dot{\phi}_t \\ -\frac{1}{J_d}(B_d \dot{\phi}_d - \tau_d - V_t(p_{O_1} - p_{O_2})\phi_t + F_{14}(\dot{\phi}_d)(\tau_{dc} + B_{dc}(p_{O_1} + p_{O_2}))) \\ -\frac{1}{C}(V_m \dot{\phi}_m + V_t \dot{\phi}_d \phi_t + (G_{O1} + G_{m1})p_{O_1} - (G_{O12} + G_{m12})p_{O_2}) \\ +\frac{1}{C}(V_m \dot{\phi}_m + V_t \dot{\phi}_d \phi_t - (G_{O12} + G_{m12})p_{O_1} + (G_{O1} + G_{m1})p_{O_2}) \\ -\frac{1}{J_m}(B_m \dot{\phi}_m - \tau_m - V_m(p_{O_1} - p_{O_2}) + F_{14}(\dot{\phi}_m)(\tau_{mc} + B_{mc}(p_{O_1} + p_{O_2}))) \end{bmatrix} \quad (5.6.1)$$

Again, as previously, if the parameters of the short line are permitted to approach zero in equation (5.6.1), equations (5.5.1) and (5.5.2) result. In the solution of (5.6.1) the limits for p_{O_1} and p_{O_2} must be observed. Since the pressure time derivatives are directly available as calculated quantities, information for proper limiting is attainable. Although the pressure equations give the appearance that the pressures are of equal magnitude, but opposite in sign, this is not at all true because of the limit requirements. The limit requirements may be interpreted as imposing a rectifying action on the solution: only pressures above a positive make-up pressure, p_m , are permitted. Without leakage both pressures are maintained above p_m in the steady state, with a pressure difference as determined by the load requirements. But, due to leakage to the atmosphere, one pressure will always return to the make-up pressure after a transient, with the other following at a

constant difference. Since the Coulomb friction characteristics of the pump and motor are adversely affected by high system pressure levels, it is clear that leakage to the atmosphere in this application is of advantage. In fact, the pump-line-motor configuration is one of the very few cases where it is important to consider leakage effects in the mathematical model.

Fig. 5.6.2 and 5.6.3 show velocity response curves of this subassembly for two different connection lines. The tiltplate was stroked by a position servo whose response lag is indicated. These curves indicate very sharply that a pump-motor subassembly is much less damped than a corresponding valve-motor subassembly. Therefore, the effect of a variation in the line capacity is much more noticeable for this subassembly than for subassembly 2.

5.7 Pump Long-Line Motor. (Subassembly 7)

Similar to the formulation procedure used in subassembly 3, the mathematical model for subassembly 7 is developed. According to the system graph of Fig. 5.7.1, one has with a 5-element line approximation the mathematical model given in (5.7.1).

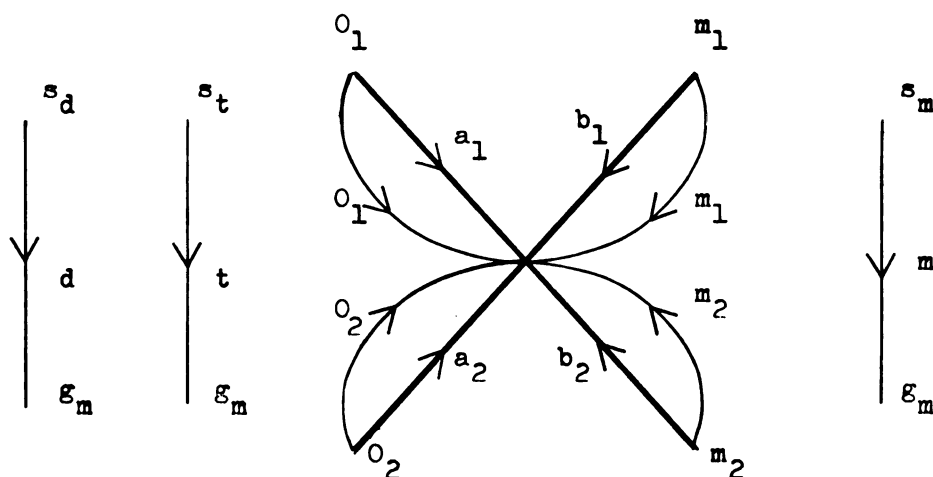


Fig. 5.7.1.--Graph of subassembly 7

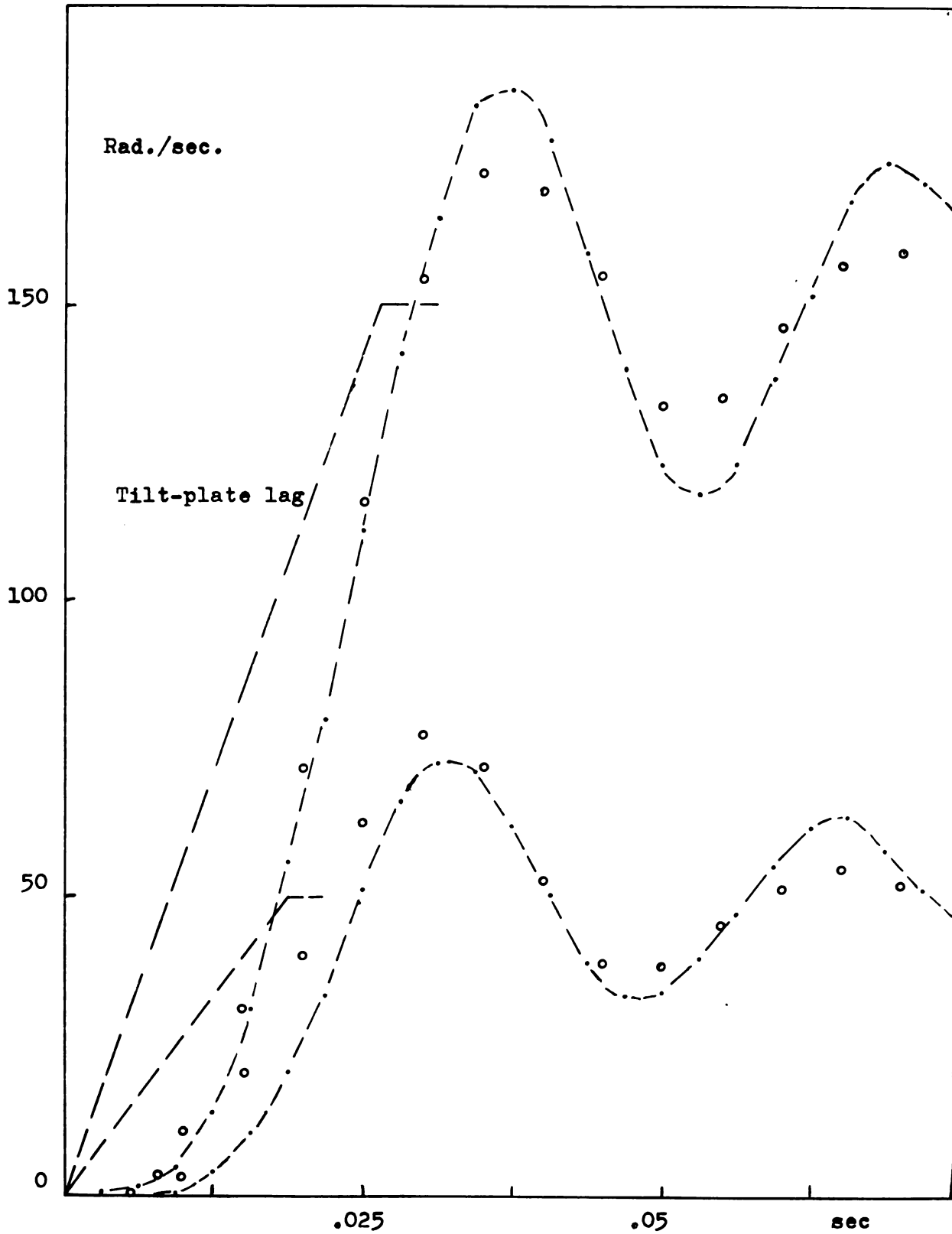


Fig. 5.6.2.--Response curves for subassembly 6.
Lines: 50 cm copper.

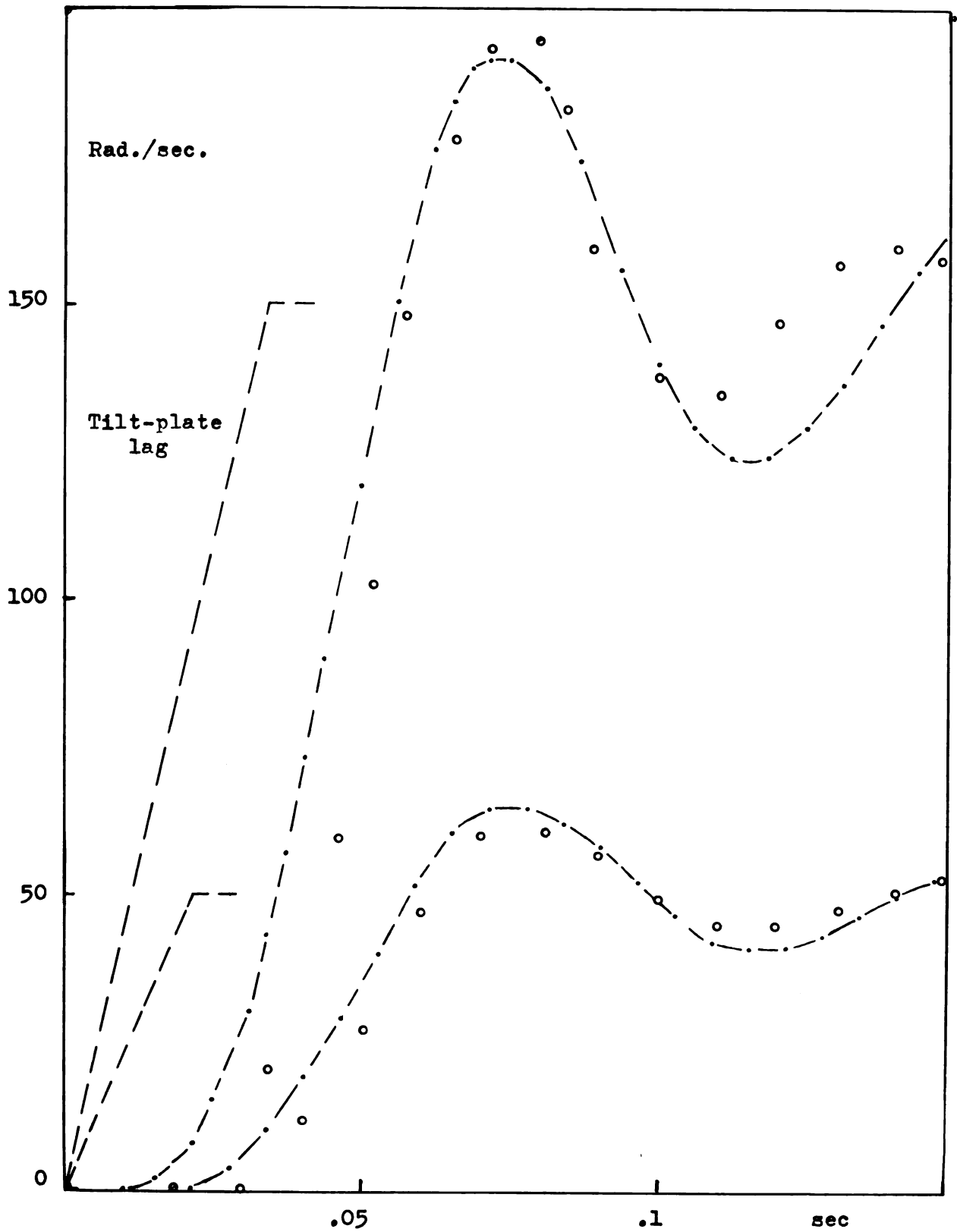


Fig. 5.6.3.--Response curves for subassembly 6.
Lines: 1 m flexible

$$\begin{aligned}
 \frac{d}{dt} \begin{bmatrix} \dot{\phi}_t \\ \phi_t \\ \dot{\phi}_t \\ p_{O_1} \\ p_{O_2} \\ p_{c_1} \\ p_{c_2} \\ \dot{g}_{ac_1} \\ \dot{g}_{ac_2} \\ \dot{g}_{cb_1} \\ \dot{g}_{cb_2} \\ p_{m_1} \\ p_{m_2} \\ \dot{\phi}_m \end{bmatrix} &= \begin{bmatrix} -\frac{1}{J_t}(B_t \dot{\phi}_t - \tau_t + F_{14}(\dot{\phi}_t)(\tau_{tc} + B_{tc} + B_{tc}(p_{O_1} + p_{O_2}))) \\ \dot{\phi}_t \\ -\frac{1}{J_d}(B_d \dot{\phi}_d - \tau_d - V_t(p_{O_1} - p_{O_2})\phi_t + F_{14}(\dot{\phi}_d)(\tau_{dc} + B_{dc}(p_{O_1} + p_{O_2}))) \\ -\frac{1}{C}(\dot{g}_{ac_1} + V_t \dot{\phi}_d \phi_t + G_{O_1} p_{O_1} - G_{O_{12}} p_{c_1}) \\ -\frac{1}{C}(\dot{g}_{ac_2} - V_t \dot{\phi}_d \phi_t - G_{O_{12}} p_{O_1} + G_{O_1} p_{O_2}) \\ \frac{1}{C}(\dot{g}_{ac_1} + \dot{g}_{cb_1}) \\ \frac{1}{C}(\dot{g}_{ac_2} + \dot{g}_{cb_2}) \\ -\frac{1}{I}(R \dot{g}_{a_2} + p_{c_1} - p_{O_1}) \\ -\frac{1}{I}(R \dot{g}_{a_2} + p_{c_2} - p_{O_2}) \\ -\frac{1}{I}(R \dot{g}_{cb_1} + p_{c_1} - p_m) \\ -\frac{1}{I}(R \dot{g}_{cb_2} + p_{c_2} - p_{m_2}) \\ -\frac{1}{C}(\dot{g}_{cb_1} + V_m \dot{\phi}_m - G_{m_{12}} p_{m_1} - G_{m_{12}} p_{m_2}) \\ -\frac{1}{C}(\dot{g}_{cb_2} - V_m \dot{\phi}_m - G_{m_{12}} p_{m_1} + G_{m_1} p_{m_2}) \\ -\frac{1}{J_m}(B_m \dot{\phi}_m - V_m(p_{m_1} - p_{m_2}) - \tau_m + F_{14}(\dot{\phi}_m)(\tau_{mc} + B_{mc}(p_{m_1} + p_{m_2}))) \end{bmatrix} \quad (5.7.1)
 \end{aligned}$$

Fig. 5.7.2 shows a set of response curves for changes in the tilt plate stroke as indicated. It is very clearly demonstrated by these curves that the high absorption and dissipation characteristics of the long line have practically eliminated any oscillatory response. If, however, an inertial load is connected to the motor, oscillation again is observed as is shown in Fig. 5.7.3.

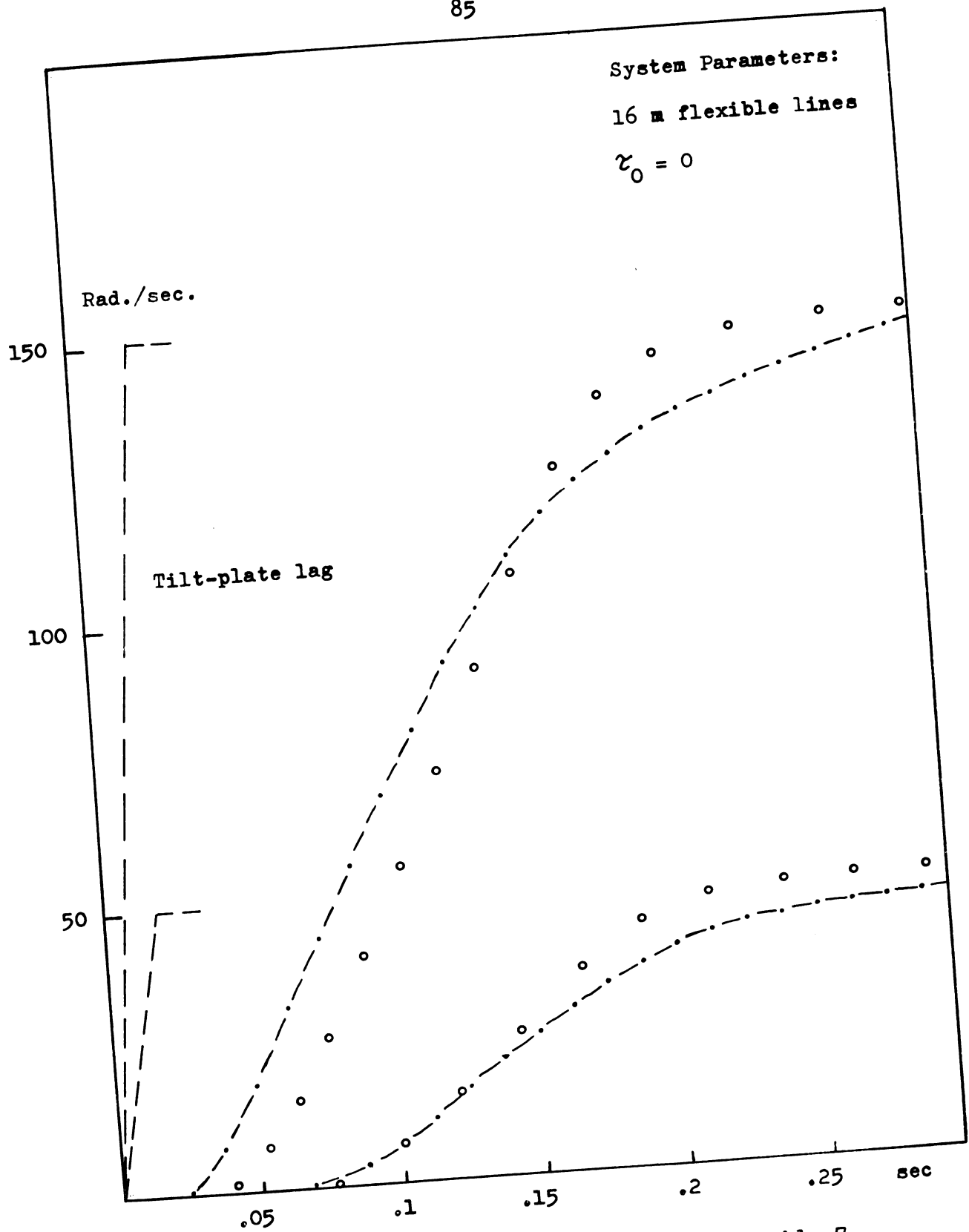


Fig. 5.7.2.--Velocity response of subassembly 7.

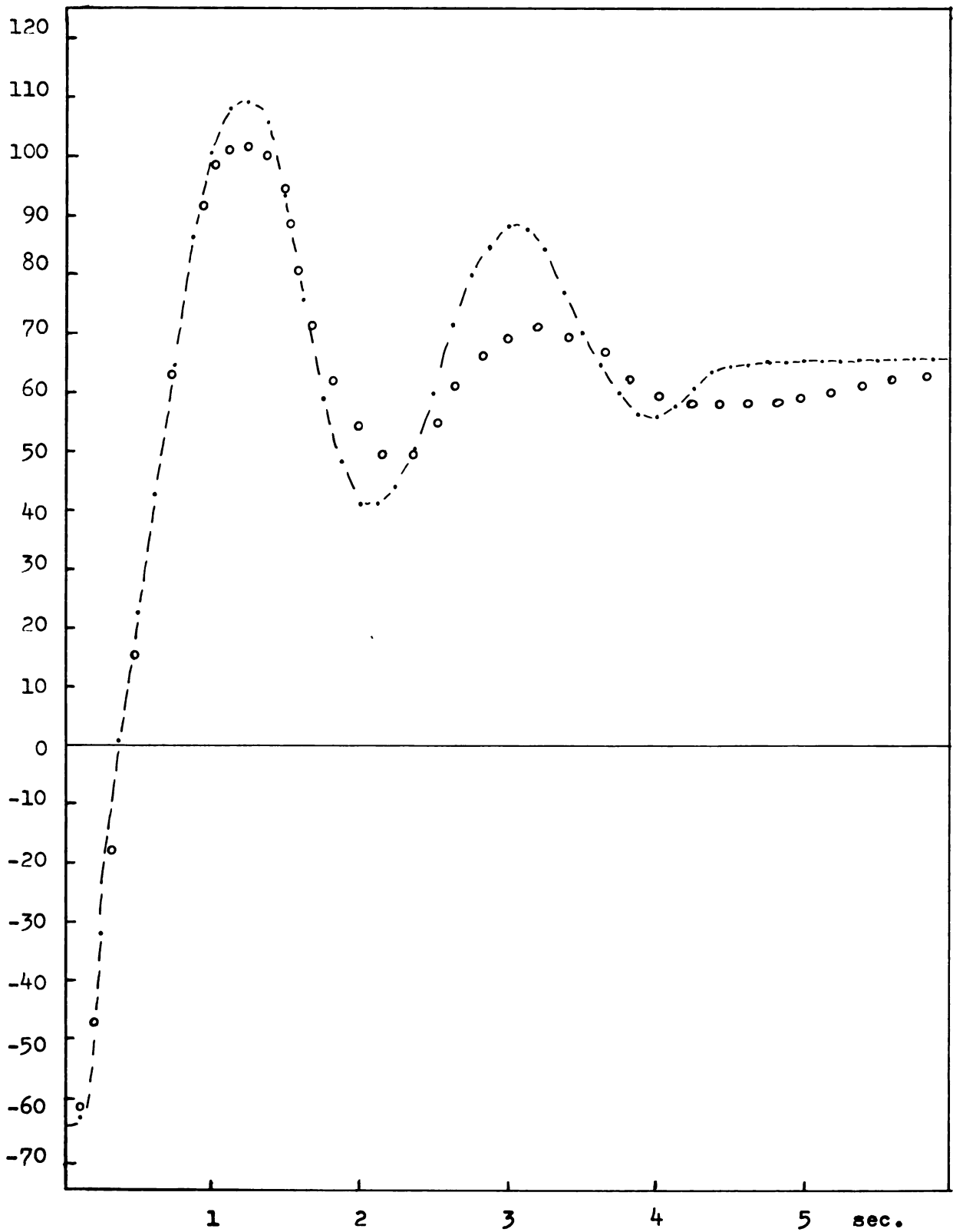


Fig. 5.7.3.--Velocity response for subassembly 7 with load

5.8 Pump Short-Line Valve Cylinder. (Subassembly 8)

In the subassemblies discussed so far, only one control element was employed to actuate a motor shaft or cylinder rod. This section presents the mathematical model of a subassembly involving two control elements, both a variable displacement pump and four-way control valve. The potentials of such a combination have well been recognized. The highly effective control action of the four-way control valve is combined with the pump which serves as a power supply, self-adjusting to power needs.

Since the valve in this subassembly is operating from a specified flow supply, the pump, it must be of totally underlapped design. It was indicated in section 2.2 for (2.2.10) that an explicit terminal representation for a valve operating from a specified flow supply is obtained by including the capacity in the connection between the flow source and the valve. For this reason, a short line is analytically inserted between the pump and the valve. The terminal representation of the valve operating under the stated conditions is given by (2.2.16). In (2.2.16) information regarding the pressures p_{h_1} , p_{h_2} and p_{h_3} is required. The existence of capacitance in both the lines connecting the pump to the motor and the cylinder chambers result in first order differential equations explicit in these pressures. Thus, the mathematical model of this subassembly may be developed in normal form.

In a pump-valve combination, it is appropriate to restrict the pump flow to one direction. One pump port may then be permanently "grounded" to the reservoir. Thus, the system graph

of subassembly 8 is established as shown in Fig. 5.8.1.

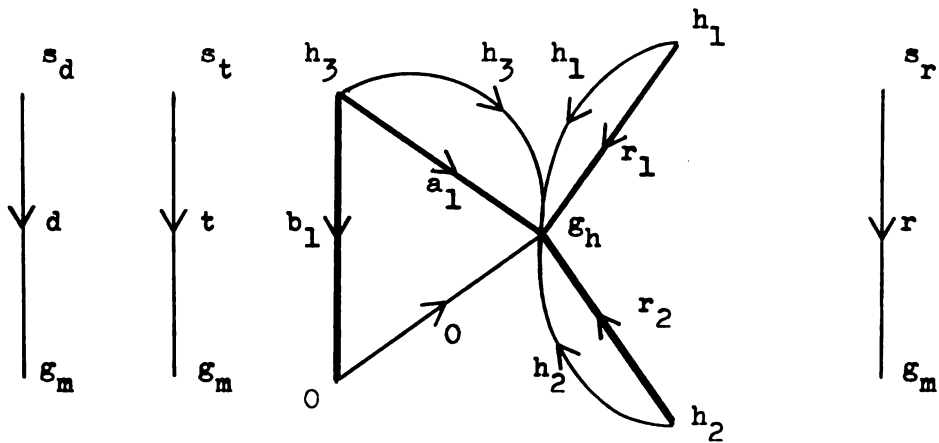


Fig. 5.8.1.--Graph of subassembly 8

The tree of this graph is selected on the basis of normal form requirements (4). This forces the line element into the tree despite the fact that the corresponding terminal equation is explicit in the derivative of a through variable. But, there is no need to solve for this through variable as it is equal to the specified flow driver as the cutset equation shows. The formulation process then yields the mathematical model

$$\begin{aligned}
\frac{d}{dt} \begin{bmatrix} \dot{\phi}_d \\ \dot{\phi}_t \\ \phi_t \\ p_{h_3} \\ p_{h_1} \\ p_{h_2} \\ \dot{\delta}_r \\ \delta_r \end{bmatrix} &= \begin{bmatrix} -\frac{1}{J_d}(B_d \dot{\phi}_d - v_t p_{h_3} \phi_t - \tau_d + F_{14}(\dot{\phi}_d)(\tau_{dc} + B_{dc} p_{h_3})) \\ -\frac{1}{J_t}(B_t \dot{\phi}_t - \tau_t + F_{14}(\dot{\phi}_t)(\tau_{tc} + B_{tc} p_{h_3})) \\ \dot{\phi}_t \\ -\frac{1}{C_e}(K_v((\Delta_u + \delta_v) \sqrt{p_{h_3} - p_{h_1}} + (\Delta_u - \delta_v) \sqrt{p_{h_3} - p_{h_2}}) \\ + v_t \dot{\phi}_d((1 + G_0 R_e \phi_t + G_0 I_e \dot{\phi}_t) + G_0 p_{h_3})) \\ -\frac{1}{C_r(\delta_r)}(K_v((\Delta_u + \delta_v) \sqrt{p_{h_1} - p_{h_3}} + (\Delta_u - \delta_v) \sqrt{p_{h_1}}) \\ + A_p \dot{\delta}_r) \\ -\frac{1}{C_r(-\delta_r)}(K_v((\Delta_u - \delta_v) \sqrt{p_{h_2} - p_{h_3}} + (\Delta_u + \delta_v) \sqrt{p_{h_2}}) \\ - A_p \dot{\delta}_r) \\ -\frac{1}{M_r}(B_r \dot{\delta}_r - A_p(p_{h_1} - p_{h_2}) + F_{14}(\dot{\delta}_r)(f_{rc} + B_{rc}(p_{h_1} + p_{h_2})) \\ - f_r) \\ \dot{\delta}_r \end{bmatrix}
\end{aligned}$$

(5.8.1)

VI. FORMULATION AND SOLUTION OF TYPICAL SYSTEMS

The subassemblies investigated in section 5 may be very effectively utilized in the construction of complete hydraulic control systems. Of interest are control systems that may be distinguished as the following types: Systems which are controlled primarily by (1) a valve, (2) a variable displacement pump, and (3) a combination of both a valve and pump.

This section deals with the presentation of mathematical models of systems of the first two types. A discussion of a system of the last type is given by Dushkes (10).

6.1 Control Systems with Valves as the Primary Control Element.

The systems under consideration are a position and a speed control system. The physical schematics of these systems are shown in Fig. 6.1.1 and 6.1.2.

The principal subassembly of these valve controlled systems is a valve-line-motor (piston) combination.

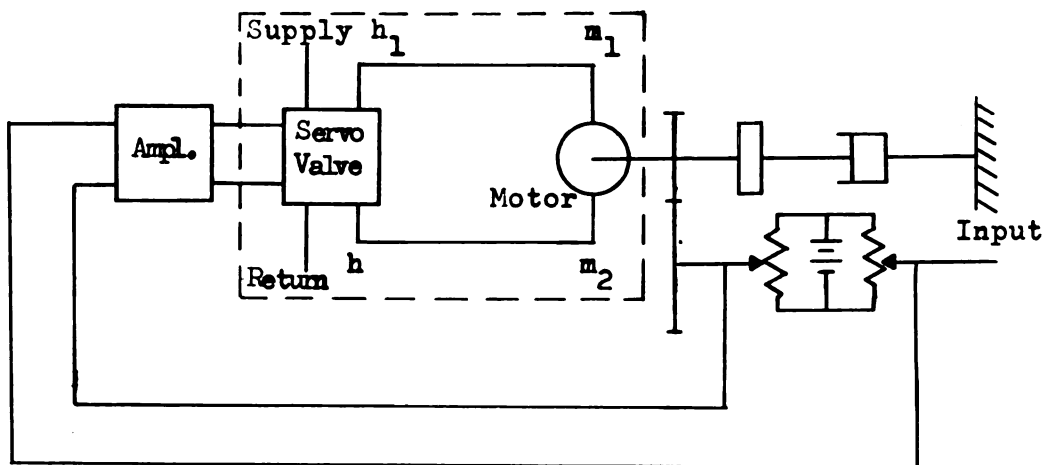


Fig. 6.1.1.--Valve controlled positioning system

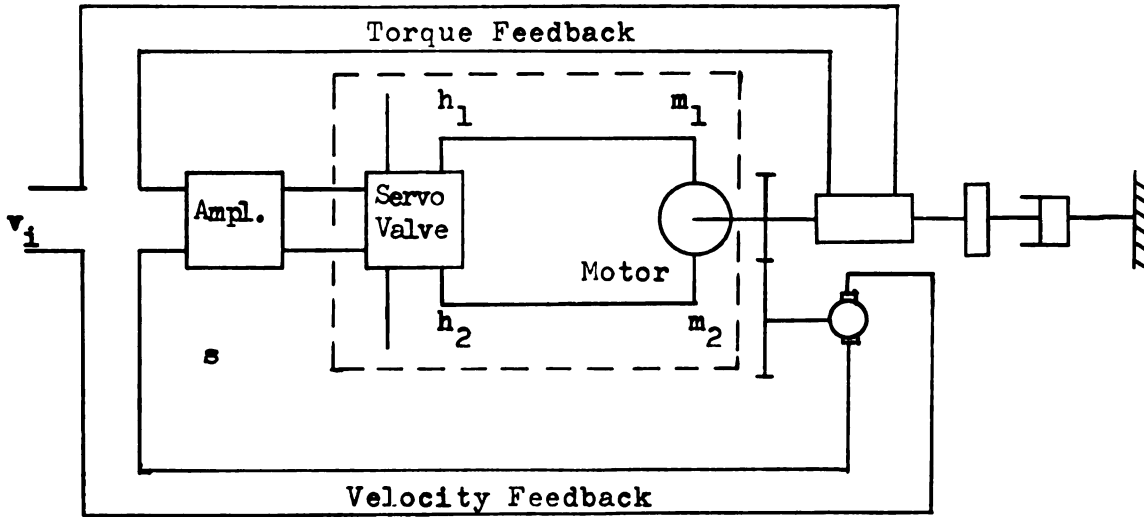


Fig. 6.1.2.--Valve controlled speed control system with load compensation.

The valves are taken as amplifier controlled four-way servovalves with characteristics as developed in section 2.5. The amplifier and feedback components are treated as ideal unilateral components with linear algebraic terminal equations. On the basis of the information provided earlier, the normal form mathematical model of the two system configurations may be readily established.

(a) Position Control System:

$$\frac{d}{dt} \begin{bmatrix} \dot{\delta}_v \\ \delta_v \\ p_1 \\ p_2 \\ \dot{\phi}_0 \\ \phi_0 \end{bmatrix} = \begin{bmatrix} -C_1 \dot{\delta}_v - C_2 (\delta_v + K_a K_p (\phi_0 - \phi_1)) \\ \dot{\delta}_v \\ -\frac{1}{C} (K_v F_{13} (\Delta + \delta_v) \sqrt{p_1 - p_s} + F_{13} (\Delta - \delta_v) \sqrt{p_1}) + V_m \dot{\phi}_0 \\ -\frac{1}{C} (K_v F_{13} (\Delta - \delta_v) \sqrt{p_2 - p_s} + F_{13} (\Delta + \delta_v) \sqrt{p_2}) - V_m \dot{\phi}_0 \\ -\frac{1}{J} (B \dot{\phi}_0 - \tau_0 - V_m (p_1 - p_2) + F_{14} (\phi_0) (\tau_c + B_c (p_1 + p_2))) \\ \dot{\phi}_0 \end{bmatrix} \quad (6.1.1)$$

where C_1, C_2 are valve constants as specified by equations (2.5.1).

$$J = J_m + J_L + 2 V_m^2 I$$

$$B = B_m + B_L + 2 V_m^2 R$$

K_p = position feedback constant

(b) Speed Control System:

$$\frac{d}{dt} \begin{bmatrix} \dot{\delta}_v \\ \delta_v \\ p_1 \\ p_2 \\ \dot{\phi}_0 \end{bmatrix} = \begin{bmatrix} -c_1 \dot{\delta}_v - c_2 (\delta_v - K_a (v_i - K_t \dot{\phi}_0 - K_e t_0)) \\ \dot{\delta}_v \\ -\frac{1}{C} (K_v F_{13} (\Delta + \delta_v) \sqrt{p_1 - p_s} + F_{13} (\Delta - \delta_v) \sqrt{p_1} + v \dot{\phi}_0) \\ -\frac{1}{C} (K_r F_{13} (\Delta - \delta_v) \sqrt{p_2 - p_s} + F_{13} (\Delta + \delta_v) \sqrt{p_2} - v \dot{\phi}_0) \\ -\frac{1}{J} (B \dot{\phi}_0 - \tau_0 - V_m (p_1 - p_2) + F_{14} (\dot{\phi}_0) (\tau_c + B_c (p_1 + p_2))) \end{bmatrix} \quad (6.1.2)$$

where K_t = velocity feedback constant

K_e = load feedback constant

Equations (6.1.1) and (6.1.2) are the equations of valve controlled systems with rotational output. Similar equations may be written for valve controlled systems with translational output.

A solution of (6.1.1) and (6.1.2) is subject to a number of constraints. These are:

$$(a) \quad p_{vap} \leq (p_1, p_2) \leq p_{max.}, \text{ in which} \quad (6.1.3)$$

the lower limit is set by the vapor pressure of the fluid. An upper limit (corresponding to a relief valve) may be arbitrarily imposed on the operation of the system to protect it from overload during transients.

$$(b) \quad |\delta_v| < \delta_{max.} \text{ (valve stem travel)} \quad (6.1.4)$$

$$(c) \quad \dot{\phi}_0 = 0, \text{ whenever } \dot{\phi}_0 \text{ changes sign}$$

$$\text{and} \quad V(p_1 - p_2) < -\tau_0 + \tau_{cs} + B_{cs}(p_1 + p_2) \quad (6.1.5)$$

Equation (6.1.5) specifies the stiction characteristics of the motor and load combined.

6.2 Solution of Position Control System.

The combination of the inherent system nonlinearities and the constraints of (6.1.3) to (6.1.5) make an analytical solution process impossible. A solution is considered for the input vector function $\dot{\phi}_1(t)$, $\tau_0(t)$. A solution may be described as the 6-dimensional trajectory with t as parameter of the state vector or more practically, a 6-variable trace with t as the independent variable. A digital computer is ideally suited to

$$T(t) = \begin{bmatrix} \dot{\delta}_v(t) \\ \delta_v(t) \\ p_1(t) \\ p_2(t) \\ \dot{\phi}_0(t) \\ \phi_0(t) \end{bmatrix} \quad (6.2.1)$$

determine such a solution vector. The various nonlinearities, logic functions and constraints are very conveniently incorporated in the numerical integration process. A solution trace for position and one of the pressures is shown in Fig. 6.2.1 and Fig. 6.2.2, with experimental traces for comparison.

Despite the insurmountable difficulty of obtaining a complete analytical solution to equations (6.1.1), some analytical investigation is possible for certain special performance characteristics: (1) steady state solution, (2) effect of variation in parameters on system performance and (3) stability behavior.

Of considerable interest in the performance study of a position control system is the steady-state solution due to the input vector.

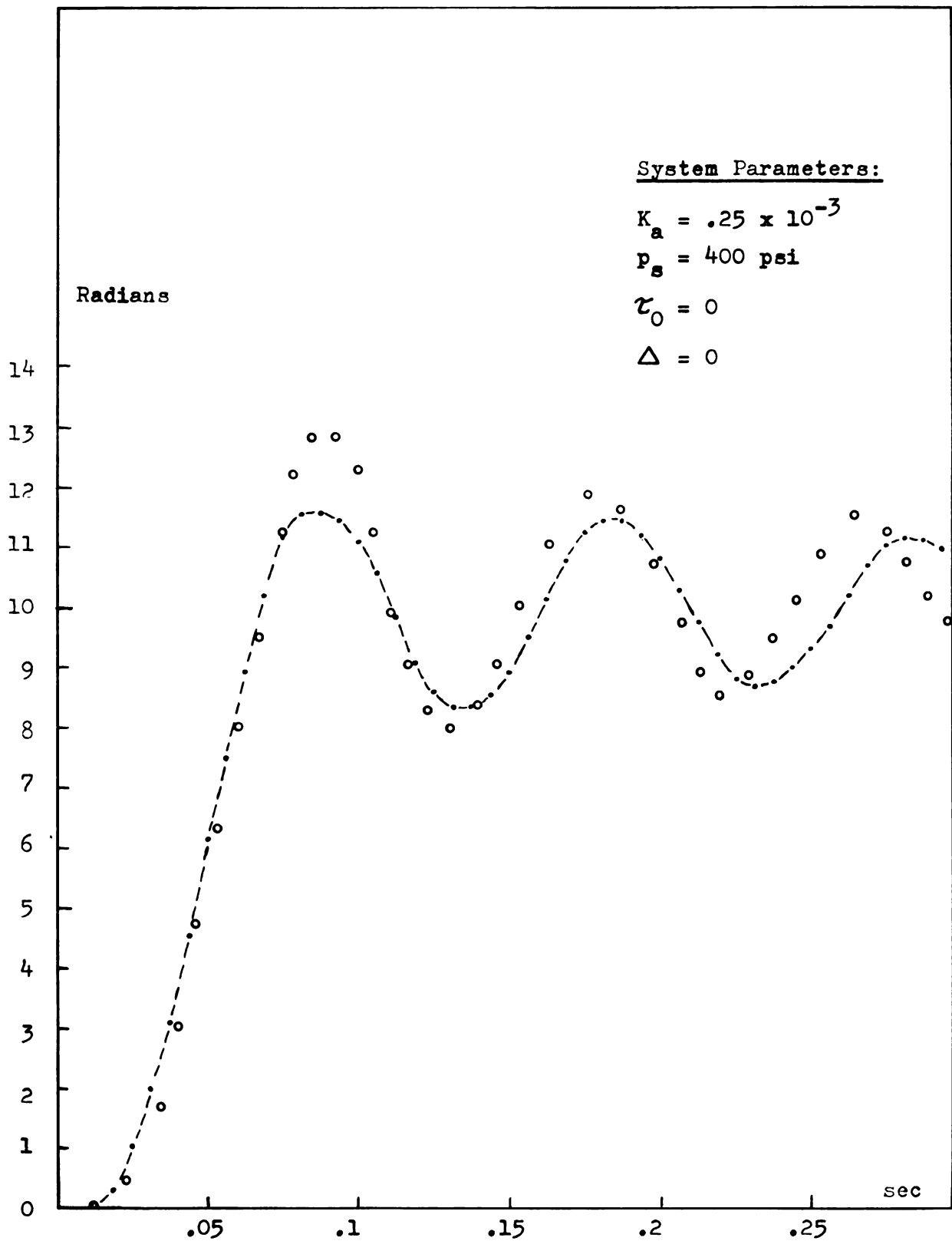


Fig. 6.2.1.--System 6.1: Position vs time for step response

$$\begin{bmatrix} \phi_1(t) \\ \tau_0(t) \end{bmatrix} = \begin{bmatrix} \Phi_1 \\ T_0 \end{bmatrix} \quad (6.2.2)$$

A solution to (6.1.1) with the inputs (6.2.2) is obtained when the derivative vector of (6.1.1) vanishes. Thus, the steady state solution $T(\infty)$ is obtained from an investigation of the condition that the right side of (6.1.1) vanishes.

From the fifth equation, one has for a given torque load

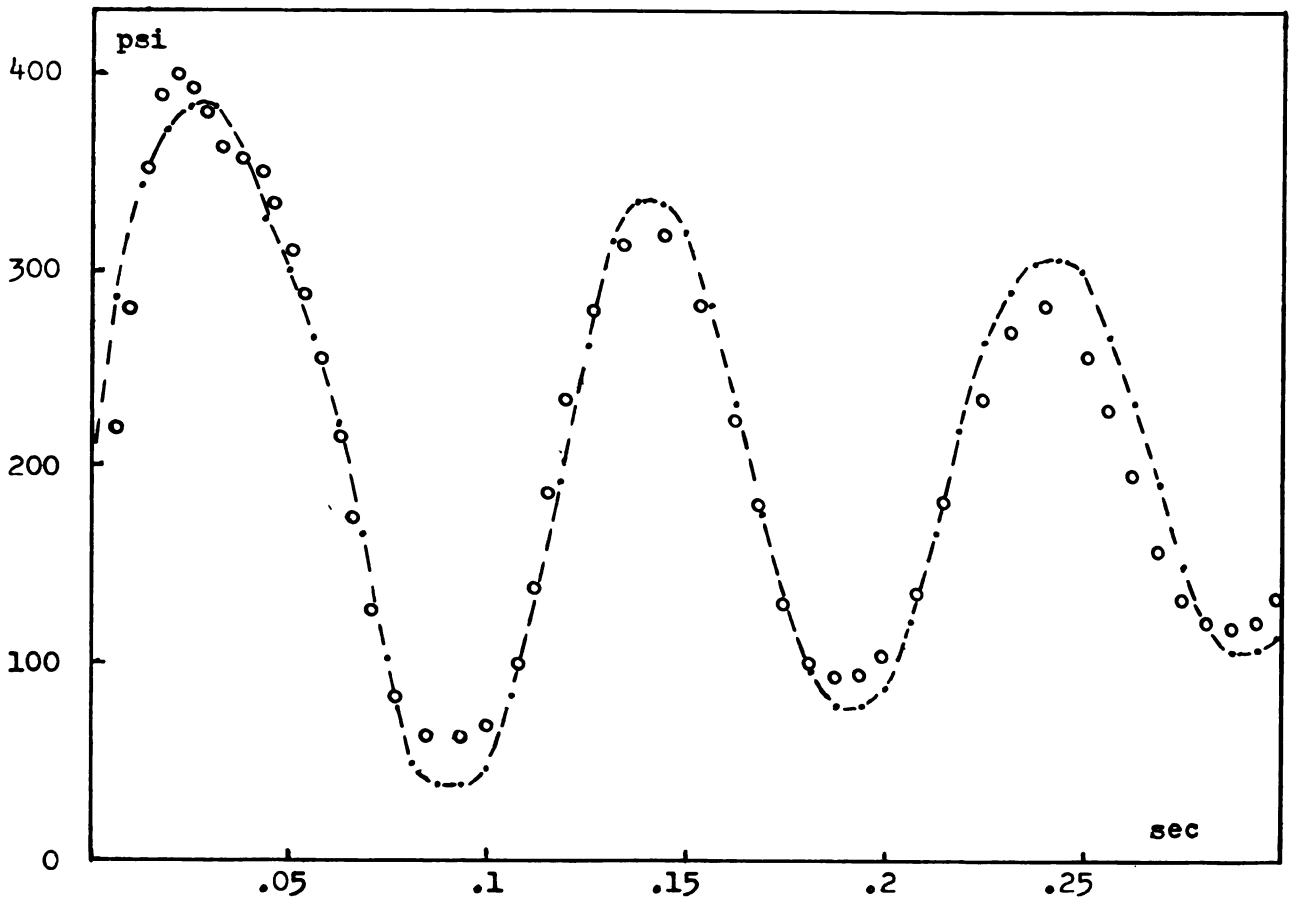


Fig. 6.2.2.--System 6.1: Pressure vs time for step response

$$p_1 - p_2 = \frac{\tau_0}{V} \quad (6.2.3)$$

It is reasonable to limit the torque to

$$\tau_0 = \alpha_p \tau_{\max} = \alpha_p V p_s \quad (6.2.4)$$

where α_p , defined as the position load factor, may vary between $0 \leq \alpha_p \leq 1$.

If it is assumed that the line pressures (p_1, p_2) have a solution symmetrically spaced about $p_s/2$, then this solution is

$$\begin{bmatrix} p_1 \\ p_2 \end{bmatrix} = \begin{bmatrix} 1 + \alpha_p \\ 1 - \alpha_p \end{bmatrix} p_s/2 \quad (6.2.5)$$

Using equation (6.2.5) and the requirement that $\dot{\phi}_0$ vanishes, one has from the third and fourth equations of (6.1.1)

$$\delta_v = \frac{\sqrt{1 + \alpha_p} - \sqrt{1 - \alpha_p}}{\sqrt{1 + \alpha_p} + \sqrt{1 - \alpha_p}} \Delta = \beta(\alpha_p) \Delta \quad (6.2.6)$$

The dimensionless ratio δ_v/Δ is plotted as a function of α_p in Fig. 6.1.4).

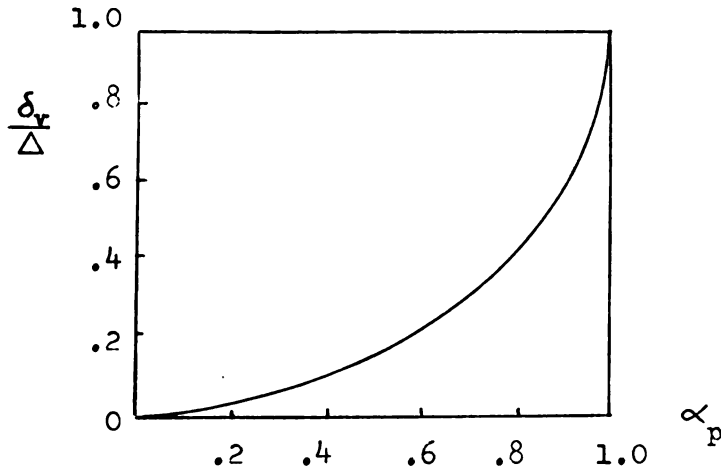


Fig. 6.2.3.--Valve stem position as a function of position load factor.

When (6.2.6) is substituted into the right hand side of

the top equation of (6.1.1), one has:

$$\phi_0 = \phi_i - \beta(\alpha_p) \frac{\Delta}{K_a K_p} \quad (6.2.7)$$

Now a complete solution vector for $\Delta \neq 0$ is

$$T(\infty) = \begin{bmatrix} \dot{\delta}_v(\infty) \\ \delta_v(\infty) \\ p_1(\infty) \\ p_2(\infty) \\ \dot{\phi}_0(\infty) \\ \phi_0(\infty) \end{bmatrix} = \begin{bmatrix} 0 \\ \beta(\alpha_p) \Delta \\ \frac{1 - \alpha_p}{2} p_s \\ \frac{1 - \alpha_p}{2} p_s \\ 0 \\ \phi_i - \frac{(\alpha_p) \Delta}{K_a K_p} \end{bmatrix} \quad (6.2.8)$$

When $\Delta = 0$, $T(\infty)$ reduces to

$$T(\infty) = \begin{bmatrix} 0 \\ 0 \\ \frac{1 + \alpha_p}{2} p_s \\ \frac{1 - \alpha_p}{2} p_s \\ 0 \\ \phi_i \end{bmatrix} \quad (6.2.9)$$

When $\alpha_p = 0$ and/or $\Delta = 0$, $T(\infty)$ reduces to

$$T(\infty) = \begin{bmatrix} 0 \\ 0 \\ p_s/2 \\ p_s/2 \\ 0 \\ \phi_i \end{bmatrix} \quad (6.2.9)$$

Several interesting conclusions may be drawn from the above development:

(1) In order to maintain the load factor within the range $0 \leq \alpha_p \leq 1$, one must satisfy, through suitable design, the condition

$$\tau_o \leq Vp_s$$

(2) For a given α_p , the steady state output position error is directly proportional to the amount of underlap Δ_u . This result may be utilized very effectively in experimentally determining the lap of a valve.

Linear approximations are quite successfully employed in predicting, with some degree of accuracy, the behavior of a nonlinear system about a point of equilibrium, i.e., a steady-state solution point.

Equations 6.1.1 and 6.1.2 may be written in the form

$$\frac{d\bar{x}}{dt} = \bar{F}(\bar{x}, \bar{y}) \quad (6.2.10)$$

where \bar{x} and \bar{y} are vector functions of the system variables and the inputs, respectively. $\bar{x} = \bar{x}_0$ is called a solution of (6.2.10) if $F(\bar{x}_0, \bar{y}) = 0$. \bar{x}_0 , of course, is the steady state response to the input \bar{y} .

If \bar{x}_0 is a solution to (6.2.10), one may express the right-hand side of (6.2.10) in the form

$$\bar{F}(\bar{x}, \bar{y}) = A(\bar{x} - \bar{x}_0) + \bar{F}_1(\bar{x}, \bar{y}) \quad (6.2.11)$$

where A is a constant matrix. If $\bar{F}_1(\bar{x}, \bar{y})$ satisfies the condition

$$\lim_{\bar{x} \rightarrow \bar{x}_0} \frac{\bar{F}_1(\bar{x}, \bar{y})}{\bar{x} - \bar{x}_0} = 0$$

then A is a unique matrix and is computable as the Jacobian matrix of (6.1.1) or (6.1.2), i.e.,

$$a_{ij} = \left. \frac{\partial F_i(\bar{x}, \bar{y})}{\partial x_j} \right|_{\bar{x}=\bar{x}_0}, \quad \begin{matrix} i = 1, 2, \dots, n \\ j = 1, 2, \dots, n \end{matrix}$$

The equation

$$\frac{d\bar{x}}{dt} = A(\bar{x} - \bar{x}_0) \quad (6.2.12)$$

is called the linear approximation to (6.2.10). The Jacobian matrix is the predominant part of (6.2.10) and hence (6.2.12) may be used to predict approximately the solution of (6.2.10) at \bar{x} near \bar{x}_0 .

For (6.2.1), the steady-state solution is given by (6.2.8) with appropriate modifications when $T_0 = 0$ and/or $\dot{\Phi}_1 = 0$. With the linear approximation of the form (6.2.12), one may make valid predictions on the effect of parameter variations on the performance of the system and the stability behavior at the steady state solution.

A linear approximation can be obtained for the above equations, since the nonlinear function $F_1(\bar{x}, \bar{y})$ corresponding to (6.1.1) or (6.1.2) satisfies the requirements for the existence of the Jacobian matrix at the steady state solution.

The linearized model for the position control system is

$$\begin{bmatrix} \dot{\delta}_v \\ \delta_v \\ p_1 \\ p_2 \\ \dot{\phi}_0 \\ \phi_0 \end{bmatrix} = \begin{bmatrix} -C_1 & -C_2 & 0 & 0 & 0 & -K_a K_p \\ 1 & 0 & 0 & 0 & 0 & 0 \\ 0 & \frac{K_v}{C} \sqrt{\frac{p_s}{2}} & -\frac{K_v}{2C} \frac{\Delta}{\sqrt{p_s/2}} & 0 & -\frac{V}{C} & 0 \\ 0 & -\frac{K_v}{C} \sqrt{\frac{p_s}{2}} & 0 & -\frac{K_v}{2C} \frac{\Delta}{\sqrt{p_s/2}} & \frac{V}{C} & 0 \\ 0 & 0 & \frac{V}{J} & -\frac{V}{J} & -\frac{B}{J} & 0 \\ 0 & 0 & 0 & 0 & 1 & 0 \end{bmatrix} \begin{bmatrix} \dot{\delta}_v \\ \delta_v \\ p_1 \\ p_2 \\ \dot{\phi}_0 \\ \phi_0 \end{bmatrix} \quad (6.2.13)$$

From (6.2.13), a linear open-loop transfer function is found to be

$$F_0(s) = \frac{K_0}{s(1 + t_1 s)(1 + t_2 s)(1 + \frac{2\zeta}{\omega_n} s + (\frac{1}{\omega_n})^2 s^2)} \quad (6.2.14)$$

where t_1 , t_2 are computable by equation (2.5.1) and

$$\zeta = \sqrt{\frac{(BC \sqrt{2p_s} + JK_v \Delta)^2}{4C \sqrt{2p_s} (2V^2 \sqrt{2p_s} - BK_v \Delta)J}}$$

$$\omega_n = \sqrt{\frac{2V^2 \sqrt{2p_s} + BK_v \Delta}{\sqrt{2p_s} JC}} \quad (6.2.15)$$

$$K_0 = \frac{2K_a K_p K_v V p_s}{2 \sqrt{2p_s} V^2 + B K_v}$$

The condition $\Delta = 0$ results in a substantial simplification in the above expressions, namely

$$\zeta = \frac{B}{2V} \sqrt{\frac{C}{2J}}$$

$$\omega_n = V \sqrt{\frac{2}{CJ}} \quad \text{for } \quad = 0 \quad (6.2.16)$$

$$K_0 = \frac{K_a K_p K_v}{2V} \sqrt{2p_s}$$

Equations (6.2.15) and (6.2.16) may be quite successfully employed to predict the effect of variation in parameter on the open-loop system behavior and serve as reliable guide lines for design. Exactly how extensive a closed-loop performance prediction may be made on the basis of (6.2.15) and (6.2.16) is questionable. Approximate relations exist between open-loop and closed-loop response for higher order systems, but at best, they are only qualitative relations. However, to remain within any given degree of accuracy, only a complete solution by computation is acceptable. Thus, if direct computation offers the only reliable method of design, the computation, of course, should be based on the nonlinear model of the system and not on its linear approximation.

The lack of reliability in a design of hydraulic system using linear approximation, is underscored by the fact that the actual system may be operating in a stable manner, while the linear model indicates instability. Computed results of an actual example represented by (6.1.1) show that the linear model is unstable at a value of loop gain of about one third the value at which the nonlinear model becomes unstable. This phenomenon is directly attributable to the fact that the third and fourth diagonal coefficients of (6.2.13) have their minimum value at

the steady-state solution. If permitted to change with the operating conditions they would monotonically increase as the actual operating point deviates from the steady-state point.

6.3 Solution of Speed Control System.

The mathematical model for the speed control system of Fig. 6.1.2 is given by (6.1.2). A steady-state solution for the input vector

$$\begin{bmatrix} \dot{\phi}_i(t) \\ \tau_0(t) \end{bmatrix} = \begin{bmatrix} \dot{\Phi}_i \\ T_0 \end{bmatrix} \quad (6.3.1)$$

is determined by finding the solution of the right hand side of (6.2.2). The bottom equation of (6.1.2) yields

$$p_1 - p_2 = \frac{1}{V} B \dot{\phi}_0 + \tau_0 + F_{14} \dot{\phi}_0 (\tau_c + B_c (p_1 + p_2)) \quad (6.3.2)$$

Similar to the development of section 6.2, a load factor

α_s , $0 \leq \alpha_s \leq 1$, may be defined such that

$$p_1 - p_2 = \alpha_s p_s \quad (6.3.3)$$

where α_s necessarily is a function of the output speed.

By using equation (6.2.5), the valve stem position is determined from the third and fourth equation of (6.1.2) with $\Delta = 0$.

$$\delta_v = \frac{\dot{v} \phi_0}{K_r \sqrt{p_s/2} \sqrt{1 - \alpha_s}} \quad (6.3.4)$$

It is immediately evident from (6.3.4) that α_s cannot be equal to unity because of the restriction (6.1.4). Substituting this result into the top equation of (6.1.2), an expression for the load feedback constant required to maintain the output at the desired level is obtained as

$$K_e = \frac{V \dot{\phi}_0}{K_a K_v \sqrt{p_s/2} \sqrt{1 - \alpha_s} \tau_0} \quad (6.3.5)$$

When τ_0 is assumed to be a viscous friction load

$$\tau_0 = B_0 \dot{\phi}_0 \quad (6.3.6)$$

then K_e is

$$K_e = \frac{V}{K_a K_v \sqrt{p_s/2} \sqrt{1 - \alpha_s} B_L} \quad (6.3.7)$$

$$\text{where } \alpha_s = \frac{(B_m + B_L) \dot{\phi}_0 + \tau_c + B_c p_s}{V p_s}$$

In order to maintain zero steady-state error, K_e must be readjusted for any changes in the input function. For zero steady-state error, the steady-state solution is then given by

$$T(\infty) = \begin{bmatrix} 0 \\ \frac{V \dot{\phi}_1}{K_v \sqrt{p_s/2} \sqrt{1 - \alpha_s}} \\ \frac{1 + \alpha_s}{2} p_s \\ \frac{1 - \alpha_s}{2} p_s \\ \dot{\phi}_1 \end{bmatrix} \quad (6.3.8)$$

A linear approximation of (6.1.2) about the steady state operating point given in (6.3.8) is

$$\begin{bmatrix} \dot{\delta}_v \\ \delta_v \\ p_1 \\ p_2 \\ \dot{\phi}_0 \end{bmatrix} = \begin{bmatrix} -C_1 & -C & 0 & 0 & -K_a K_t \\ 1 & 0 & 0 & 0 & 0 \\ 0 & a_{32} & -a_{33} & 0 & -\frac{V}{C} \\ 0 & -a_{32} & 0 & -a_{33} & \frac{V}{C} \\ 0 & 0 & \frac{V}{J} & -\frac{V}{J} & -\frac{B}{J} \end{bmatrix} \begin{bmatrix} \dot{\delta}_v \\ \delta_v \\ p_1 \\ p_2 \\ \dot{\phi}_2 \end{bmatrix} \quad (6.3.9)$$

where $a_{32} = \frac{K_v}{C} \sqrt{\frac{1 - \alpha_s}{2}} p_s$

$$a_{33} = \frac{V \dot{\phi}_1}{C(1 - \alpha_s) p_s}$$

It is obvious that as both the load and the operating speed increase, a_{32} decreases while a_{33} increases. This has a profound influence on the stability of the system when operating about an equilibrium point. This can be seen from the open-loop transfer function $F_0(s)$ of the linear model which reads

$$F_0(s) = \frac{K_0}{(1 + t_1 s)(1 + t_2 s)(1 + \frac{2\zeta}{\omega_n} s + \frac{1}{\omega_n^2} s^2)} \quad (6.3.10)$$

where $K_0 = \frac{2K_a K_t V C a_{32}}{2V^2 + B C a_{33}}$

$$\omega_n^2 = \frac{2V^2 + B C a_{33}}{J C}$$

$$\zeta^2 = \frac{(B + J a_{33})^2 C}{(2V^2 + B C a_{33}) 4J}$$

For an increase in either operating load or speed, the linear small-signal model becomes more stable. The change in linear stability characteristics as a function of operating point is very effectively demonstrated by the response curves of Fig. 6.3.1. The velocity and torque feedback constants are adjusted at a

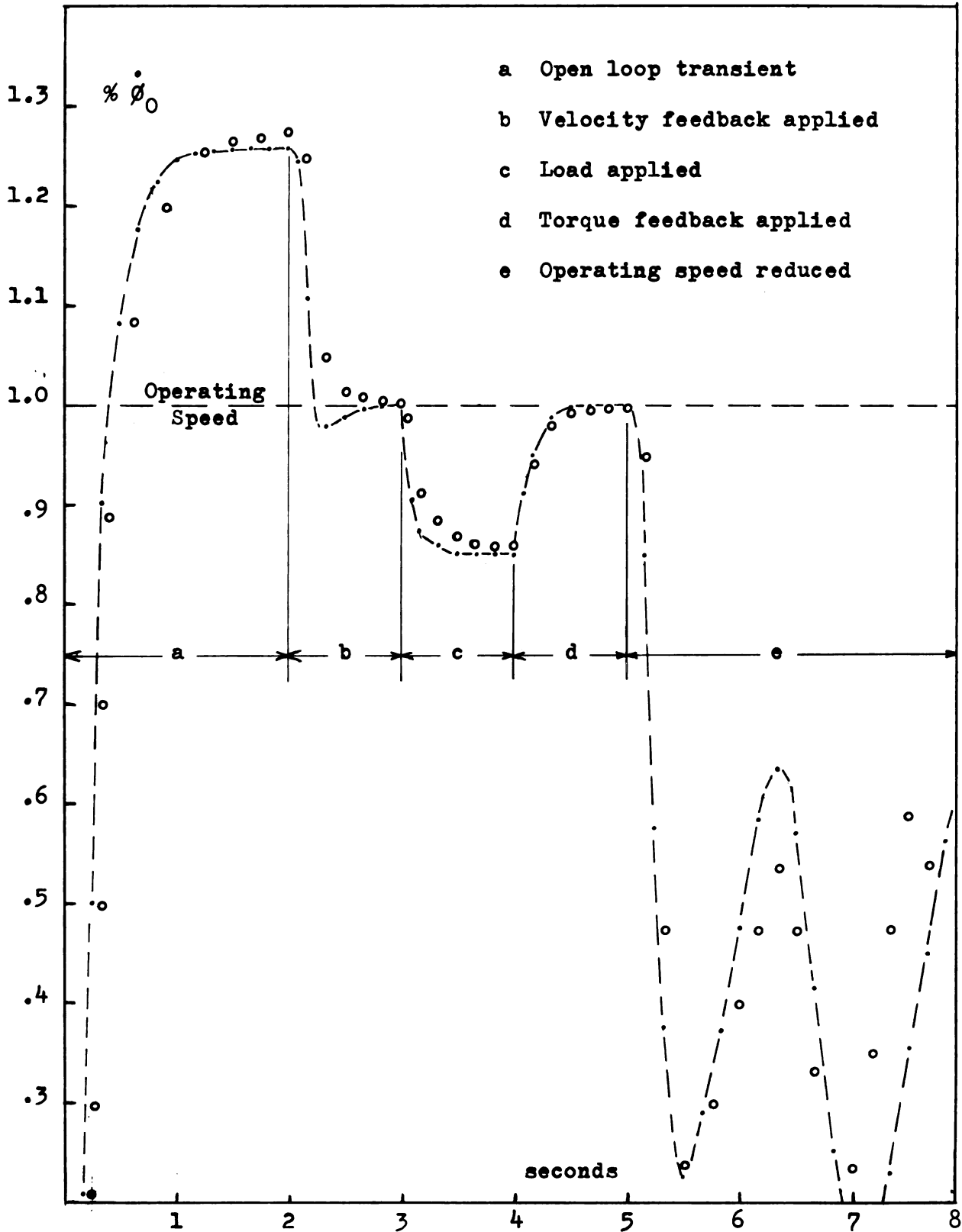


Fig. 6.3.1.--Response curves for system 6.2.

As in the valve controlled system, all components employed in the feedback networks are treated as ideal unilateral

characterized by linear algebraic terminal equations.

The control valve of the tilt-plate stroke assembly is assumed to be of zero-lap design. The piston rod is connected to the tiltplate by a lever of length R_t . The mathematical model of the system as obtained by combining the component equations with the circuit and cut-set equations of the system graph is

$$\begin{aligned}
 \frac{d}{dt} \begin{bmatrix} \dot{\delta}_v \\ \delta_v \\ p_{h1} \\ p_{h2} \\ \dot{\delta}_r \\ \delta_r \\ p_{m1} \\ p_{m2} \\ \dot{\phi}_m \end{bmatrix} &= \begin{bmatrix} -2\zeta\omega_n \dot{\delta}_v - \omega_n^2(\delta_v - K_a(v_1 - K_p \delta_r - K_t \dot{\phi}_m)) \\ \dot{\delta}_v \\ -\frac{1}{C_r}(K_v |\delta_v| \sqrt{p_{h1} - F_{12}(\delta_v) p_s} + A_p \dot{\delta}_r) \\ -\frac{1}{C_r}(K_v |\delta_v| \sqrt{p_{h2} - F_{12}(-\delta_v) p_s} - A_p \dot{\delta}_r) \\ -\frac{1}{M_r + R_t^2 J_t}((B_r + R_t^2 B_t) - A_p(p_{h1} - p_{h2}) \\ \quad + F_{14}(\dot{\delta}_r)(f_{rc} + R_t^2 B_{tc}(p_{m1} + p_{m2}))) \\ \dot{\delta}_r \\ -\frac{1}{C_1}(v_t \dot{\phi}_s \delta_r + v_m \dot{\phi}_m + (G_{01} + G_{m1}) p_{m1} - (G_{02} + G_{m2}) p_{m2}) \\ +\frac{1}{C_1}(v_t \dot{\phi}_s \delta_r + v_m \dot{\phi}_m + (G_{02} + G_{m2}) p_{m1} - (G_{01} + G_{m1}) p_{m2}) \\ \frac{1}{J_m + 2v_m^2 I_{11}}((B_m + 2v_m^2 R_1) \dot{\phi}_m - \tau_m - v_m(p_{m1} - p_{m2}) \\ \quad + F_{14}(\dot{\phi}_m)(\tau_{mc} + B_{mc}(p_{m1} + p_{m2}))) \end{bmatrix} \\
 &\quad (6.4.1)
 \end{aligned}$$

The variables in (6.4.1) are subject to the following bounds imposed by physical limitations and geometric design considerations:

(a) The tilt-plate stroke is limited to a maximum $\delta_{r_{\max}}$,
i.e.

$$|\delta_r| \leq \delta_{r_{\max}} \quad (6.4.2)$$

$$(b) \quad p_m \leq (p_{m_1}, p_{m_2}) \quad (6.4.3)$$

The line pressures in the pump-motor connection cannot drop lower the make-up system pressure, which itself must be above atmospheric pressure to be effective.

Additional bounds are set by equations (6.2.2) through (6.3.4).

Insight to the steady state performance of the system in Fig. 5.4.1 may be obtained by solving (5.4.1) when the derivative vector is zero. The input vector for which a solution is of interest is

$$\begin{bmatrix} \tau_m(t) \\ v_i \end{bmatrix} = \begin{bmatrix} T_m \\ V_i \end{bmatrix} \quad (6.4.4)$$

For simplicity, let the make-up system pressure be $p_m = 0$. Then, the last equation of (6.4.1) gives

$$p_{m_1} = \frac{1}{V_m - B_{mc}} (T_m + \tau_{mc} + (B_m + 2V_m^2 R_e) \dot{\phi}_m)$$

$$p_{m_2} = 0$$

Substituting (6.4.5) into the seventh equation of (6.4.1) the required tilt-plate displacement is obtained as

$$\delta_r = \frac{1}{V_t \dot{\phi}_d} (V_m \dot{\phi}_m + \frac{G_{m1} + G_{01}}{V_m - B_{mc}} (T_m + \tau_{mc} + (B_m + 2V_m^2 R_2) \dot{\phi}_m)) \quad (6.4.6)$$

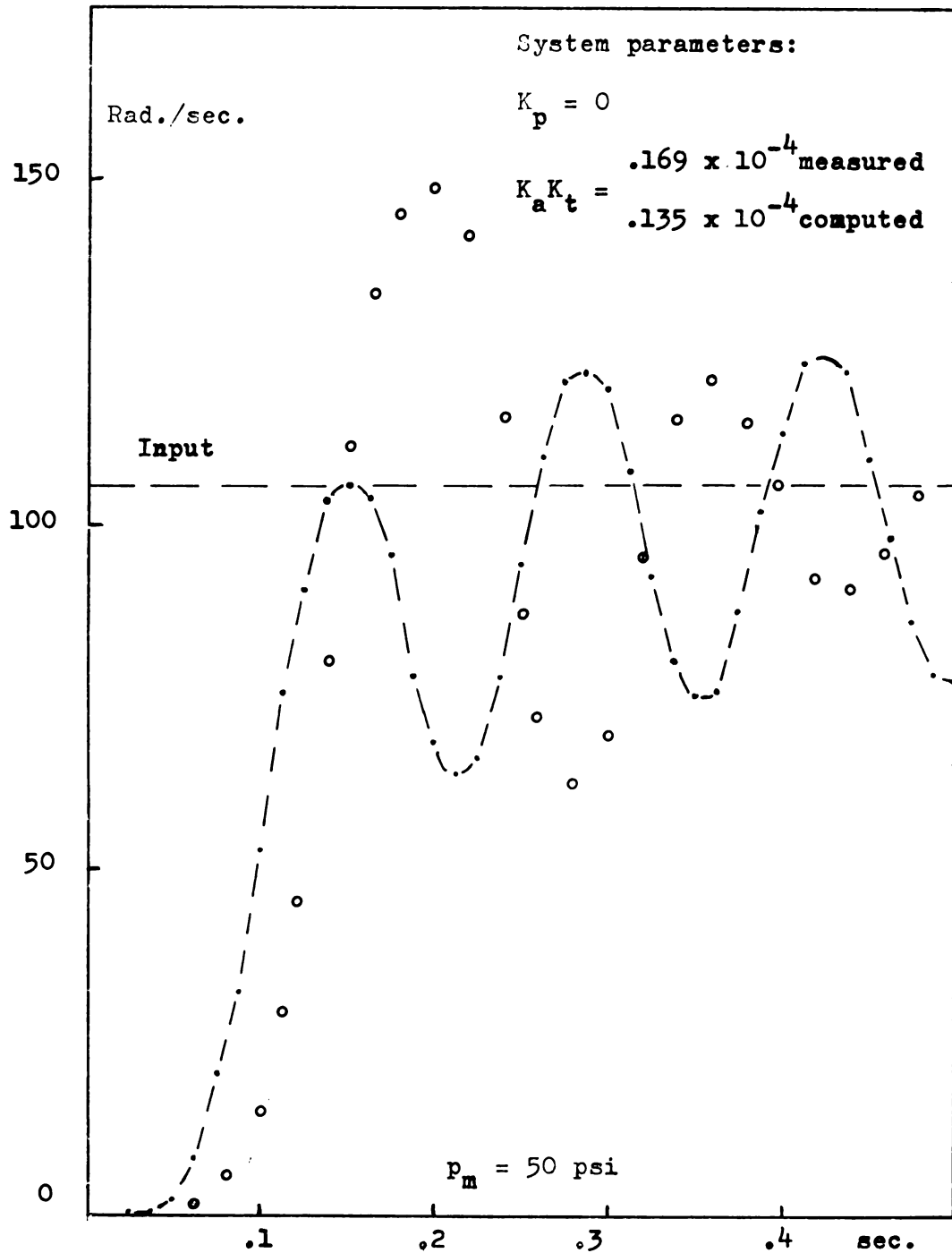


Fig. 6.4.2.--Response curves for speed control system.

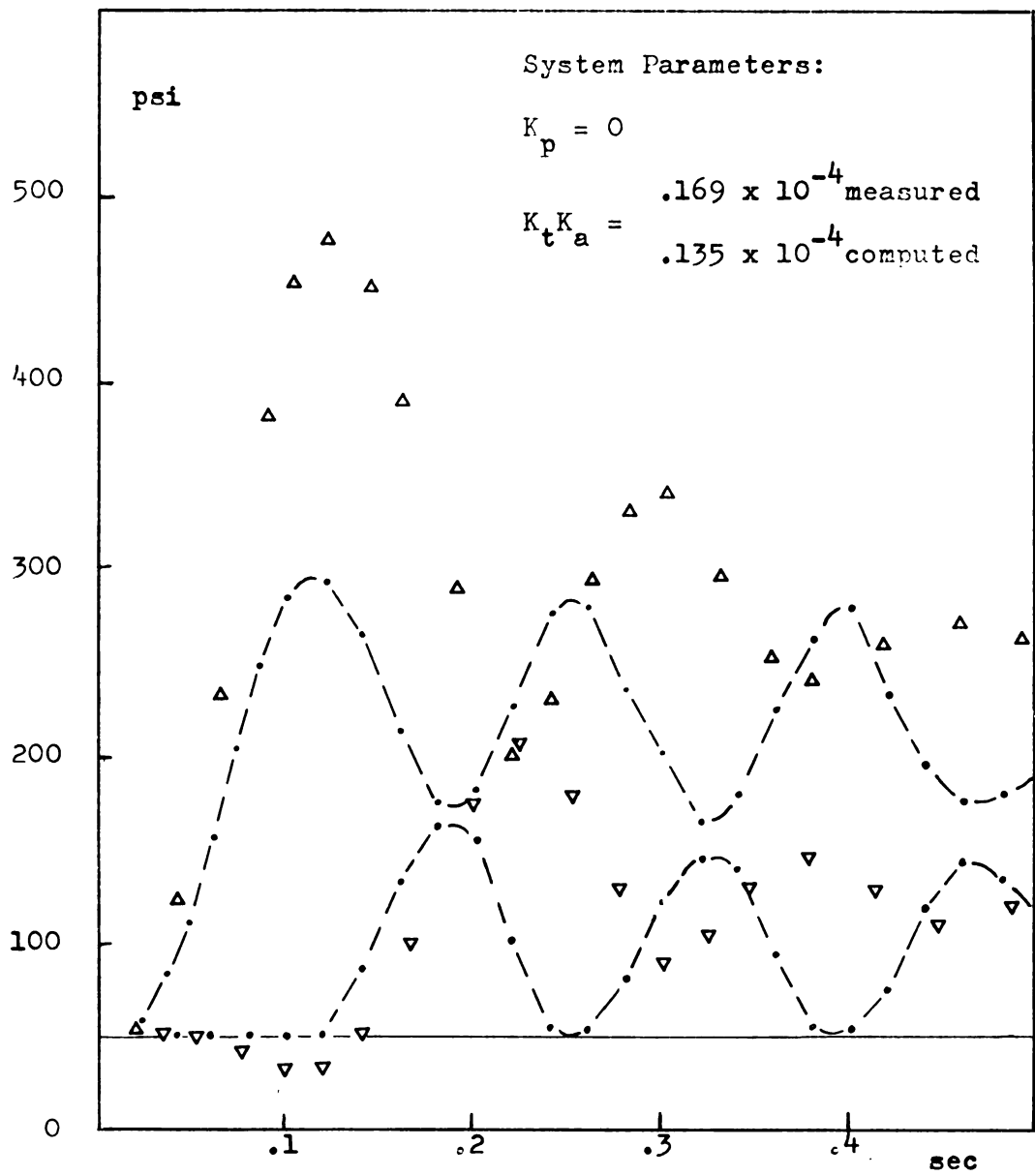


Fig 6.4.2.--Pressure response curves for speed control system

It can be seen from (6.4.6) that the tilt plate displacement is a function of the load torque only through the pump to atmosphere leakage coefficients. Thus, for a system with no leakage, the output speed is independent of the load torque. Equation (5.2.6) offers a convenient method of determining the leakage coefficients.

On the basis of the steady-state analysis of system 5.1, it can be said that

$$\begin{bmatrix} p_{h1} \\ p_{h2} \end{bmatrix} = \frac{1}{2} \begin{bmatrix} p_s \\ p_s \end{bmatrix} \quad (6.4.7)$$

$$\dot{\phi}_e = v_1 - K_t \dot{\phi}_m = K_p \delta_r \quad (6.4.8)$$

Hence, the steady-state velocity error is directly proportional to the tilt-plate angle when tilt-plate position feedback is employed. It is zero when no tilt-plate position feedback is used.

VII. CONCLUSION

In the presence of the inherent nonlinearities in the mathematical models of hydraulic system components the analysis and design of hydraulic systems is most effectively carried out in the time-domain.

Time-domain solutions by computer methods require that the derived mathematical models of the systems is given in normal form. Normal form models for hydraulic systems may always be established when the effect of hydraulic capacitance is included in the models of the components.

Computer solutions are most conveniently generated on the digital computer as the nonlinearities encountered are more suitably handled by numerical integration procedures than through analog calculations.

On the basis of correlation obtained between computer solutions and laboratory measurements for the functional subassemblies and systems considered, it can be said that the nonlinear mathematical models serve effectively to predict performance characteristics, and thus may be reliably employed in the design of hydraulic system.

APPENDIX A

NUMERICAL VALUES OF COEFFICIENTS

Note: All units are consistent with the MKS system.

1. Valve. RAD Model 410, Raymond Atchley

$$K_v = .7 \times 10^{-4}$$

$$K_a = .5 \times 10^{-5} \text{ variable to } .25 \times 10^{-3}$$

$$\text{max.} = .2 \times 10^{-3}$$

$$n = 250$$

$$= 1.0$$

2. Hydraulic Cylinder. 4" Bore, 6" Stroke,

Cylinders & Valves, Inc.

$$A_p = .253 \times 10^{-3}$$

$$F_r = .465 \times 10^{-3}$$

$$M_r = .2145$$

$$F_{cr} = 0$$

$$f_{cr} = 0$$

$$F'_{cr} = 0$$

$$f'_{cr} = 1.25$$

3. Variable Displacement Pump

$$0 - .2 \text{ cu in / rev.}$$

Modified from Vickers Hydraulic Transmission.

$$J_d = .161 \times 10^{-3}$$

$$B_d = .395 \times 10^{-2}$$

$$R_t^2 B_{dt} = 32$$

$$V_t = .967 \times 10^{-4}$$

$$t_{cd} = .54 \times 10^{-1}$$

$$B_{cd} = .587 \times 10^{-7}$$

$$R_t^2 J_t = 2.3$$

$$t_{ct} = 10$$

$$B_{ct} = .35 \times 10^{-5}$$

$$t'_{ct} = 15$$

$$B'_{ct} = .43 \times 10^{-5}$$

4. Fixed Displacement Motor

.08 cu. in. / rev

Vickers Aircraft Hydraulic Motor

$$J_m = .513 \times 10^{-4}$$

$$B_m = .77 \times 10^{-3}$$

$$V_m = .219 \times 10^{-6}$$

$$t_{cm} = .392 \times 10^{-1}$$

$$B_{cm} = .213 \times 10^{-7}$$

$$t'_{cm} = .5 \times 10^{-1}$$

$$B'_{cm} = .413 \times 10^{-7}$$

5. Hydraulic Line

1/4" I. D. H-C-4

Weatherhead Hose

$$R = .85 \times 10^9$$

$$C = .33 \times 10^{-12} \quad \text{per meter}$$

$$I = .269 \times 10^8$$

LIST OF REFERENCES

1. Koenig, H. E. and Blackwell, W. A. Electromechanical System Theory. McGraw-Hill Book Co., N. Y., 1961.
2. Reeves, E. I., "Contributions to Hydraulic Control-7, Analysis of the Effects on Nonlinearity in a Valve-Controlled Hydraulic Drive. Trans. ASME vol. 79 (1957), pp. 427-33.
3. Zaborsky, J. and Harrington, H. J. A series of 4 papers on Describing Functions for Electrohydraulic Valves. AIEE Transactions, vol. 76, pt. I, May, 1957, pp. 183-98 and vol. 76, pt. II, January, 1958, pp. 394-408.
4. Wirth, J. L. Analysis in the time domain and existence of solutions, Ph.D. Thesis, 1962, Michigan State University.
5. Wang, P. C, K. Mathematical Models for Time-Domain Design of Electro-Hydraulic Servomechanisms. AIEE ITG on Automatic Control, Volume 1, No. 1, Winter 61/62.
6. Blackburn, J. F. Contributions to Hydraulic Control-3, Pressure-Flow Relationships for 4-Way Valves. Trans. ASME, vol. 74, 1952, pp. 1163-70.
7. Blackburn, J. F. Contributions to Hydraulic Control-4, Notes on the Hydraulic Wheatstone Bridge. Trans. ASME, Vol. 75, (1953), pp. 1171-73.
8. Blackburn, J. F., Shearer, J. L. and Reethof, G. Fluid Power Control. Wiley--Technology Press. 1960.

9. Thaler, G. J. and Pastel, E. S. Analysis and Design of Nonlinear Feedback Control Systems. McGraw-Hill Book Co. N. Y. 1962.
10. Dushkes, S. Z. Bootstrapped Variable Displacement Pump Servo. Control Engineering. McGraw-Hill Book Co., April, 1962, pp. 123-25.
11. Struble, G. Nonlinear Differential Equations. McGraw-Hill Book Co. N. Y. 1962.

ROOM USE ONLY:

Room No. 101

MICHIGAN STATE UNIVERSITY LIBRARIES



3 1293 03145 1606